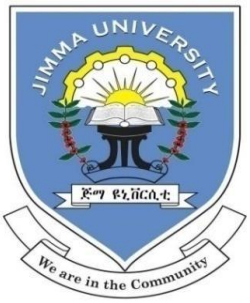

JIMMA UNIVERSITY
JIMMA INSTITUTE OF TECHNOLOGY
FACULTY OF MECHANICAL ENGINEERING
SUSTAINABLE ENERGY ENGINEERING

Modeling and Simulation of Energy and Exergy Analysis of closed Brayton cycle Combined with organic Rankine cycles for Parabolic Trough Solar Power Plant.

A thesis report submitted to the School of Graduate Studies of Jimma University in Partial Fulfillment of the Requirements for the Degree of Master of Science in Sustainable Energy Engineering.

BY: YOHANNES ALEMU

Advisor: BALEWGIZE AMARE (Assistant Prof.)

Co-Advisor; ABDULEHAK ALEMU (MSc.)

December 2018

JIMMA, ETHIOPIA

JIMMA UNIVERSITY
JIMMA INSTITUTE OF TECHNOLOGY
FACULTY OF MECHANICAL ENGINEERING
SUSTAINABLE ENERGY ENGINEERING

Modeling and Simulation of Energy and Exergy Analysis of closed Brayton cycle Combined with organic Rankine cycles for Parabolic Trough Solar Power Plant.

BY:

YOHANNES ALEMU

APPROVAL BY BOARD

Signatures

ABDULEHAK ALEMU _____

Chairperson

BALAWGIZE AMARE _____

Advisor

ABDULEHAK ALEMU _____

Co-advisor

_____

Examiner

Date; _____

DECLARATION

I, the under signed, declare that this thesis entitled by *"Modeling and Simulation of Energy and Exergy Analysis of closed Brayton cycle Combined with organic Rankine cycles for Parabolic Trough Solar Power Plant."* is my original work, and has not been presented by any other person for an award of a degree in this or any other University, and all sources of materials used for the thesis have been duly acknowledged.

Name: Yohannes Alemu

Signature _____

Acknowledgment

First, I would like to thank almighty God for blessing and being with me and give the strength to realize my aspiration.

I would like to express my warmest thanks to my advisor Mr. Balewgize Amare and co-advisor Mr. Abdulehak Alemu for their immense guidance and supervision all the way throughout this proposal work with good heart and patient.

A special thanks address to Jimma University, Institute of Technology, Mechanical Department Staffs Prof Vinkata Ramarya, Henoke Mekonnen, Eshetu Taddes for their support until the completion of the study.

Special thank goes to all my friends and my family for their support and encouragement during the development of a thesis proposal

Abstract

Concentrating Solar Power (CSP) technology offers an interesting potential for future power generation and research on CSP systems of all types, particularly those with parabolic trough solar system has been attracting a lot of attention recently.

In this paper, both energy and exergy performances of solar power plant, under different design and operating conditions are investigated. The E-draw Max and Engineering Equation Software (EES) software are used to model the power system and simulations prospectively. In the state-of-the-art PTCs, technologies are considered to set the design parameters used in the modeling of the solar field. Therminol VP-1 is the heat transfer fluid on PTC similarly Supercritical Carbon dioxide (*S-CO_2) as working fluid for closed Bryton cycle and R123 for Organic Rankine Cycle.*

The combination of S-CO_2 closed Brayton cycle and organic Rankine cycle (ORC) integrated with Solar Parabolic Trough Collectors (*SPTC) has been used to produce power, in which S-CO_2 cycle and ORC are arranged as a topping and bottoming cycle. The uses of S-CO2 as the working fluid, and organic Rankine cycles that are employed to recover the waste heat from the Brayton cycle. Now the power cycle system are assessed thermodynamically both the first and second law viewpoints. In thermodynamics, closed Brayton and ORC power cycle in the heat exchanger one and condenser sections, where the maximum exergy destruction and energy loss occurred respectively.*

Furthermore, the effects of varying some design and operating conditions on the energy and exergy performance of the PTCs and the S-CO_2 closed Brayton combined with ORC power cycle are investigated. These parameters include Direct Normal Irradiance, Pressure Ratio, and Gas turbine inlet temperature. Subsequently, the resultant impacts of changing these parameters on the overall solar power plant energy and exergy efficiencies are examined. The energy and exergy efficiencies of the power cycle are found to be 53.7% and 60.59%, respectively. Thus, the overall combined CSP efficiency reached 13.7% at the pressure ratio of 2.5 and 850 W/m^2 solar radiation.

Key words; Solar energy, Parabolic Trough Collectors, Supercritical CO_2, Combined cycle, Exergy analysis, Organic Rankine cycle.

Table of Contents

List of Figures

List of Tables

List of Abbreviations

CSP	Concentrated Solar Power
CSPS	Concentrated Solar Power System
CPTS	Concentrated Parabolic Trough Solar
CCHP	Combined Cooling Heating Power
DNI	Direct Normal Irradiance
FPL	Florida Power & Light Company
GHG	Green House Gas
GWh	Giga Watt hour
HTF	Heat Transfer Fluid
IEA	International Energy Agency
ISCCS	Integrated Solar Combined Cycle System
Mteo	Million Tone
MWe	Megawatt Electric
MWh	Megawatt Hour
NASA	National Aeronautics and Space Administration
ORC	Organic Rankine Cycle
PTC	Parabolic Trough Collector
PTSC	Parabolic Trough solar collector
SEGS	Solar Electric Generation Systems
S-CO2	Supercritical CO_2
SPTC	Solar Parabolic Trough Collector
SWERA	Solar and Wind Energy Resource Assessment
TES	Thermal Energy Storage

Nomenclatures and Symbols

λ	Wavelengths of spectral intensity range
ω	Hour Angle
L_{st}	Standard meridian time
L_{loc}	Local zone time
E	Equation of the time
$\emptyset$	Latitude angle
δ	Solar Declination
θ_z	Zenith Angle
α	Solar altitude
γ_{sun}	Solar Azimuth Angle
θ	Angle of incidence
ε	Effectiveness
η_{II}	Second law efficiency
η_I	First law efficiency
$\dot{E}_d$	Net exergy destruction rate
e_f	Flow exergy
D	Distance between collector rows
F	Focal length
l	Length of the not irradiated part
L	Length of collector
n	Number of days in years
ST	Solar time
W	Collector aperture width

CHAPTER ONE

1. Introduction

Energy consumption is one of the most important indicators showing the development stages of companies and living standards of the community. Population increment, urbanization, industrializing and technological development results directly in an increase of energy consumptions.

Solar energy is recognized as one of the most promising energy alternatives that are maturing and expected to play a major role in mitigating the CO_2 emission through a gradual replacement of current fossil fuel energy systems. According to the international energy agency (IEA), the total world energy supply in 2014 reached 13,699 Mtoe, out of which 81% is coming from oil, coal, and natural gas, while 19% is supplied by non-fossil resources with only less than 1.5% renewables contribution, including geothermal, solar, and wind [1].

Parabolic troughs are currently the most used means of power generation option of solar sources. Solar electric generation systems (SEGS) employ solar collectors to track the sun and use its energy to produce steam and hot gas. The PTC replace the boiler part of a conventional Brayton and Rankine Cycle power plant with solar fields that are used to increase the temperature of HTFs (heat transfer fluids)and the PTC is used as a heat source for Brayton cycle . The solar field area must be wide enough to satisfy the power demand [2].

1.1. Current Status of the Solar Electric Generation Systems (SEGS) Plants

Parabolic trough collectors are the most mature solar technology to generate heat at temperatures up to 400°C for solar thermal electricity generation or process heat applications. The biggest application of this type of system is the nine southern California power plants known as solar electric generating systems (SEGS), which have a total installed capacity of 354 MWe (Kearney and Price, 1992). Details on these plants are given in Table 1 (LUZ, 1990). As can be seen, SEGS I is 13.8 MWe, SEGS II–VII are 30 MWe each, and SEGS VIII and IX are 80 MWe each. These have been designed, installed, and operated in the Mojave Desert of southern California, the first one since 1985 and the last one since 1991. These plants are based on large parabolic trough concentrators providing steam to Rankine power plants. They generate peaking power, which is

old to the Southern California Edison utility. These plants were built in response to the 1970s oil crises when the U.S. government gave tax and investment incentives on alternative energy, totaling to nearly 40% of their costs [2] [3].

The average gross solar output for all nine plants at SEGS is around 75MWe a capacity factor of 21%. In addition, the turbines can be utilized at night by burning natural gas. Florida power & light company (FPL) claims that the solar plants power 232,500 homes and displace 3,800 tons of pollution per year that would have been produced if the electricity had been provided by fossil fuels. The facilities have 936,384 mirrors and cover more than 1,600 acres (6.5 km^2). Lined up, the parabolic mirrors would extend over 229 miles (370 km). The SEGS power plants were built by Luz Industries and commissioned between 1984 and 1991. Kramer Junction employs about 95 people and 45 people work at Harper Lake [3].

Table1.1 Characteristics of SEGS Plants Solar[3].

SEGS Plant	1st Year of Operation	Net Output (MWe)	Solar Field Outlet Temp. (°C)	Solar Field Area (m^2)	Solar Turbine Eff. (%)	Fossil Turbine Eff. (%)	Annual Output (MWh)
I	1985	13.8	307	82,960	31.5	-	30,100
II	1986	30	316	190,338	29.4	37.3	80,500
III/IV	1987	30	349	230,300	30.6	37.4	92,780
V	1988	30	349	250,500	30.6	37.4	91,820
VI	1989	30	390	188,000	37.5	39.5	90,850
VII	1989	30	390	194,280	37.5	39.5	92,646
VIII	1990	80	390	464,340	37.6	37.6	252,750
IX	1991	80	390	483,960	37.6	37.6	256,125

From the table1.1 there is increasing the parabolic trough solar plant installation and capacity are improved.

Figure 1.1 Aerial view of SEGS III, IV, and V, three of the Luz plants located on the Mojave Desert of southern California. Photo courtesy of Luz International, Inc [3].

1.2. Description of the PTC Power Plants

During 1984-1990, nine Solar Electric Generating Station power plants were built in the southern California desert. Each plant used parabolic trough solar collectors to heat either a mineral oil or synthetic heat transfer oil; thermal energy in the oil was used to generate steam, and the steam drove a conventional Rankine cycle power plant. However, for a variety of economic reasons, no new domestic or international parabolic trough power plants have been constructed since that time. To improve system cost and efficiency, Integrated Solar Combined Cycle System (ISCCS) proposed as a means of integrating a parabolic trough solar plant with modern combined cycle power plants. An integrated plant consists of a conventional combined cycle plant, a solar collector field, and a solar steam generator. During sunny periods, feed water is withdrawn from the combined cycle plant heat recovery steam generator and converted to saturated steam in the solar steam generator. The saturated steam is returned to the heat recovery steam generator, and the combined fossil and solar steam flows are superheated in the heat recovery steam generator [3][4]. However, taking into consideration the growth of population and the ongoing development in countries of transition and developing countries, a significant increase in energy consumption along with GHG emissions will be noticed. Therefore, the transition to renewable energy resource is more environmentally friendly.

Ethiopia is one of the countries where significant increase in energy consumption has been experienced recently. Electricity sales increased from 3,131.26 GWh in 2008 to 3,264.42 GWh in 2009 by 4.25 % [5]. Therefore, to compensate for the increase in demand and to mitigate climate change, different energy potentials should be explored.

1.3. Energy Potential of Ethiopia

In Ethiopia, substantial renewable energy resources do exist consisting mainly, hydropower, wind, geothermal, biomass and solar energy. The country also has considerable non-renewable energy resources especially natural gas and coal. The source of energy is currently dominated by traditional biomass consumption, other energy sources such as hydropower and the rest renewable energy resources can potentially offer the nation for major economic development opportunities. Many governments started incentive plans to promote generation and integration of energy into the grid by means that minimize the environmental impact.

Ethiopia has great potential for solar energy as receives a solar irradiation of 5,000-7,000Wh/m^2 depending on the locale and the season. However, less than 1% of the potential has been exploited so far. According to the recent data collected by energy information administration and development follow up core process, within the last 6 years, the total generated energy from solar photovoltaic is more than 35 MWh, more than 6MW than the installed capacity. Solar water heating systems with the total energy generation of 299 MWh and ten water pumps with pumping installed capacity of 10 kW have been installed in different parts of the country by governmental and nongovernmental organizations [5].

1.4. Solar Technology

Comparing this outstanding potential with the currently limited utilization is the main motivation for further research and development to make solar technologies reliable and economically competitive. The broad solar energy research can generally, be categorized into three broad themes: (1) solar photovoltaic (PV) cells which focus on the utilization of solar light (photonic energy) in a direct conversion process involves the use of semiconductor devices, (2) solar thermal systems which concentrate and capture solar radiation to be used as heat or converted to power in a thermodynamic cycle; and (3) fuel production by solar energy where chemical and photochemical processes are used to produce fuel such as hydrogen out of solar energy. The current

study falls under the second category where thermal energy is concentrated and captured using parabolic trough collector (PTC). The heat is subsequently converted to power using thermodynamic power cycle [3].

The key factor that affects the CSP plant size, performance and land occupation, is the direct normal irradiation of the selected site. United Nations Environment Program study revealed that a minimum threshold value of 1,800 kWh/m^2/year of direct normal irradiance (DNI) as a prerequisite for CSP installations [6].

Thermal Power plants generate more than 80% of the total electricity produced in the world where as rest of the electricity is compensated from different sources like hydraulic, nuclear, wind, solar, geothermal, biomass etc. The economic growth of any country depends upon the cheap and abundant supply of electricity. Modern life is totally dependent on the electrical power in such a way that the per capita consumption of electricity is often taken as index of economic development prosperity and standard of living of a nation [7].

The mostly used method for the analysis of energy conversion system is the first law of thermodynamics. The energy analysis based on first law of thermodynamics cannot provide the true measure of efficiency and thermodynamic losses. So there is increasing interest in the combined utilization of first and second law of thermodynamics.

1.5. Definition of Energy and Exergy analysis in Different Component

In the power generation system, exergy analysis (or second law analysis) has proven to be a powerful tool in thermodynamic analyses of the system. Exergy is defined as the maximum useful work that can be done by a system interacting with a reference environment. Different from the conventional energy analysis that is based on the first law analysis, the exergy analysis can give a clearer assessment of various losses occurring in energy system both quantitatively and qualitatively. Exergy analysis can evaluate quantitatively the causes and locations of the thermodynamic imperfection in the energy system, and thus indicate the possibilities of thermodynamic improvement. As a result, exergy analysis has been widely used in the design, simulation and performance evaluation of energy systems. The conclusions from the exergy analysis play a significant role in improving the existing processes, components or systems, or developing new processes or systems [8].

Exergy analysis based on the second law of thermodynamics provides the clear distinction between energy loss to the environment and internal irreversibilities in the process. It is a methodology for the evaluation of performance of devices and process and involving the exergy at different point in series of energy conversion steps. Exergy of a thermodynamic process shows the efficiency or inefficiency of that process. Exergy provides us with a better understanding of processes for qualifying energy. Therefore, it would better to use exergy to locate, qualify and quantify energy destruction. For this reasons, the modern approach to process analysis uses exergy analysis that provides a more realistic view of a process and useful tool for engineering evaluation. Whenever the two system in different states, there is the possibility of producing useful work and principle work can be developed as the two are allowed to come into equilibrium. When one of the two systems is a suitably idealized system called an environment and the other is some system of interest, exergy is the maximum theoretical useful work (shaft work or electrical work) obtainable as the systems interact to equilibrium, heat transfer occurring with the environment only [16].

In this project, further development of Ethiopia's research capacity in alternative energy systems with particular emphasis on parabolic trough solar power generation is considered. In doing so, a particular site called Adigala, which is found in the province of Somalia in Ethiopia located at latitude 10.41^{o} and longitude 42.21^{o} with annual averaged direct normal radiation of 7.24 ($kWh/m^2/day$) is chosen for a power plant simulation capacity of 1 MWe.

1.6. Problem statement

Energy production is essential to develop the country. Now a day energy consumption increases proportionally to the gross national product. Therefore, Conservation of energy management is an essential parameter to Lower Annual Energy Usage and Reduce Operating Cost. However, over the last few years, there have been limited study under taken on the energetic and exergetic evaluation of an integrated solar combined Waste heat recovery system. Now a day in solar thermal technology the parabolic trough design combined with S-CO_2 Bryton cycle require a large amount of water or absorption refrigeration system is needed to cool the condenser in order to continuous cycle process [1]. Nevertheless, a large amount of heat is rejected from the condenser. This is one of the energy loss in the condenser in order to conserve this energy and to cool the condenser temperature it needs additional cycle.

Many of the problems lie with the effects of varying some operating conditions on the energy and exergy performance of the Parabolic Solar Trough integrated with Supercritical CO_2 Brayton power cycle. These parameters include beam radiation intensity, pressure ratio, the inlet temperature of the turbine and the heat transfer working fluid selection. Subsequently, the resultant of changing these parameters on the overall solar power plant thermal efficiencies are varied.

Now in thermodynamics closed Brayton power cycle the maximum energy loss occurs in the condenser. Therefore, the possible solution in order to minimize energy loss by connecting into organic Rankine cycle for the application of like waste heat recovery and cogeneration process. Based on the previous literature R123 organic Rankine cycle fluid was selected because of a better energy and exergy efficiency as well as lowest exergy destruction [9]. This Combined cycle will minimize the energy loss in the condenser; similarly it produces additional output work and improves the overall thermal efficiency of the system.

1.7. The objective of this Thesis

1.7.1. General Objective

The major objective of this thesis is to Modeling and Simulation of Energy and Exergy Analysis of closed Brayton cycle Combined with organic Rankine cycles for Parabolic Trough Solar Power Plant.

1.7.2. Specific Objectives

- Modeling of CPTS combined with S-CO_2 closed Brayton cycle and ORC.
- To evaluate the Energetic and Exergetic performance of the combined S-CO_2 and ORC power cycle.
- To predict the Energy and Exergy efficiency of the combined S-CO_2 and ORC plant, with the behavior of internal disturbances and external disturbance.
- Optimize and simulation of the maximum efficiency and energy power production.
- Performance comparison of present work with previously work power cycles.

1.8. The scope of the Project

The scope of this work is

- Modelling and simulation of parabolic trough solar and S-CO_2 combined with ORC power plant using EES software and only theoretical study are done.
- All the systems are working in steady state conditions which means does not consider transient analysis.
- Validate the results using a secondary validation method; (by using data from pervious literature) therefore primary validation (experimental validation) is beyond the scope of this research.
- The Thermal Energy Storage system is beyond the scope of this research.

1.9. Significant of this Project

The solar energy has received much attention as a promising renewable energy source to replace fossil fuels. Therefore, the growing energy supply, demand has created an interest towards the plant equipment efficiency and the optimization of CPTS power plants. Most of the power plants are designed by the energy performance criteria based on the first law of thermodynamics only. The real useful energy loss cannot be justified by the fist law of thermodynamics, because it does not differentiate between the quality and quantity of energy. The present study deals with the energy and exergy analysis of closed Brayton cycle combined with organic Rankine cycles for parabolic trough solar power plant. This research has a great significant to improve the performance energy loss and exergy destruction occurred in the condenser, increasing green energy economic, reduce fossil fuels consumption and increasing energy production.

1.10. Methodology

1.10.1. General Approach and site selection

After conducting relevant materials review on parabolic trough collectors and power production from the Brayton cycle Combined with organic Rankine cycles, modeled by E-DRAW MAX software. The system was simplified into control volumes with distinct energy inflows and outflows from each volume representing the different process flows. The processes were approximated to steady or quasi steady- state flow conditions.

In this thesis, concentrated parabolic trough solar (CPTS) power plant, detailed thermodynamic, and heat transfer analyses are conducted to assess heat losses, exergy destructions, and energy plus exergy efficiencies. The state-of-the-art PTCs technologies will consider setting the design parameters used in the modeling of the solar field. In doing so, a particular site called **Adigala**, which is found in the province of Somalia in Ethiopia located at latitude 10.41^{o} and longitude 42.21^{o} with an daily averaged direct normal radiation of 7.24 (kWh/m^2/day) and Relevant data were acquired and processed using an Excel spreadsheet. A mathematical model was created by using EES software for analysis of each subsystem and draw the graph by using origin software. By inputting the real operation and design parameters, the exergy balance and energy performance evaluation were performed. Overall Capacity of S-CO_2 closed Brayton cycle Combined with organic Rankine cycle power plant was simulated and a factor which affects the overall capacity

of the power plant were evaluated. These factors are beam radiation intensity, pressure ratio, and inlet temperature of the turbine. The reference environment is going to define as being the local environment of the **Adigala** area. The limitations and simplifying assumptions were stated and finally, conclusions and suggestions were made.

1.10.2. Data Collection

Primary and secondary data is collected from concerned bodies. The weather data for selected sites were collected from National metrological agency office. Considering numerous criteria such as ground structure, water bodies, slope, protected or restricted areas, forest, and agricultural covered areas for the detection of land resources, which would permit the placement of concentrating solar collector fields installed, data is collected in map format.

In addition, weather data was collected from SWERA and National Solar Radiation Data Base (NASA) for data analysis and simulation of the model. Different Literature surveys like energy books, journal articles are reviewed.

1.10.3. Data Analysis

To accomplish the desired objectives, reviewing literature and other resources, which are relevant to this thesis work, are followed. E-DRAW MAX software is used to model the SPTC and power plant using from E-DRAW MAX library.

In Thermodynamic, cycle the simulation code that is programmed by using EES software. The EES software extracts the thermodynamic properties from its library of property functions and calculates all of the unknown parameters including state point thermodynamic properties and heat and work interactions as well as exergy rates for each stream.

By using EES software simulation of the power plant is used to find different state reference values (pressure, steam temperature, enthalpy) which are used as to evaluate of the energetic and exergetic performance of the combined S-CO2 and ORC power system integrated with SPTCs plant and plot the graph by using Origin software. Next to that to analysis and simulate the factor affect the total power plant, like internal and external disturbances (DIN, pressure ratio, the inlet temperature of the gas turbine) was analyzed. Similarly, to analysis was done for the total maximum energy, exergy power production in MW and efficiency.

1.11. Thesis Organization

There are seven chapters in this thesis. The first chapter covers the introduction part, which deals with the background and objective of the thesis. The second chapter deals with the literature review previous work describing the main elements of the plant system namely Parabolic Trough Concentrated Solar Power Plant, Working Fluid of Cycle. Chapter three general terminology of about solar radiation and Estimation of Solar Radiation Data the selected site in Adigala Chapter four is on modeling of Solar Thermal S-CO_2 Brayton Cycle Combined with ORC Power Plant Mathematical Modeling using EES. The fifth chapter deals with the Thermodynamic Analysis of S-CO_2 and ORC Power Cycles modeling formulas.

The sixth chapter deals with the simulation result and discussion. this chapter shows like the Energy and Exergy efficiency of the combined S-CO_2 and ORC plant with the behavior of internal disturbances etc. chapter seven the conclusions and recommendations are included.

CHAPTER TWO

2. Literature Review

Climate change has drastically increased causing global warming due to the emission of greenhouse gas with the provision of energy services that community of the world uses. In order to work against this trend, varieties of researches are necessary to avoid the negative impacts of global warming. Among the various forms, of utilizing energy mechanisms that curtails the emission of greenhouse gases is solar energy electricity production [6].

Utilization of solar energy has become crucial and it is expected to increase significantly in the near future. Therefore, there is a need to improve the performance of thermal power plants integrated with solar thermal energy. Parabolic trough solar collector (PTSC) technology is considered the most established solar thermal technology for power production. It has been used in large power plants since the 1980s in California and has demonstrated a promising renewable energy technology for the future. Hence, this technology has been selected for this study [10].

2.1 Parabolic Trough Concentrated Solar Power Plant

Parabolic trough concentrated solar power (CSP) plants are mainly comprised of a solar field, Thermal Energy Storage (TES), and a power generation block. The solar field consists of parabolic mirrors, receivers, and a single-axis-tracking system. The parabolic mirrors reflect and concentrate sunlight onto the receivers, which are positioned along the focal line of the parabolic trough. Receivers, in turn, are connected in a series to form a loop through which heat transfer fluid (HTF) is circulated to absorb the heat generated by a concentrated solar beam.

The HTF leaves the field loop with a high temperature to be pumped through a hot header to the TES or directly to the power generation block based on the operating condition. The parabolic trough CSPs are mature technologies, they have been in use since the 1980s when nine Solar Electric Generating Systems (SEGS) were built in the Mojave Desert of Southern California. These SEGS plants have a total of 354 MW installed capacity and achieved an efficiency of 10% [11].

Thereby, parabolic trough CSP systems are considered the most advanced and commercially proven technology compared with all other types of CSP plants. PTC has a concentration ratio of 70 to 80 suns and an operating temperature in the range of 290–550 °C [12].

The peak efficiency of PTC-based CSPs is between 14 and 20%, and the annual solar-to-electricity net efficiency is about 11–16%, as reported by Kuravi et al [13]. numerous studies some of which focused on the development and the optimization of the solar field [22][23], while others investigated the conversion cycles and improving their conversion efficiencies [16]. On the performance of PTC studied the incidence angle modifier for a PTC and investigated the relationship between a PTC test and long-term performance prediction of a solar field. Gupta and Kaushik [17] studied a direct steam generation in a trough-based CSP and conducted an energy and exergy analysis for different plant components. Hence, for the purpose of exergy analysis, SPTC system considered as the efficient heat source.

2.2 Solar Parabolic Trough Collector Working Fluid

As reported by Bellos E et al. PTCs operate with numerous working fluids and a lot of research has been focused on this domain. Water/steam is conventional working fluid and there are applications that include operation with water at low temperature, as well as with water/steam in direct steam production systems. The use of thermal oils as Syltherm 800, Therminol VP-1, Therminol D12, Marlotherm TH, Dowtherm A and Sandotherm-59 is usual in indirect systems with heat exchangers for the heat production [18]. However, the utilization of the thermal oils set upper limits up to 400 °C [19]. Therminol PV-1 is able to be kept in the liquid phase up to 400^{o}C while it has to operate over 12^{o}C for avoiding crystallization [20]. The next generation of working fluids is focused on the molten salts (especially nitrate salts) because these can operate up to 550–600 °C giving higher margin in the solar energy to electricity conversion [21]. These working fluids can be exploited as working fluids in PTCs, as well as a storage medium for concentrating solar power plants. However, the molten salts have to be kept upper to a lower limit close to 200 °C due to solidification danger [18]. On the other hand Tzivanidis et al reported that six working fluids are examined energetically and exergetically in a commercial PTC Water, Therminol VP-1, Molten salt, Air, CO2 and Helium are examined Every working fluid is examined in the proper temperature range from 300 K to 1300 K The global maximum exergetic efficiency achieved for

Molten salt at 800 K (47.48%), however CO_2 and helium are the most suitable working fluids for extremely high temperatures [18]. G. Srilakshmi et al. Reported that molten salt as HTF, a heat exchanger is used to transfer thermal energy from the HTF to water in order to generate steam. Steam Rankine cycle is used for power generation. One of the advantages of using this as the working fluid is that the HTF used is the same as the storage media. When the plant is not in operation, HTF from the receiver has to be drained out as the freezing temperature of molten salt is relatively high, its value is around 238°C [22].

In conclusion, these techniques aim to increase the effective thermal conductivity in the flow and to increase the heat transfer coefficient between the absorber and the working fluid. Therefore, from the previous literature reported that Molten salts is limited to about 600°C by its thermal stability and also maximum energetic and exergetic efficiency. However, the current study is the working temperature up to 400°C. Therefore Therminol VP-1 is well known to maintain their liquid state above 400°C, allowing the system to operate at much higher temperatures, energetic and exergetic efficiency and low pressure both for energy capture and heat storage.

2.3 Supercritical CO_2 Brayton Cycle

Nowadays, the S-CO2 cycle and organic Rankine cycle integrated with various renewable heat sources are considered for the purpose of power generation and improved efficiency. C. Zhou et al [23].The supercritical CO_2 cycle can effectively use different heat sources including coal power, solar thermal power, and waste heat from the high temperature fuel cell, geothermal energy and natural gas. Y. Ahn et al. [24], However, the rise of the novel S-CO_2 power cycle, that promises higher energy efficiency and much smaller plant footprint, expected to positively impact the performance and the economic competitiveness of CSP plants. A. A. Alzahrani et al carried out a study to analyze the dynamic behavior of S-CO_2 power cycle integrated with a concentrated solar power system (i.e. central receiver), hot and cold energy storage, heat exchange device, recuperator and multi-stage compression-expansion subsystem along with the intercooler and re-heater as an integral component employed between the compressor and turbine [1]. Their results showed that the process efficiency and maximum power output is 21% and 1.6 MW respectively. Further, few researchers considered the integrated SPTC with ORC for various applications like waste heat recovery and cogeneration process. J. D. Osorio et al [25]. The use of CO_2 as a working fluid in a

power cycle has been proposed by several researchers as a novel and promising cycle. Recently, the CO2 cycles have regained more interest due to their potential to improve the conversion efficiency. J. D. Osorio et al. [25]. Therefore, AlZahrnai et al. have focused trans-critical and supercritical CO2 power cycles such as a reheat Rankine [26], combined trans-critical and regenerative Brayton cycles [27]. Similarly, Wang et al. have examined the performance of various CO2 power cycle configurations [28]. It was concluded that S-CO_2 power cycles are very promising technologies as it offers energy conversion efficiency of as high as 50% for high-temperature application, while for low-grade applications it provides a reasonable performance compared with organic Rankine cycles. X. Li, H. Huang. [29]. In spite, the fact that CO_2 turbomachinery is still in the research and demonstration stage, CO_2 cycles are expected to significantly reduce the power plants' foot print and subsequently reduce costs associated with materials and space. Additionally, these power cycles, with small volume, can be adapted for other small-scale renewable energy systems. The specific location of Al Madinah in Saudi Arabia, and the total CSP plant targeted capacity is one MW electric output. The rise of the novel S-CO_2 power cycle, that promises higher energy efficiency and much smaller plant footprint, expected to positively impact the performance and the economic competitiveness of CSP plants.

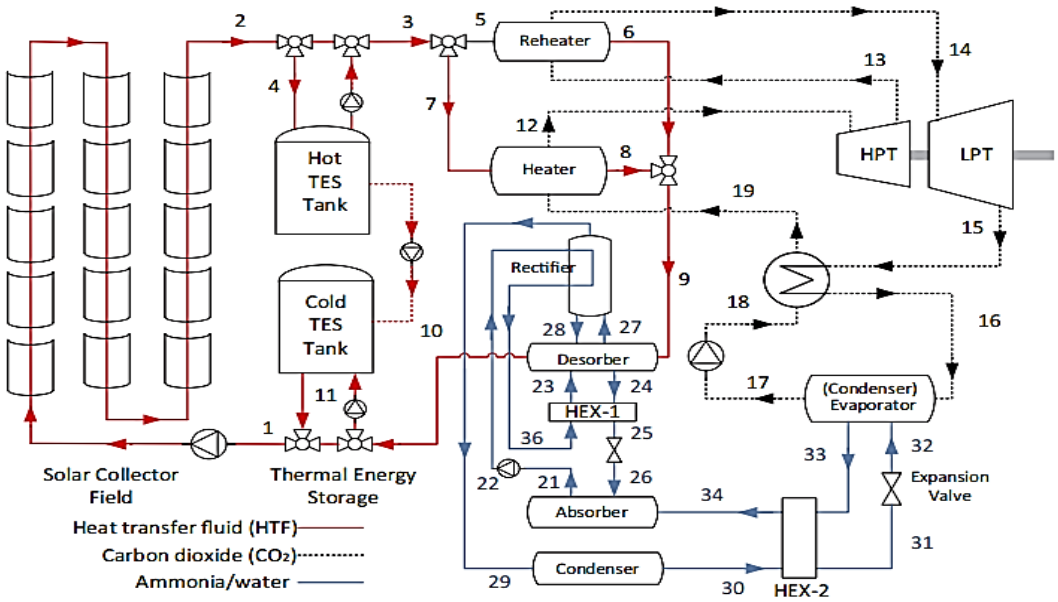

Figure 2.1 Schematic diagram Al Madinah in Saudi Arabia of the integrated CSP systems layout[1].

Reddy et al reported that maximum energy loss occurred in the condenser and the PTCs solar field. However, maximum exergy destruction rate was reported to occur in the PTCs solar field [18]. Abdullah A. et al Presented the shares of exergy destruction rate within each subsystem to the total exergy destruction rate within the entire integrated system. The figures show that most of the exergy is destroyed within the PTCs solar field, which represents about 65% of the total exergy destruction. Then, the exergy destruction rate shares of the ARS and the S-CO_2 power cycle are 18% and 17%, respectively [1].

In conclusion , from the above lecturer the only purpose Absorption refrigeration system (ARS) has been connected into the (condenser evaporator) to maintain a continuous cooling effect nevertheless it does not produce work. During the work production the hot temperature of S-CO2 exit from the turbine, which is contained, a large amount of waste heat is rejected from the condenser. Therefore, in order to minimize energy loss and exergy destruction from the condenser, by substituting ARS cycle into two organic Rankine cycles for the application of like waste heat recovery and cogeneration process to produced additional work and to get higher overall thermal efficiency.

2.4 Organic Rankine cycle

Nowadays, the S-CO_2 cycle and organic Rankine cycle integrated with various renewable heat sources are considered for the purpose of power generation [23]. C**.** Sarmiento et al. conducted an exergy analysis of combined steam and ORC power system integrated by SPTC and he found that R134a shows the highest exergy efficiency of 26% which has the maximum amongst other refrigerants followed by R152a [30]. Cardemil et al carried out an optimal arrangement of the solar collectors with a supercritical CO_2 based solar Rankine cycle system along with three different modes of collector arrangement, i.e. five units only in series, parallel and cascade with each five units in series. Lastly, their results found that solar collectors in a cascade arrangement produce a large amount of electric power [31].

Garga et al conceded out a thermodynamic study of CO_2 based power cycles (i.e. Rankine or Brayton) with four different working fluids such as ethane, toluene, D4siloxane and water for the purpose of relative performance assessment. Ultimately, this study reveals that the first law efficiency of power cycle based on CO_2 could be lower than other fluids, while the exergetic

efficiency of CO_2 could be crucially higher than competing fluids [30]. Carried out a study to assess the performance of a novel system integrated with SPTC and ORC for combined cooling, heating and power (CCHP). They used the part of waste heat from ORC for cooling as well as heating cogeneration and examined the different output parameters. Finally, his study reveals that the electrical efficiency significantly enhances from 15% to 94% for a solar mode without energy storage J. Andreasen et al [32].Apart from ORC, S-CO2 power cycle can be utilized for the exhaust/waste heat recovery process. Firms such as Echogen -power systems LLC (Ohio, USA) and General Electric (New York, USA) have already patents related to this application [31].

H. Singh et al. reported on the detailed energy and exergy analysis of solar parabolic trough collectors (SPTCs) driven a combined power plant. The combination of (S-CO_2) cycle and (ORC) integrated with SPTCs has been used to produce power, in which S-CO_2 cycle and ORC are arranged as a topping and bottoming cycle. Five organic working fluids like R134a, R1234yf, R123, R1234ze, and R245fa were selected for a low temperature bottoming ORC.As can be seen, R123 combined cycle has the maximum exergetic as well as thermal efficiency which is around 78.07% at 0.95 kW/$m^2$and 43.49% at 0.95 kW/m^2, respectively.

In conclusion, the R134a and R245fa combined cycle yields fewer promising results with the marginal difference in their performance. As inferred from the study that S-CO_2 turbine and evaporator has a certain amount of exergy destruction, which is around 9.72% and 8.54% of the inlet exergy, and almost, 38.10% of the total exergy destruction in case of R123 combined cycle. Finally, this study concludes that R123 combined cycle has a minimum fuel depletion ratio of 0.2583 for a solar collector and possess the highest power output of 3740 kW [33]. Based on the above literature R123 organic Rankine cycle fluid was selected because of a better energy and exergy efficiency as well as it has the lowest exergy destruction.

CHAPTER THREE

3. Solar Radiation

The sun is a sphere with a radius of 6.95x108 m and a distance of $1.5x10^{11}$ m from the earth. The temperature of the sun is 5777 K, and the estimated temperature at the center of the sun is $8x10^6$ to $40x10^6$ K. Its density is 100 times greater than the density of the water. The sun is a continual fusion reactor, and there are many fusion reactions, which have been proposed to supply the sun's energy. The main reaction is a process of forming helium (one helium nucleus) by combining hydrogen (four photons). The sun's energy is emitted constantly in all directions, and it is divided into two forms; extraterrestrial and terrestrial [34].

Wavelengths of spectral intensity range between 0.3μm (10^{-6} to over 3μm as shown in Figure 3.1. At 0.48 μm, maximum spectral intensity is occurring. Approximately 6.5% of total energy is included in the ultraviolet region (less than 0.38). In the visible region $0.38\mu m < \lambda < 0.78\mu m$ around 48% of the total energy is contained. The rest of energy, which is 45.6%, is contained in the infrared region, $\lambda > 0.78$.

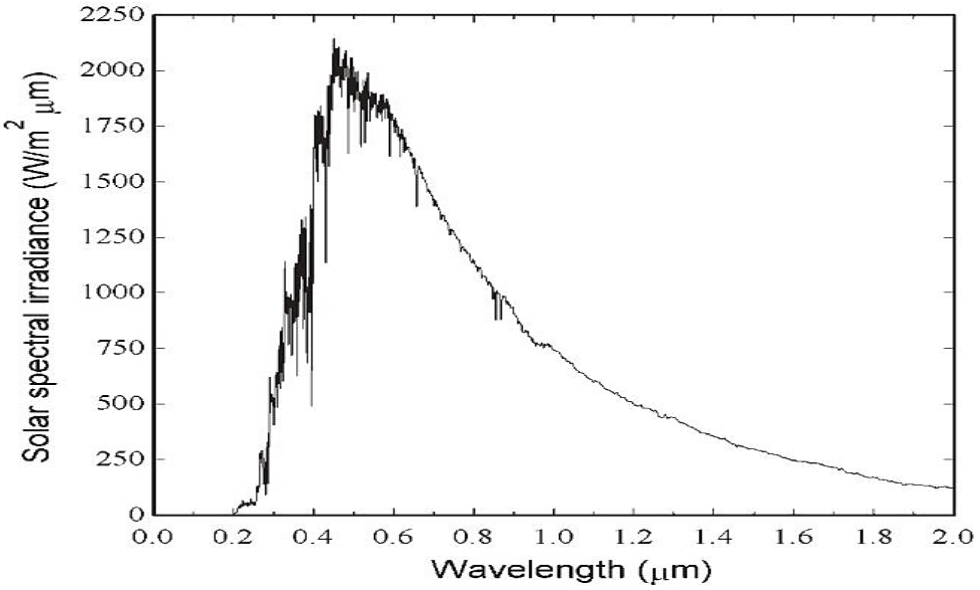

Figure 3.1 Spectral solar irradiance [34]

3.1. Earth-Sun Geometric Relationship

The annual amount of solar radiation received by the earth varies due to the changeable distance between the earth and the sun as illustrated in Figure 3.2. The Earth Sun distance has a minimum value of $1.47x10^{11}$ which is called, perihelion, on December 21 and a maximum value of $1.512x10^{11}$ which is called, aphelion, on June 21. The average distance between the earth and the sun that is called the astronomical unit (AU) is $1.419x10^{11}$. The earth revolves around itself within an axis that has a tilted angle of 23.45° with respect to its orbital plane axis. This angle is the cause of the changeable solar radiation throughout the year[35].

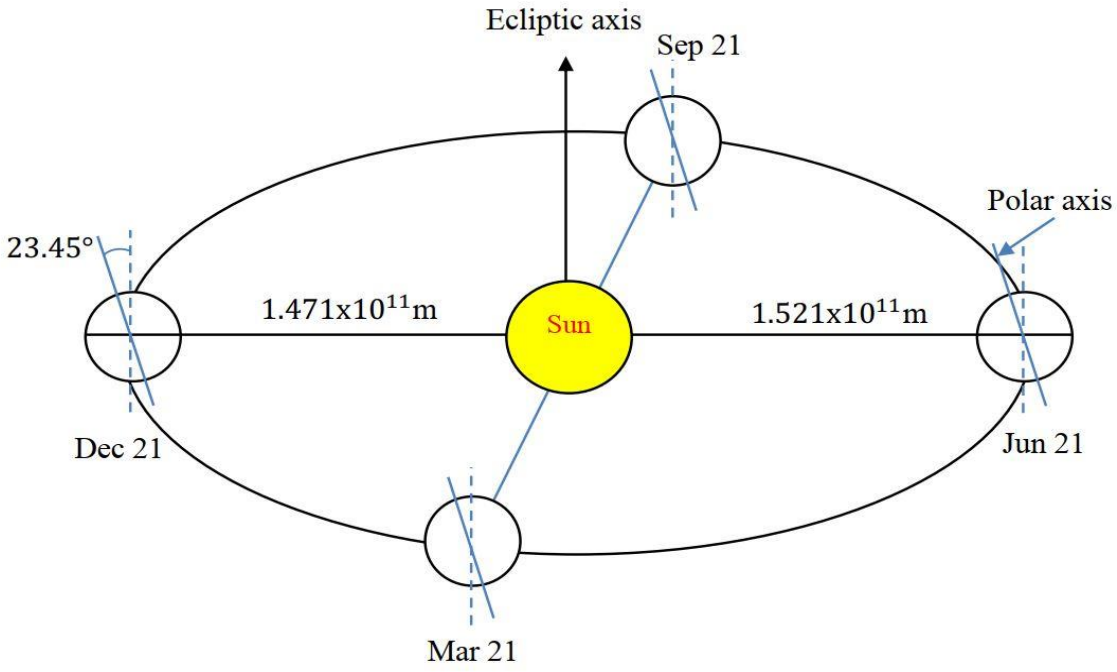

Figure 3.2 Motion of the earth around the sun

3.1.1. Hour Angle (ω)

The hour angle can be known as the angle through which the earth has to revolve to get the meridian of any point straight under the sun. Hour angle varies throughout the day as seen in Figure 3.3. For any place, at sunrise, the hour angle has a maximum negative value of -180°, then, it slowly increases, 15° per hour, while the sun is rising until it reaches zero at noon. For the period from afternoon to sunset, hour angle increases from zero to the maximum positive value, which is +180°. The hour angle (in degrees) can be calculated from the following equation [35]:

$$\omega = 15(ST - 12) \quad (3.1)$$

Where ST is the solar local time.

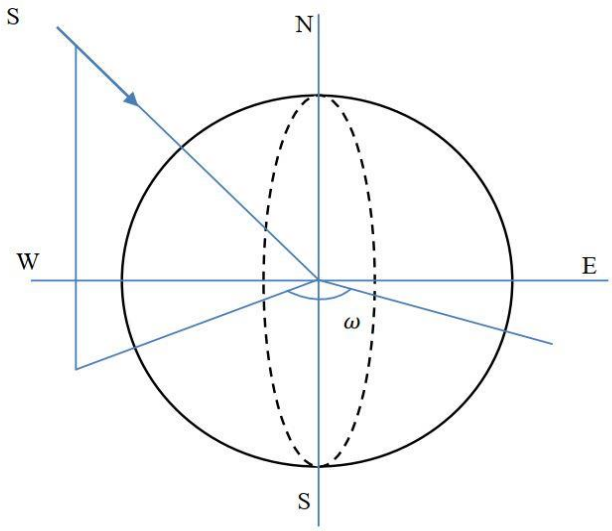

Projection if sun's ray in equatorial plane

Figure 3.3 Hour angle ($\boldsymbol{\omega}$) Adopted from [35]

Solar local time ST is not the same as the standard time. Therefore, it is important to convert the local clock time to solar time. The conversion depends on the longitude, local standard meridian, and day of the year. It is given by the following expression

$$\text{Solar time} = \text{Standard time} + 4(L_{st} + L_{loc}) + E \quad (3.2)$$

Where L_{st} stands for the standard meridian of local zone time (30° for Adigala). Represents longitude of the location (42.233 °for Adigala). The term called the equation of the time (in minutes), and it can be determined by to apply the following equation [35].

$$E = 229.2(0.000075 + 0.001868\cos B - 0.032077\sin B - 0.014615\cos 2B - 0.04089\sin 2B) \quad (3.3)$$

Where B measured in degrees can be calculated using the next equation

$$B = (n-1)\frac{360}{365}$$

Where n represents the day of the year ($1 \leq n \leq 365$). The equation time is plotted and shown in Figure 3.4.

Figure 3.4 Variation of the constant B throughout the year

3.1.2. Latitude angle (∅)

Assume that there is a point P at a location on the earth. By drawing a radial line connecting the earth center with the projection of this radial line on the equatorial plane, an angle is derived, and it is known as the latitude angle varies between +90 and -90 but (10.424° for Adigala).as shown in Figure 3.5

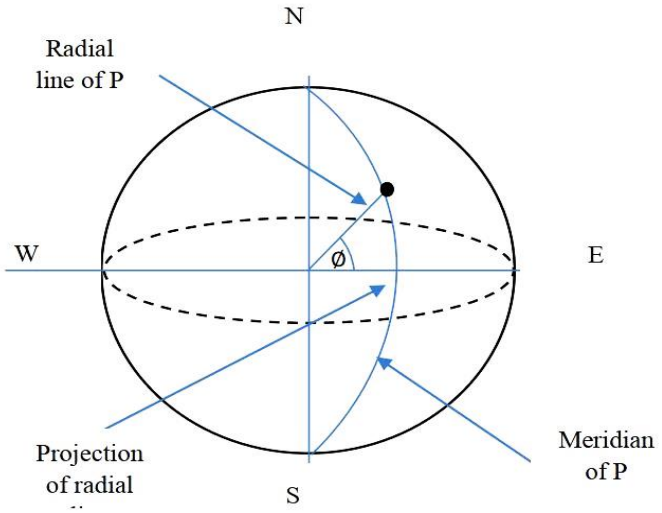

Figure 3.5 Latitude angle (∅)

3.1.3. Solar Declination(δ)

Solar declination is an angle between a line connecting the earth's and the sun's centers and the projection of the line upon the equatorial plane of the earth. The solar declination varies throughout the year because of the earth's revolving around its axis. It varies between a value of +23.45° on June 21 and a value of -23.45° on December 21]. Solar declination angle can be determined using Cooper's equation [3]:

$$\delta(in\ degrees) = 23.45\sin\left[\frac{360}{365}(284+n)\right] \quad (3.4)$$

Where n represents the day of the year ($1 \leq n \leq 365$). The plotting of the equation is shown in Figure 3.6

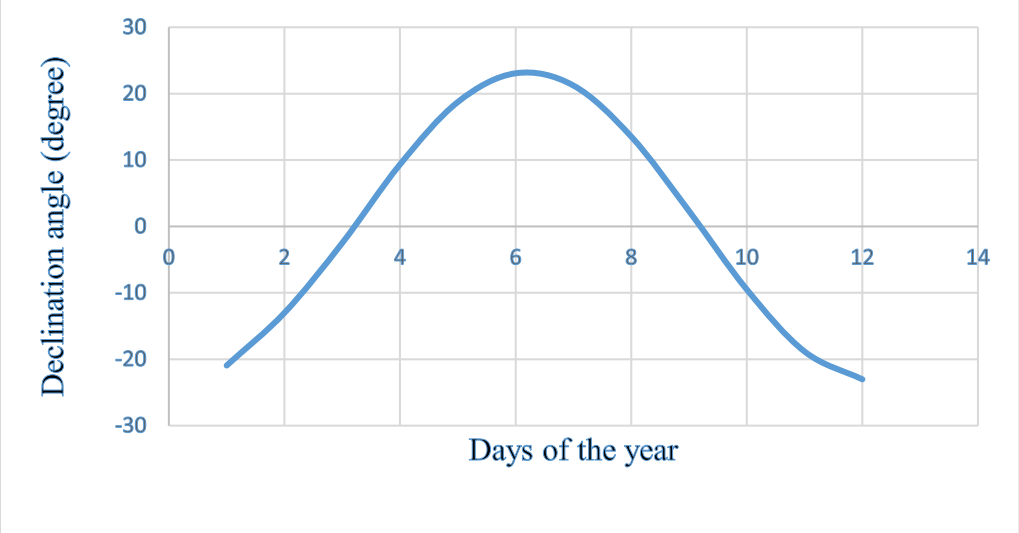

Figure 3.6 Variation of solar declination (δ) throughout the year

3.1.4. Zenith Angle (θ_z)

Consider a point P on a surface of the earth, the direction PN is called, zenith direction, and the direction SP is known as sun's beam direction. The angle between the zenith direction (PN) and the ray of the sun direction (SP) is called as the zenith angle (θ_z), Figure 3.7. At sunrise or sunset, the zenith angle (θ_z) is about 90°. However, at noon, the zenith angle become very close to 0° [3].

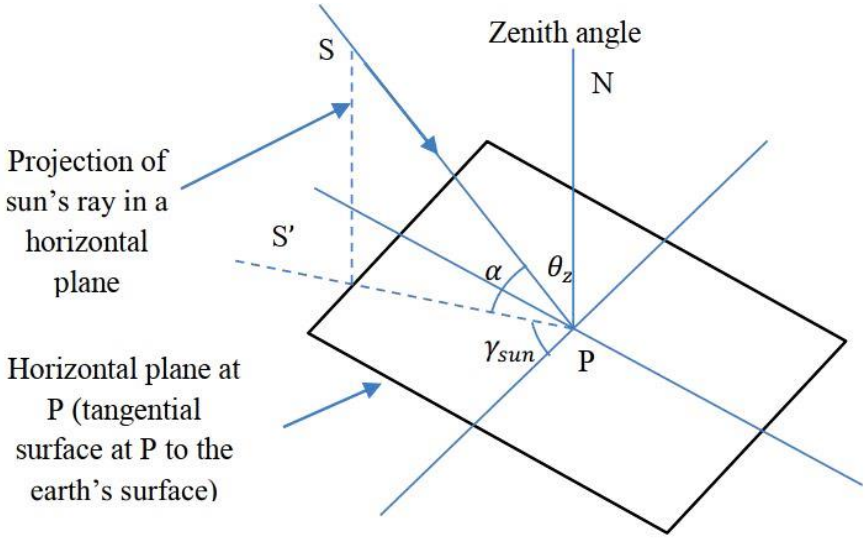

Figure 3.7 Zenith, solar altitude, and solar azimuth angles

3.1.5. Solar altitude(α)

The solar altitude(α) is the angle between the horizontal direction (S'P) and the sun's beam direction (SP), Figure 3.7, i.e. S'PS is the solar altitude. The summation of zenith angle (θ_z)and solar altitude (α) is equal to 90° [3]

$$\theta_z + (\alpha) = 90° \tag{3.5}$$

The Solar altitude angle changes with the sun movement. At sunrise or sunset, the solar altitude angle is near to zero while at noon, it becomes near to 90°. Solar altitude angle can be determined using the following expression [3]:

$$\text{Sin}(\alpha) = \text{Sin}(\emptyset)\ \text{Sin}(\delta) + \text{Cos}(\emptyset)\ \text{Cos}(\delta)\ \text{Cos}\ (\omega) \tag{3.6}$$

3.1.6. Solar Azimuth Angle (γ_{sun})

The solar azimuth angle is the angle measured between the south direction and the sun's ray as shown in Figure 3.7. The expression used to estimate the solar azimuth angle is given by [3]:

$$\sin(\gamma_{sun}) = \frac{\cos(\delta)\sin(\omega)}{\cos(\alpha)} \tag{3.7}$$

According to Duffie [3], the angle of incidence is defined as the angle between the sun rays hitting a surface and the normal to that surface. The angle of incident varies throughout the day and the

year, and it greatly affects the solar energy gained by the receiver. In other words, the solar radiation is reduced by increase the cosine of this angle. For a plane tilted with an angle of as shown in Figure 3.8, the angle of incidence correlation is given by:

$$\cos\theta = \sin\delta\sin\phi\cos\beta - \sin\delta\cos\phi\sin\beta\cos\gamma + \cos\delta\cos\phi\cos\omega + \cos\delta\sin\phi\sin\beta\cos\gamma\cos\omega + \cos\delta\sin\beta\sin\gamma\sin\omega \quad (3.8)$$

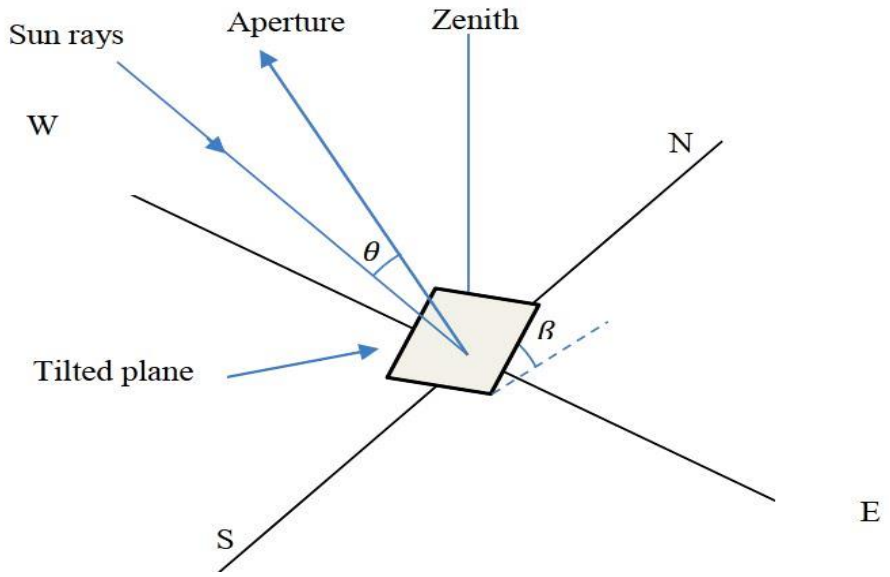

Figure 3.8 Angle of incidence (θ)

In order to minimize the angle of incidence and then maximize the solar radiation, the solar collectors must move in prescribed ways to track the sun. There are two tracking systems for the collectors. First, the collectors rotate about two axes, which is considered the best way. The second system is that the collectors rotate about a single axis; horizontal north-south, horizontal east-west, vertical, or parallel to the earth's axis. For the prototype used in this study, the parabolic trough collector rotates about a single axis, which is horizontal east-west as seen in Figure 3.9. Thus, the angle of incidence, in this case, is equal to the zenith angle because the tilting angle β is zero [3]

$$\mathrm{Cos}\,\theta = \mathrm{Cos}\,\theta_z \quad (3.9)$$

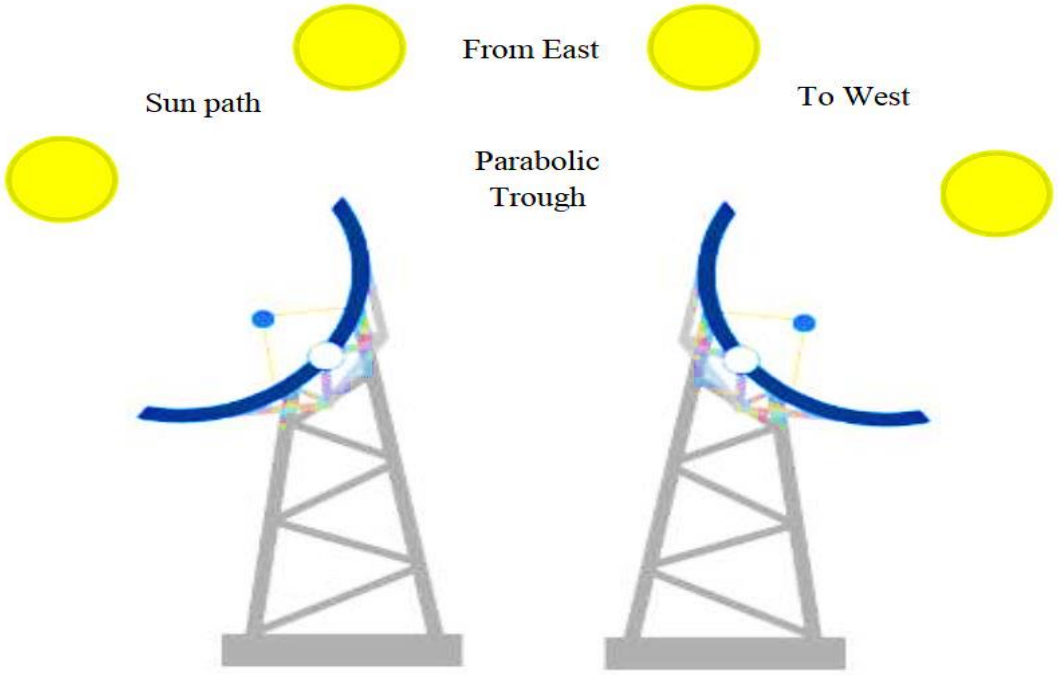

Figure 3.9 Horizontal East-West Tracking System

3.2 Estimation of Solar Radiation Data in Adigala

3.2.1 General Description of Selected Site

In Ethiopia, there are different sites that have rich solar potential. Among these, the Somalia region is one of them. Somalia region is divided into Woredas. Shinle Woreda is one of them; it consists of different kinds of land topology but mostly flat lands. In this Woreda, a place called Adigala is chosen for this particular study. Geographically, the system's site is located at latitude 10.41^{o} and longitude 42.21^{o} with an annual averaged direct normal radiation of 7.24 (kWh/m^2/day).

3.2.2. Land uses

To identify major locations for CSP installation, land assessment has to be considered. Areas with <1km^2 should be eliminated. Thus, assessment criteria are required. Some of the criteria that will be used can be seen as optional. For instance, tourist areas or agricultural areas can be transformed into potential sites for CSP plants. Other information like the slope of the terrain or water availability can be understood as necessary criteria. For example, if the slope of the terrain is greater than 2.1% the placement of a CSP plant will be impossible, considering the state of the current technologies, impossible[36]. Table 3.1 lists the necessary and optional criteria.

Table 3.1: Necessary and optional criteria an area must fulfill for being considered as a possible construction site for a CSP plant.

Excluded criteria	Necessary	Optional
Slope of terrain		
>2.1%	X	
Land cover		
Inland water	X	
Forest		X
Swamp	X	
Agriculture		X
Hydrology		
Permanent inland water	X	
Non- permanent inlet water		X
Regularly Flood area		X
Land use		
Settlements		X
Airport		X
Road	X	
Mine, quarry		X
Protected and Restricted area		X

3.2.3. Geomorphologic Features

For CSP project flat land is a requirement. As can be seen from Figure 3.10. The geomorphologic features of the land of north eastern Ethiopia, which is marked in red star, is suitable for CSP installation considering the plain surface of the area.

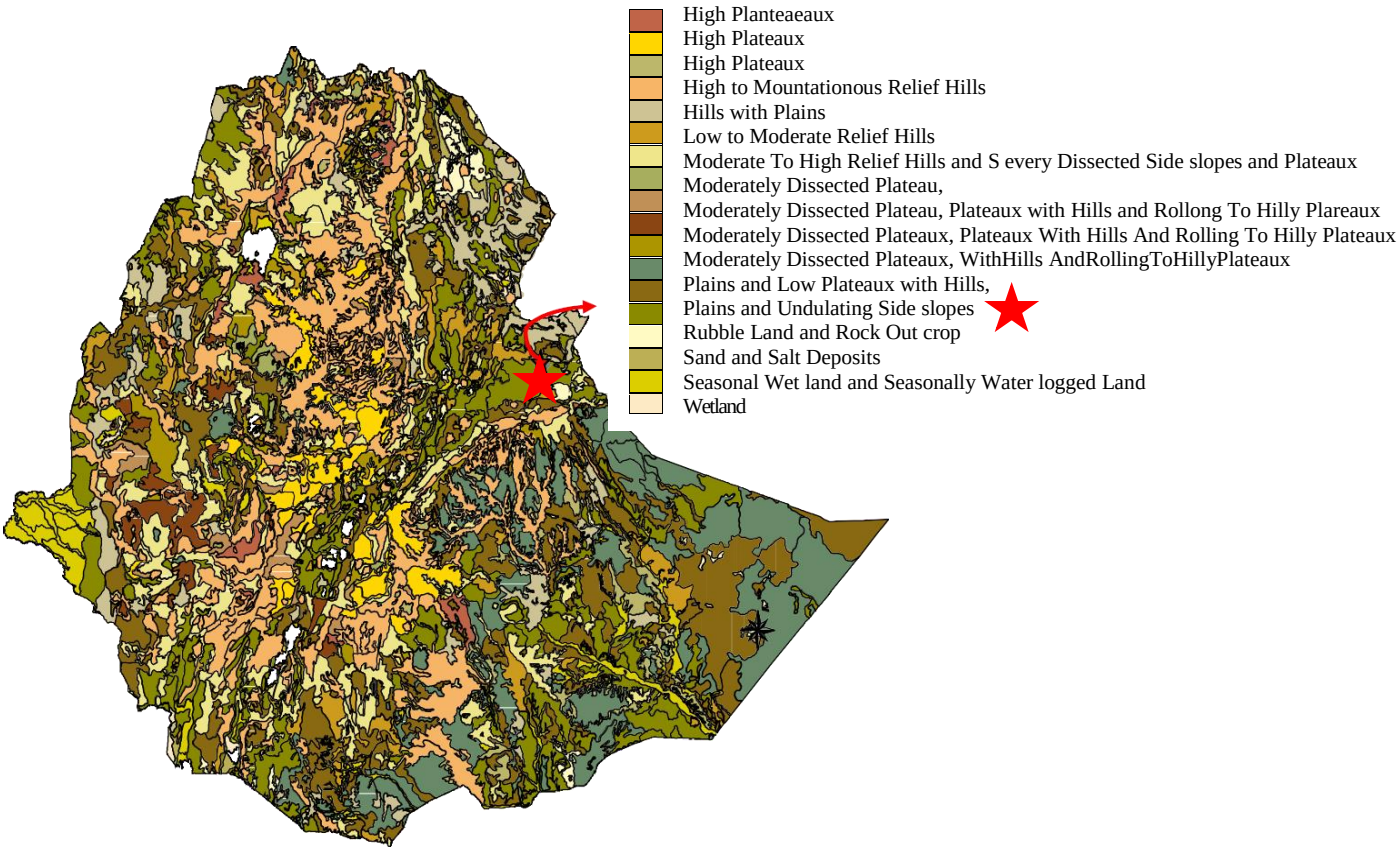

Figure 3.10: Geomorphologic features Ethiopia

The site selection and modification of Concentrated Parabolic Trough Solar system require precise knowledge regarding the availability of global solar radiation and its components at the location of interest. Since the solar radiation reaching the earth's surface depends upon climatic conditions of the place, a study of solar radiation under local climatic conditions is essential. In developing countries such as Ethiopia, due to absence or malfunction of measuring instruments, reliable solar radiation data is not available. In the absence and scarcity of trustworthy solar radiation data, the use of an empirical model to predict and estimate solar radiation seems inevitable. These models use climatological parameters of the location under study. Among all such parameters, sunshine hours are the most widely and commonly used.

3.3. Prediction of Monthly Average Daily Global Radiation on a Horizontal Surface

The first empirical correlation using the idea of employing sunshine hours for the estimation of global solar radiation was proposed by Angstrom. The Angstrom correlation was modified by Prescott and Page. The simplest model used to estimate monthly average daily solar radiation on a horizontal surface is the well-known Angstrom equation [35].

$$\frac{\overline{H}}{\overline{H_O}} = a + b\frac{\overline{n_s}}{N_s} \tag{3.10}$$

$\overline{H}$ - Monthly average daily radiation on the horizontal surface.

$\overline{H_O}$ - Monthly average radiation outside of the atmosphere (ETR on the horizontal surface) for the same location.

a, b - empirical constants, (Values are obtained by regression).

$\overline{n_s}$ - Monthly average daily hours of bright sunshine.

N_S -Monthly average of the maximum possible daily hours of bright sunshine

The regression parameters a and b can be determined from

$$a = -0.11 + 0.235\cos\phi + 0.323\left(\frac{\overline{n_s}}{N_S}\right)$$

$$b = 1.449 - 0.533\cos\phi + 0.694\left(\frac{\overline{n_s}}{N_S}\right)$$

$\overline{H_O} = Can\ be\ obtained\ by\ the\ Klein\ relationship:$

$$\overline{H_o} = \left[\frac{24*3600}{\pi} I_{SC}\right]\left[1.0 + 0.033\cos\left(\frac{360n}{365}\right)\right]\left[\cos\phi\cos\delta\sin\varpi_s + \frac{\pi}{180}\varpi_s\sin\delta\sin\phi\right] \tag{3.11}$$

$\varpi_s = sunrise\ hour\ angle$

$\overline{H_O}$ = *In Wh / m²day*

I_{SC} = 1367W/m², (solar constant)

The length of sunshine hours ($\overline{N_S}$) is computed from Cooper's formula:

$$\overline{N_S} = \frac{2}{15}\varpi_S \tag{3.12}$$

$$\varpi_S = \cos^{-1}(-\tan\phi\tan\delta) \tag{3.13}$$

$$\delta(in\ degrees) = 23.45\sin\left[\frac{360}{365}(284+n)\right]$$

Where: *N* is recommended average days for the month.

3.3.1. Prediction of Monthly Average Daily Diffuse Radiation and Global on a Horizontal Surface Adigala

The monthly average daily diffuse radiation on a horizontal surface can be determined from the monthly average daily global radiation on a horizontal surface and the number of bright sunshine hours [34].

$$\frac{\overline{H_d}}{\overline{H}} = 0.931 + 0.814\frac{\overline{n_s}}{\overline{N_s}} \tag{3.14}$$

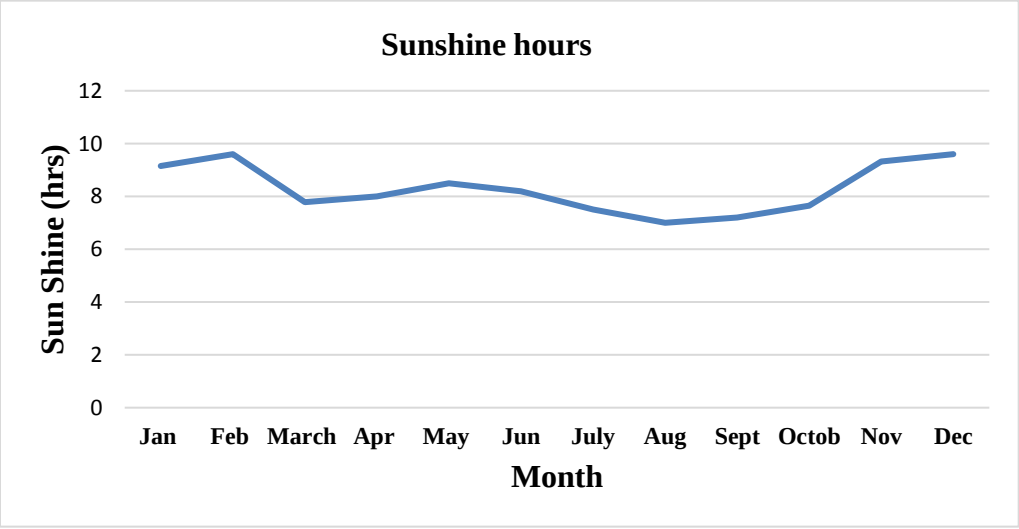

Figure 3.11. Monthly Average Daily Sunshine Duration in Adigala **[**Appendix A1]

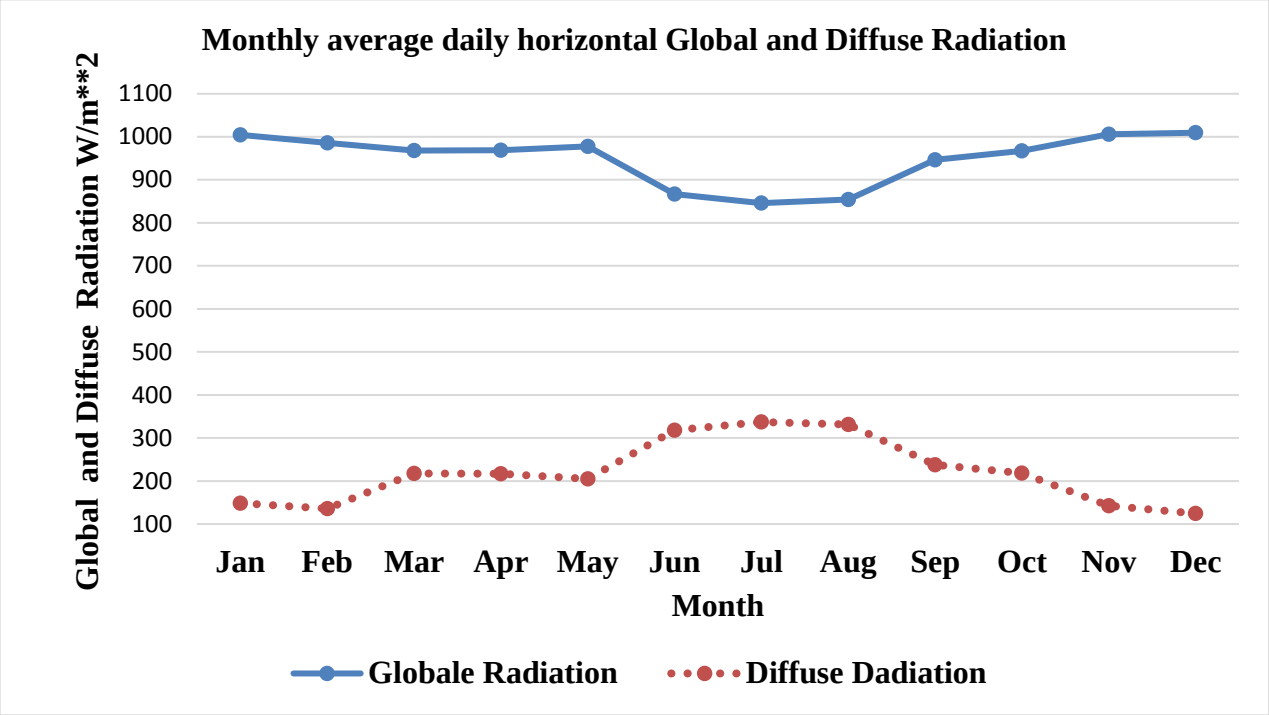

Figure 3.12 Monthly Averages of Daily Mean Global and diffuse Radiation on the Horizontal Surface for Adigala, Data available at **[**Appendix A1]

3.3.2. Prediction of Monthly Average Hourly Global Radiation on a Horizontal Surface

The monthly average hourly global radiation on a horizontal surface can be calculated from the knowledge of the monthly average daily global radiation on a horizontal surface [34]

$$\frac{\bar{I}}{\bar{H}} = \frac{\pi}{24}(a + b\cos\varpi)\frac{\cos\varpi - \cos\varpi_s}{\sin\varpi_s - \frac{\pi}{180}\varpi_s\cos\varpi_s} \tag{3.15}$$

Where: $a = 0.409 + 0.501\sin(\varpi_s - 60)$

$$b = 0.6609 - 0.4767\sin(\varpi_s - 60)$$

3.3.3. Prediction of Monthly Average Hourly Diffuse Radiation on a Horizontal Surface

The monthly average hourly diffuse radiation on a horizontal surface can be calculated from the

knowledge of the monthly average daily diffuse radiation on a horizontal surface [34].

$$\frac{\overline{I_d}}{\overline{H_d}} = \frac{\pi}{24}\frac{\cos\varpi - \cos\varpi_s}{\sin\varpi_s - \frac{\pi}{180}\varpi_s\cos\varpi_s} \tag{3.16}$$

3.3.4. Prediction of Monthly Average daily Maximum, Minimum and Average Temperature on Horizontal Surface in Adigala.

The monthly average daily Maximum, Minimum and Average Temperature on Horizontal Surface can be calculated by the knowledge of the monthly average hourly variation of temperature on the year 2012 to 2017 from collected data.

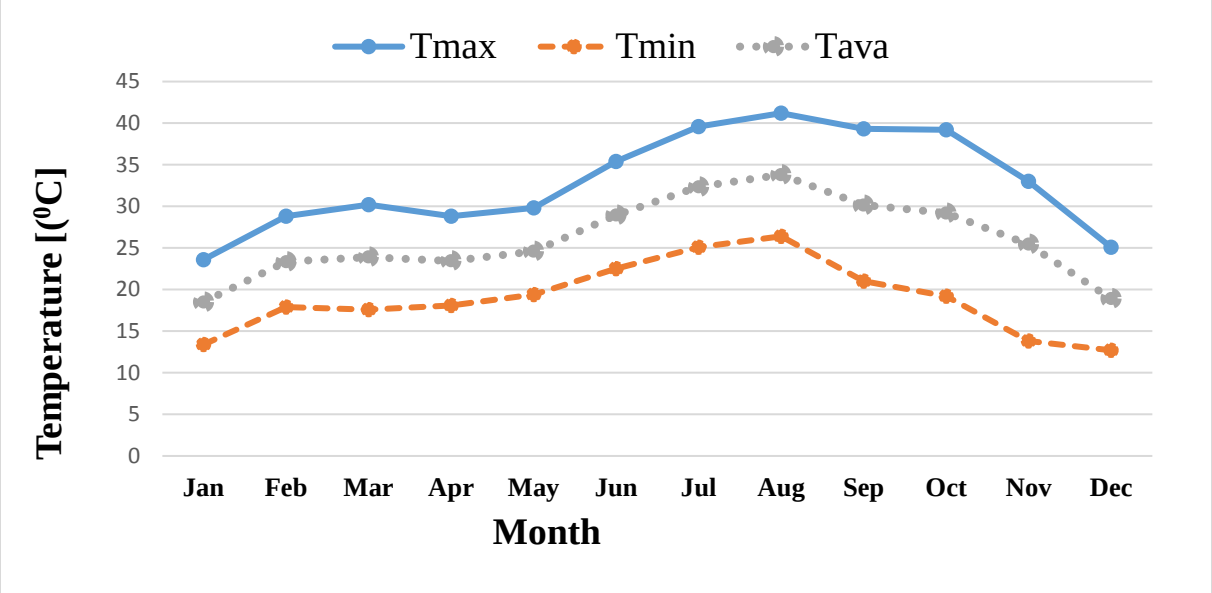

Figure 3.13 Monthly Ambient Temperature Pattern in Adigala, from 2012 to 2017 Years [Appendix A1]

3.4. The Selected Site Technical Potential

A site is considered to have a technical potential for a CSP plant when the yearly average direct normal irradiation is 2642.6 kWh/m^2/year and above. Taking into consideration economic factors, CSP starts to become feasible with a higher irradiation. In addition, the selected site yearly average hourly direct normal irradiation is 872 W/m^2 this qualifies a suitable value for operating a CSP plant.

CHAPTER FOUR

4. Parabolic Trough Solar Thermal S-CO_2 Brayton Cycle Combined with ORC Power Plant Mathematical Modeling

In order to assess solar thermal CO_2 Brayton Cycle Combined with ORC Power Plant configurations, thermodynamic models in the simulation environment EES software has been established. The plant model consists of two major components, which are described here, in this chapter:

- ❖ Solar field (SF)
- ❖ Power block (PB)

The simulation study is performed for both the chosen cycle configurations of divided into three phases:

1. Choice of the thermodynamic parameters of the cycle at the design point.
2. Off-design analysis, which corresponds to the operating conditions, which vary from the nominal point at a behavior of the external disturbances like DNI, Pressures Ratio inlet temperature of the gas turbine
3. Evaluation of energy and exergy simulation data and optimize.

4.1. Preliminary Sizing

In the simulation of both cycles, the solar field is assumed to equal. The solar field is characterized by its aperture area, type and number of collectors. In order to determine the total aperture area (A_{eff}) and the number of collectors, a preliminary sizing for an effective direct normal irradiation DNI_{eff} of 850 W/m^2 is made. The following assumptions are considered:

1. The chosen type of collectors is the Luz-3 with the Schott receiver PTR70.
2. The proposed power plant the solar field compared to the power block must be oversized. The solar multiple (SM) represents the solar field size related to the power block, in terms of nominal thermal power. In this case, a SM equal to 2 is fixed [37].
3. The gross electrical power of both plants $W_{PB,\,nom}$ is set to be 1MW_{el}, while the nominal cycle efficiency $\eta_{th,nom}$ is assumed approximately range from 35% up to 42%[37].

4. The nominal solar field efficiency $\eta_{th,SF}$ is assumed to be equal to a range from 65% up to 75%[37]. In fact, this value is overestimated in order to balance the assumed $\eta_{th,nom}$.

Table 4.1. Summarizes the data used for the preliminary sizing.

Parameters	**Specification**
Solar field technology	Luz LS-3+ Schott PTR 70
$W_{PB,nom}$	1MWel,
$\eta_{th,nom}$	35% [38]
SM	2 [42]
DNI_{eff}	850W/m^2
$\eta_{th,SF}$	75% [37]

The sizing process is now described as follows. The total aperture area is determined using the design-point power cycle rating, the solar field efficiency $\eta_{th,SF}$ and the desired solar multiple SM. Since SM is defined as the ratio between the thermal power produced by the solar field at the design point $\dot{Q}_{SF,nom}$ and the thermal power required by the power block at the nominal condition $\dot{Q}_{PB,nom}$.

$$SM = \frac{\dot{Q}_{SF,nom}}{\dot{Q}_{PB,nom}} \tag{4.1}$$

The solar field thermal output at design $\dot{Q}_{SF,nom}$ is calculated according to the following equation

$$\dot{Q}_{SF,nom} = \frac{W_{PB,nom} x SM}{\eta_{th,nom}} \tag{4.2}$$

Hence, the total incident thermal energy $\dot{Q}_{inc,nom}$ can be determined by dividing the total thermal energy output by the solar field efficiency, as shown in Equation (4.3)

$$Q_{in,nom} = \frac{\dot{Q}_{SF,nom}}{\eta_{th,SF}} \tag{4.3}$$

Therefore, the effective aperture area is given by

$$A_{eff} = \frac{\dot{Q}_{inc,nom}}{DNI_{eff}} \tag{4.4}$$

Therefore, the effective number of collectors is calculated by

$$n_{coll} = \frac{A_{eff}}{A_{coll}} \tag{4.5}$$

Since the aperture, the area of the single collector in Luz-3 is 545 m^2 [41]. By rounding off this value and estimating to an even number to obtain the symmetry of the collectors in each loop, the chosen number of collectors is equal to 16. In all, the Total reflective aperture area is 8,963.59 m^2.

The total Land area needed to install the plant is given by

Solar field area = SM x Total reflective aperture area in the field (4.6)

The non-solar field land area multiplier is 1.4 [42]. (4.7)

Total land area =1.4 x Solar field area (4.8)

4.2. Heat collecting element (HCE) performance model

The HCE performance model is based on an energy balance on the collector and the HCE. The energy balance includes the direct normal solar irradiation incident on the collector, optical losses from both the collector and HCE, thermal losses from the HCE, and the heat gain into the HTF. Temperature gradient on the receiver can be accounted for by a flow factor F_R to allow the use of inlet fluid temperature in energy balance equation. Thus it is required to drive appropriate expression for the collector efficiency factor F', the loss coefficient U_L, and the heat removal factor F_R to numerically evaluate the outlet temperature. For short receivers (< 100 m) a one-dimensional energy balance gives reasonable results; for longer receivers, a two-dimensional energy balance becomes necessary [25]. All the equations and relationships used in one-dimensional HCE performance models are described in the following sections.

4.3. One-Dimensional Energy Balance Model

The HCE performance model uses an energy balance between the HTF and the atmosphere and includes all equations and correlations necessary to predict the terms in the energy balance, which

depend on the collector type, HCE condition, optical properties, and ambient conditions. Figure 4.2 shows the one-dimensional steady-state energy balance for a cross-section of an HCE, and Figure 4.3 shows the thermal resistance model and subscript definitions. For clarity, the incoming solar energy and optical losses have been omitted from the resistance model. The optical losses are due to imperfections in the collector mirrors, tracking errors, shading, and mirror and HCE cleanliness. The effective incoming solar energy (solar energy minus optical losses) is absorbed by the selective coating ($\dot{q}'_{3solAsbs}$) some energy that is absorbed into the selective coating is conducted through the absorber ($\dot{q}'_{23Cond}$) and transferred to the HTF by convection ($\dot{q}'_{12Conv}$); remaining energy is transmitted back to the environment by convection ($\dot{q}'_{35Conv}$) and radiation ($\dot{q}'_{34rad}$). The model assumes all temperatures, heat fluxes, and thermodynamic properties are uniform around the circumference of the HCE. In addition, all flux directions are shown in Figure 4.2(a), 4.2b are positive, and all the terms in the above paragraph are defined in Table 4.2. Dotted variables indicate rates and the prime indicates per unit length of the receiver. A double prime will indicate per unit normal aperture area.

Table 4.2. Heat flux definitions

Heat Flux (W/m)	**Heat Transfer Type**	**From**	**To**
$\dot{q}'_{12Conv}$	Convection	Absorber inner surface	Heat transfer fluid
$\dot{q}'_{23Cond}$	Conduction	Absorber outer surface	Absorber inner surface
$\dot{q}'_{3solAsbs}$	Radiation	Sun	Absorber outer surface
$\dot{q}'_{3solAsbs}$	Radiation	Sun	Glass envelope outer surface
$\dot{q}'_{34Conv}$	Convection	Absorber outer surface	Glass envelope inner surface
$\dot{q}'_{34rad}$	Radiation	Absorber outer surface	Glass envelope inner surface
$\dot{q}'_{45rad}$	Conduction	Glass envelope inner surface	Glass envelope outer surface
$\dot{q}'_{56rad}$	Convection	Glass envelope outer surface	Surrounding air
$\dot{q}'_{57rad}$	Radiation	Glass envelope outer surface	Sky

With the help of Figure 4.2b, the energy balance equations are determined by conserving energy at each surface of the HCE cross-section.

$$\dot{q}'_{12Conv} = \dot{q}'_{23Cond} \tag{4.9}$$

$$\dot{q}'_{3solAsbs} = \dot{q}'_{23Cond} + \dot{q}'_{34Conv} + \dot{q}'_{34rad} \tag{4.10}$$

$$\dot{q}'_{HeatLoss} = \dot{q}'_{35Conv} + \dot{q}'_{34rad} \tag{4.11}$$

$$\dot{q}'_{3solAsbs} = I_b \cos\theta Ap\eta_{opt} IAM \tag{4.12}$$

$$\dot{q}'_{SolarAbsbyGlass} = I_b x \cos\theta xApx \frac{\eta_{opt}}{\tau_{gl} x\alpha_{glass}} xIAMx\alpha_{glass} \tag{4.13}$$

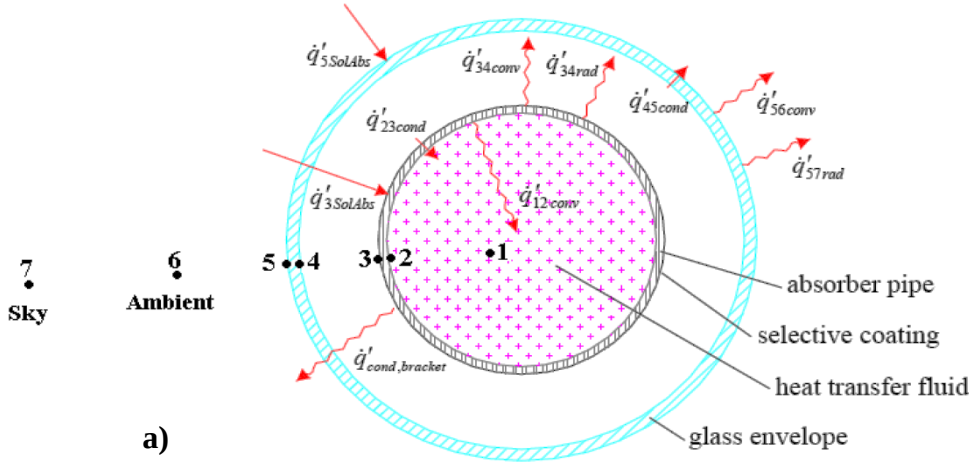

a)

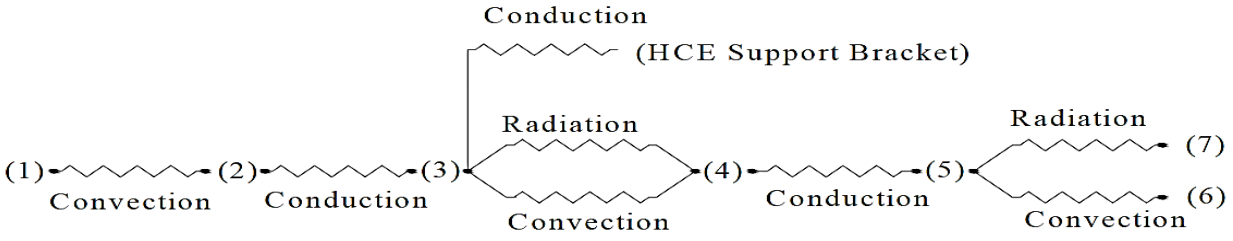

b)

Figure 4.2 **a)** One-dimensional steady-state energy balance **b)** Thermal resistance model for a cross-section of an HCE

1. Heat Transfer Fluid
2. Absorber Inner Surface
3. Absorber Outer Surface
4. Glass Involve Inner Surface
5. Glass Involve Outer Surface
6. Surrounding Air
7. Sky

4.3.1. Convection heat transfer between the HTF and the absorber

From Newton's law of cooling, the convection heat transfer from the inside surface of the absorber pipe to the HTF is

$$\dot{q}'_{12Conv} = h_1 D_1 \pi (T_2 - T_1) \text{ (W/m)} \quad (4.14)$$

Where;

h_1 is the convective heat transfer coefficient. It depends on the thermos physical properties of the HTF, the diameter of the tube, the flow rate, and the temperatures of the HTF and inner absorber surface. Burkholder, F [39] fully describes its calculation. For typical conditions in the loop of an operating plant (Therminol VP1, 6.6 cm inner diameter absorber, average HTF temperature of 340°C), the convective coefficient can be calculated from the mass flow rate from 4 kg/s to 12 kg/s as

$$h_1 = 522 + 478 x\dot{m}$$

Where;

h_1 =convection heat transfer coefficient inside the tube

D_1 = inside diameter of the absorber pipe (m)

T_1 = mean (bulk) temperature of the HTF (^oC)

T_2 = inside surface temperature of the absorber pipe (^oC)

4.3.2. Conduction heat transfer through the absorber wall

Fourier's law of conduction through a hollow cylinder describes the conduction heat transfer through the absorber wall [40].

$$\dot{q}'_{23Cond} = \frac{2\pi k_{23}(T_2 - T_3)}{\ln\left(\frac{D_2}{D_1}\right)} \text{ (W/m)} \quad (4.15)$$

$$k_{abs} = 14 \cdot 8 + 0.153 x T_{abs}$$

Where:

k_{23} = absorber thermal conductance at the average absorber temperature $(T_2+T_3)/2$(W/mK)

T_2 = absorber inside surface temperature (K)

T_3 = absorber outside surface temperature (K)

D_1 = absorber inside diameter (m)

D_2 = absorber outside diameter (m)

In this equation, the conduction heat transfer coefficient is constant and is evaluated at the average temperature between the inner and outer surfaces

4.3.3. Heat Transfer from the Absorber Wall to the Atmosphere

The heat will transfer from the glass envelope to the atmosphere by convection and radiation. The convection will be either forced or natural, depending on whether there is wind. Radiation heat loss occurs due to the temperature difference between the glass envelope and sky.

- **Convection heat transfer**

The convection heat transfer from the glass envelope to the atmosphere ($\dot{q}'_{35Conv}$) is the largest source of heat loss, especially if there is a wind. From Newton's law of cooling

$$\dot{q}'_{35Conv} = h_{35} D_2 \pi (T_3 - T_5) \quad (4.16)$$

$$h_{amb} = 4.9 + 4.9 x U - 0.18 U^2$$

Where:

h_{35} is the convective heat transfer coefficient to ambient. It is strongly a function of wind speed. Burkholder, F [39] presents the detailed calculation, but for the PTR70 geometry and expected ambient temperatures the convection coefficient can be estimated from

T_3 = glass envelope outer surface temperature (^oC)

T_5 = ambient temperature (^oC)

h_{35} = convection heat transfer coefficient

U= is the wind speed in m/s.

k_3 = thermal conductance of air at $(T_3-T_5)/2$ (W/m K)

D_2 = glass envelope outer diameter (m)

4.3.4. Radiation Heat Transfer

The useful incoming solar irradiation is included in the solar absorption terms. Therefore, the radiation transfer between the outer surface of the tube and sky is caused by the temperature difference between the outer surface of the tube and the sky. To approximate this, the outer surface of the tube is assumed to be a small convex gray object in a large blackbody cavity (sky).

The net radiation transfer between the glass envelope and sky becomes[40]

$$\dot{q}'_{34rad} = \sigma\pi D_2 \varepsilon_3 (T_3^4 - T_4^4) \tag{4.17}$$

Where:

σ = Stefan-Boltzmann constant (5.670E-8) ($W/m^2\text{-}K^4$)

D_2 = the outer surface tube diameter (m)

ε_3 = emissivity of the outer surface tube

T_3 = the outer surface tube temperature (K)

T_4 = effective sky temperature (K)

Thus, after determining the loss coefficient U_L and determining the heat transfer resistance from the outer surface of the receiving tube to the fluid in the tube, the overall heat transfer coefficient (i.e. the sum of heat gain and heat loss of the heat collecting tube) which is given by

$$\frac{1}{U_O} = \left[\frac{1}{U_L} + \frac{D_2}{h_1 D_1} + \frac{D_2 \ln\left(\frac{D_2}{D_1}\right)}{2k_{23}} \right] \tag{4.18}$$

Where:

U_L - The sum of convection and radiation heat loss from the heat collecting tube

4.3.5. Solar Irradiation Absorption

Using basic energy balance equation, the useful energy gained per unit collector length expressed in terms of the local receiver tube temperature and the absorbed solar radiation per unit of the aperture area, which is the difference between the absorbed solar radiation and the thermal loss and is given by:

$$\dot{q}'_{used} = \frac{A_a \dot{q}_{ab} - A_t U_L (T_t - T_a)}{L} \tag{4.19}$$

$$\dot{q}_{ab} = \alpha_o I_t \tag{4.20}$$

$$A_t = \pi D_2 L$$

Where:

$\dot{q}'_{used}$ - Useful energy gained by HTF

UL - The sum of convection and radiation heat loss from the heat collecting tube

Aa - Aperture area

L - Parabolic trough length

T_t - Receiver tube temperature

Ta- Ambient temperature

I_t - Solar intensity

α_o - absorptivity of the tube

D_2 - Receiver tube outer diameter

In terms of the energy transferred into the working fluid at a local fluid temperature

$$\dot{q}'_{used} = \left[\frac{\left(\frac{A_t}{L}\right)(T_t - T_f)}{\frac{D_2}{h_1 D_1} + \frac{D_2}{2k}\ln\left(\frac{D_2}{D_1}\right)} \right] \tag{4.21}$$

F' is the collector efficiency factor which is given by

$$F' = \left[\frac{\frac{1}{U_L}}{\frac{1}{U_L} + \frac{D_2}{h_1 D_1} + \frac{D_2}{2k}\ln\left(\frac{D_2}{D_1}\right)} \right] \tag{4.22}$$

This can be rewritten in the form of:

$$F' = \frac{U_O}{U_L} \tag{4.23}$$

The actual useful energy collected by the fluid is given by

$$\dot{q}'_{used} = F_R \left[\frac{A_a \dot{q}_{ab} - A_t U_L (T_t - T_a)}{L} \right] \tag{4.24}$$

Where FR is the collector heat removal factor, defined as the ratio of the actual useful energy gain to the useful energy gain if the entire collector was at the fluid inlet temperature T_{fi} and it is expressed as:

$$F_R = \frac{\dot{m} C_{pf} (T_{fo} - T_{fi})}{\frac{A_a}{L}\left[\dot{q}'_{ab} - \frac{A_t}{A_a} U_L (T_{fi} - T_{fi}) \right]} \tag{4.25}$$

After rearranging the above equation including collector efficiency factor it becomes

$$F_R = \frac{\dot{m} C_{pf}}{A_t U_L}\left[1 - \exp\left(\frac{A_t U_L F'}{\dot{m}_f C_{pf}} \right) \right] \tag{4.26}$$

Where;

Cpf - Specific heat of the working fluid

$\dot{m}_f$ - Mass flow rate of the working fluid

Finally, rearranging the above equations in the form of T_{fo}, then the exit temperature of the water

in the heat collecting tube can be calculated by the following formula,

$$T_{fo} = T_{fi} + \frac{\dot{q}'_{used}}{\dot{m}_f C_{pf}} \tag{4.27}$$

Finally, the thermal efficiency of the collector and HCE is calculated with

$$\eta_{th} = \frac{\dot{q}'_{12Conv}}{\dot{q}'_{i,oinc}} \tag{4.28}$$

Where

η_{th} is the thermal efficiency of the collector and HCE

qi,0inc is the insolation on the trough aperture at zero incidence angle, (W/m)

$$\dot{q}'_{i,oinc} = I_b x A_{eff} \tag{4.29}$$

Note that the denominator of the efficiency equation does not contain cos θ, which would correct for the decreased insolation on the aperture at non-zero incidence.

4.4. Detailed Parabolic Trough Collector Solar Field and Input Data Specification

The PTCs solar field includes the area that harvests sun radiation energy (heat) through a set of arrays of parabolic troughs. Each PTC is comprised of parabolic mirrors, receivers, and a single-axis-tracking system. The parabolic mirrors reflect and concentrate the solar beam radiation onto the receivers, which are positioned along the focal line of the parabolic troughs. The heat generated by the concentrated solar beam is then absorbed by the HTF, which is continuously circulated through the receivers. The solar field consists of three loops connected in series; where each loop is composed of a number of solar collector assemblies (SCA).

The SCA is about 100 m in length and includes reflectors, receivers, supporting structures and an independent tracking system. The PTC type selected for the current study is Luz system LS-3

collectors. These collectors are manufactured of galvanized steel and have been used in SEGS power plants where they have demonstrated a high reliability [41]. The dimensions and specifications of LS-3 are presented in table 4.3.

Table 4.3 Solar collector technology and specifications, data from[42]

Component	**Specification**
Trough type	Luz LS-3
Aperture Width	5.75m
SCA length	100m
Focal length	2.1m
SCA Aperture reflective area	$545m^2$
Concentration ratio	82
Tracking error and twist	0.99
Geometric accuracy	0.935
Mirror cleanliness (average)	0.98
Heat Collection Elements [HCEs]	4.08m
Number of HCEs in the loop	134m

The receivers, or the so-called heat collection elements (HCEs), are configured to maximize the concentrated radiation absorption while minimizing heat losses to the surrounding environment. Thus, a receiver consists of a metal tube coated with a special material to increase absorptivity and reduce emissivity. The metal tubes are enclosed in a glass envelope to reduce the convective heat losses to the environment.

The absorber tube is made mainly from stainless steel coated with a special material, with bellows at inlet and outlet. These bellows are glass-to-metal seals designed to minimize heat conduction loss to the supporting structure while maintaining the vacuum enclosed by the glass cover. The receiver, manufactured by SCHOTT solar, (SCHOTT PTR® 70) is selected for the present study. The dimensions and specification of the SCHOTT PTR® 70 receivers are given in Table 4.4

Table 4.4 Technical specifications of the SCHOTT PTR® 70 receivers, data from[39]

Components	**Specification**
Dimension	Length: 4.060 m at 20 °C
Absorber	Outer diameter: 0.07 m
Glass envelope	Material: steel DIN 1. 304L or similar Absorptivity, $\alpha \geq 0.955$ Thermal emittance, $\varepsilon_r \leqslant 0.095$ at 400 °C Material: borosilicate glass Outer diameter: 0.125 m Solar transmittance, $\tau \geq 0.965$
Vacuum	Gas pressure $\leq 10^{-3}$ mbar
Operating pressure	≤40 bar (absolute)

Table 4.5 Design point parameters for PTCs solar field based on Adigala, Somalia Ethiopia, data from[43]

Parameter	**Value**
Longitude (°)	42.21^{o}N
Latitude (°)	10.41^{o}E
Altitude	758 m
Time zone	GMT +3
Direct normal radiation, Ib	850 W/m2
Optical efficiency	0.75
Incidence angle, θ (deg)	0
Loop inlet temp (°C)	280
Wind speed (m/s)	2
Ambient temperature (°C)	30
Mass flow rate (kg/s)	8

Table 4.6 Relevant properties of the heat transfer fluid (Therminol-PV1), data from[44]and [Appendex B]

Parameter	Value
Composition	Biphenyl and diphenyl oxide
T_{Max} [°C]	400°C
Crystallization point [°C]	12°C
Fire point[°C]	127°C
Auto-ignition point	621°C
Kinematic viscosity at 40°C to 100 °C	2.48 mm^2/s- 0.99 mm^2/s
Density at 25 °C [Kg/m^3]	1060 Kg/m^3
Optimum use range (Liquid phase) °C	12-400°C

4.5. Basic program structure for computing parabolic solar trough thermal power output

The simulation is intended to accurately reproduce of the thermodynamics process occurring in parabolic trough concentrated solar power plant located in **Adigala, Somalia Ethiopia**. At the moment, not even one CSP plant, exclusively powered by solar energy is installed in Ethiopia. Consequently, predictions for the future have to be undertaken. To make these predictions reasonable, information about potential and available areas is taken and processed in a realistic way for a further performance calculation. The following in fig.4.5 shows pseudo flowchart gives a common overview of how this is put to execution.

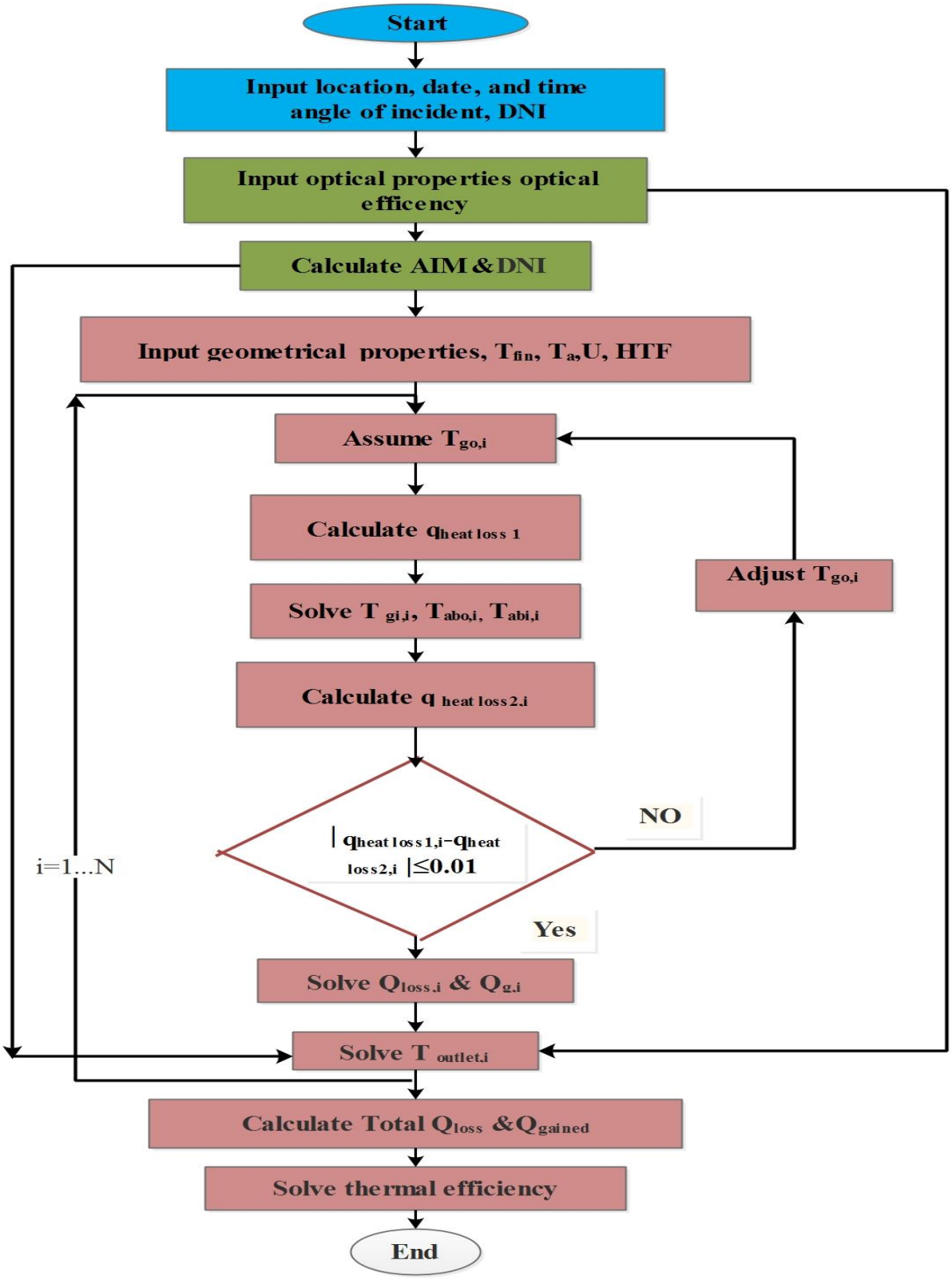

Figure 4.3. The pseudo Flowchart of the solar parabolic trough model

CHAPTER FIVE

5. Thermodynamic Analysis of S-CO_2 and ORC Power Cycles

5.1 Thermodynamic Modelling of S-CO_2 and ORC system

The thermodynamic system analysis consists of three statements concerning three system properties: mass, energy and entropy. These encapsulated the mass conservation law, the energy conservation law (first law of thermodynamics), and the exergy (second law of thermodynamics).

Exergy is not conserved as energy, which is destructed in the system due to internal and external irreversibility. For a real process, the exergy input always exceeds the exergy outputs; this unbalance is due to irreversibility, a process known as exergy destruction. Thus, thermodynamic inefficiencies and the processes that cause them are identified. Illustration of the above three indifferent mathematical forms can be shown as follows:

Mass Balance

The mass rate balance for control volumes with several inlets and exits which is commonly employed in engineering is[45].

$$\frac{dm_{cv}}{dt} = \sum_i \dot{m}_i - \sum_e \dot{m}_e \qquad (5.1)$$

Where the subscripts

cv = the control volume

I = inlet

e = outlet

$\dot{m}$ = mass flow rate of the fluid stream

For steady state, $\frac{dm_{cv}}{dt} = 0$ so equation (5.1) becomes [5],

$$\sum_i \dot{m}_i - \sum_e \dot{m}_e = 0$$

$$\Rightarrow \sum_i \dot{m}_i = \sum_e \dot{m}_e \tag{5.2}$$

Energy Balance

An accounting balance for the energy of the control volume is [5].

$$\frac{dE_{cv}}{dt} = \dot{Q}_{cv} - \dot{W}_{cv} + \sum_i \dot{m}_i (h_i + \frac{V_i^2}{2} + gz_i) - \sum_e \dot{m}_e (h_e + \frac{V_e^2}{2} + gz_e) \tag{5.3}$$

Where, $\frac{dE_{cv}}{dt}$ the time rate of change of energy of control volume

$\dot{Q}_{cv}$ The time rate of heat input in the control volume

$\dot{W}_{cv}$ The time rate of work output in the control volume

h enthalpy

V bulk velocity of the working fluid

z altitude of the stream above the sea level

g specific gravitational force

Exergy balance

The control volume exergy rate balance considering several inlets and exits in control volume is [45].

$$\frac{dEx_{cv}}{dt} = \sum_i (1 - \frac{T_0}{T_j}) \dot{Q}_j - (\dot{W}_{cv} - p_0 \frac{dV_{cv}}{dt}) + \sum_i \dot{m}_i e_{fi} - \sum_e \dot{m}_e e_{fe} - \dot{E}_d \tag{5.4}$$

Where

$\dot{Q}_j$ - Time rate of heat transfer at the location on the boundary where the instantaneous temperature is T_j

$\dot{W}_{cv}$ - Time rate of energy transfer by work other than flow work

$\dot{E}_d$ - Net exergy destruction rate within CV

Flow exergy (e_f) of a fluid in a steady flow is defined as the maximum work output that can be obtained as the fluid is changed reversibly from the given state to a dead state in a process where any heat transfer occurs solely with the environment The specific flow exergy is given by [45],

$$e_f = (h - h_0) - T_0(s - s_o) + \frac{V^2}{2} + gz \tag{5.5}$$

Neglecting kinetic and potential energy [45],

$$e_f = (h - h_0) - T_0(s - s_o) \tag{5.6}$$

5.2 Mathematical Model

5.2.1. Energy and Exergy analysis of the cycle components

In this section, individual components' energy and exergy balance of the cycles are introduced under the assumed conditions of the present study.

5.2.1.1. Energy Analysis

To analyze the possible realistic performance, a detailed energy analysis of the topping S-CO2 gas turbine cycle and bottoming ORC has been carried out by ignoring the kinetic and potential energy balance. For steady state flow the energy balance for the thermal system can be written modifying the equation (5.3) as below [45]:

$$0 = \dot{Q}_{cv} - \dot{W}_{cv} + \sum_i \dot{m}_i (h_i + \frac{V_i^2}{2} + gz_i) - \sum_e \dot{m}_e (h_e + \frac{V_e^2}{2} + gz_e) \tag{5.7}$$

Neglecting kinetic and potential energy [45],

$$0 = \dot{Q}_{cv} - \dot{W}_{cv} + \sum_i \dot{m}_i h_i - \sum_e \dot{m}_e h_e \tag{5.8}$$

For one inlet and one exit system [45],

$$0 = \dot{Q}_{cv} - \dot{W}_{cv} + \dot{m}_i h_i - \dot{m}_e h_e \tag{5.9}$$

$$\Rightarrow 0 = \dot{Q}_{cv} - \dot{W}_{cv} + \dot{m}(h_i - h_e) \tag{5.10}$$

For single component analysis, equation (5.10) will be used in this study. The energy or first law efficiency (η_I) of a system and/or system component is defined as the ratio of energy output to the energy input to system/component [45], i.e.,

$$\eta_I = \frac{Desired\ Output\ Energy}{Input\ Energy\ Supplied} \tag{5.11}$$

5.2.1.2. Exergy Analysis

Exergy Analysis is a method that uses the conservation of mass and conservation of energy principles together with the second law of thermodynamics for the analysis, design and improvement of energy systems. An exergy method is a useful tool for furthering the goal of more efficient energy-resource use. Many engineers and scientists suggest that the thermodynamic performance of a process is best evaluated by performing an exergy analysis in addition to or in place of conventional energy analysis because of exergy analysis appears to provide more insights and to be more useful in furthering efficiency improvement efforts than energy analysis [46].

The exergy (second law) analysis has become one of the significant methods to evaluate the performance of any thermal system application because the exergy analysis deals with the quality of energy. Exergy can be defined as availability, the highest available work, which is an evaluation of the maximum useful work that can be obtained when a system is brought to a state of equilibrium with the environment in a reversible process. For a real process, the exergy input always exceeds exergy outputs; this unbalance is due to irreversibility, which is known as exergy destruction.

A general form of the exergy equation for an open system control volume already stated in equation (5.4). For steady state flow, the exergy balance for a thermal system is given in equation (5.12), where time rate variations are neglected [45].

$$0 = \sum_i (1 - \frac{T_0}{T_j})\dot{Q}_j - (\dot{W}_{cv} - p_0 \frac{dV_{cv}}{dt}) + \sum_i \dot{m}_i e_{fi} - \sum_e \dot{m}_e e_{fe} - \dot{E}_d \tag{5.12}$$

Rearranging equation (5.12) gives the exergy destruction of a steady state open system for a control volume [45].

$$\dot{E}_d = \sum_i (1 - \frac{T_0}{T_j})\dot{Q}_j - (\dot{W}_{cv} - p_0 \frac{dV_{cv}}{dt}) + \sum_i \dot{m}_i e_{fi} - \sum_e \dot{m}_e e_{fe} \tag{5.13}$$

If the system is adiabatic, then $Q_j = 0$ So, for a steady state adiabatic system equation (4.12) becomes [45],

$$0 = -\dot{W}_{cv} + \sum_i \dot{m}_i e_{fi} - \sum_e \dot{m}_e e_{fe} - \dot{E}_d \tag{5.14}$$

So, for 1-inlet, 1-exit system [45],

$$0 = -\dot{W}_{cv} + \dot{m}(e_{fi} + e_{fe}) - \dot{E}_d$$

$$\Rightarrow \dot{E}_d = \dot{m}(e_{fi} + e_{fe}) - \dot{W}_{cv} \tag{5.16}$$

Total exergy of a system consists of four different components:

$$Ex_{total} = Ex_{ph} + Ex_{kn} + Ex_{pt} + Ex_{ch} \tag{5.17}$$

Neglecting the potential and kinetic exergy, the equation can be written as

$$Ex_{total} = Ex_{ph} + Ex_{ch} \tag{5.18}$$

5.2.2. Thermodynamic Relationships in the S-CO2 and ORC

The schematic representation of the S-CO2 and ORC is demonstrated in Figure 5.1. In the system, a Parabolic Trough Collector, as a well- known and commercialized technology, is used to heat up the Therminol PV-1 as the heat transfer fluid (HTF) to temperatures of around 390.4°C and then its thermal energy is transferred to the S-CO_2 in the heat exchanger one (HE1) and heat exchanger two (HE2) as the figure indicates. The heated S-CO2 exiting from the HE (state 6) and (state 8) is expanded in the high-pressure turbine and low-pressure turbine respectively to generate power to run the generator and compressors. S-CO_2 exiting the turbine (state 9) passes through the recuperator before entering the evaporator1 (state 10) in the evaporate it drops its temperature before entering the low-pressure compressor (state 1). After being compressed in a low-pressure

compressor, S-CO_2 enter to the intercooler (state 2) between the two stages of compression. The S-CO_2 exiting the high-pressure compressor (state 4) passes the recuperator where it is heated and then returned to the HE1 (state 5). In the combined cycle, ORC1 is used to recover some part of the low-temperature waste heat.

The following assumptions are made in the present work:

1. The systems are working in steady state conditions.

2. Changes in kinetic and potential energies and exergies are neglected.

3. For the S-CO_2 flow through the Brayton cycle, appropriate values for pressure losses will be taken from previous literature

4. The pressure losses for the ORC system are neglected.

5. The gas turbine and the compressors in the Brayton cycle have polytropic efficiencies while for the turbine and pump in the ORC isentropic efficiencies will be from previous literature

a)

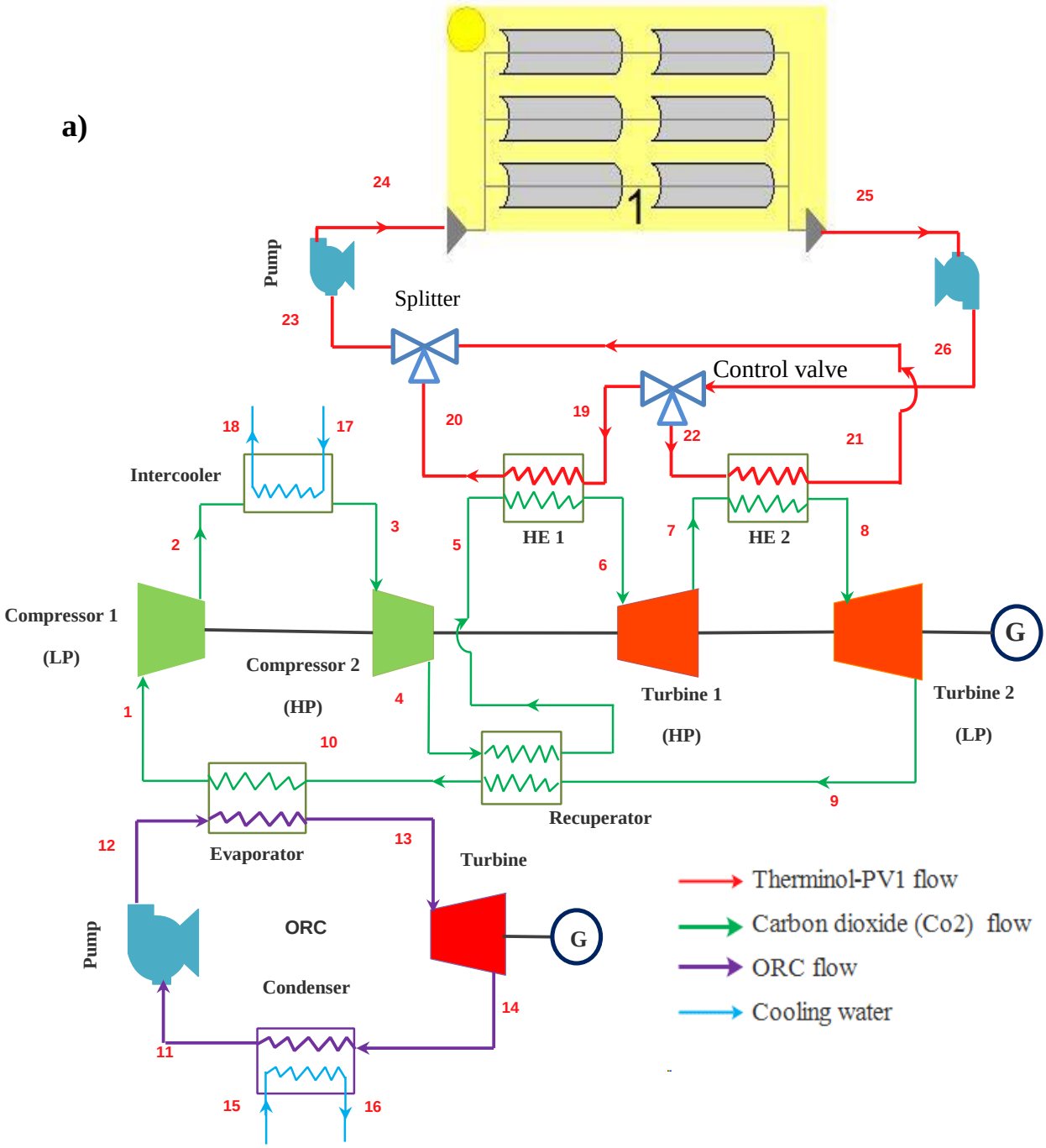
1
24
25
Pump
Splitter
23
26
Control valve
18
17
20
19
22
21
Intercooler
HE 1
HE 2
2
3
5
7
8
6
Compressor 1
(LP)
Compressor 2
(HP)
Turbine 1
(HP)
Turbine 2
(LP)
G
1
4
10
9
Recuperator
Evaporator
12
13
Turbine
Pump
ORC
G
Condenser
14
11
15
16
Therminol-PV1 flow
Carbon dioxide (Co2) flow
ORC flow
Cooling water

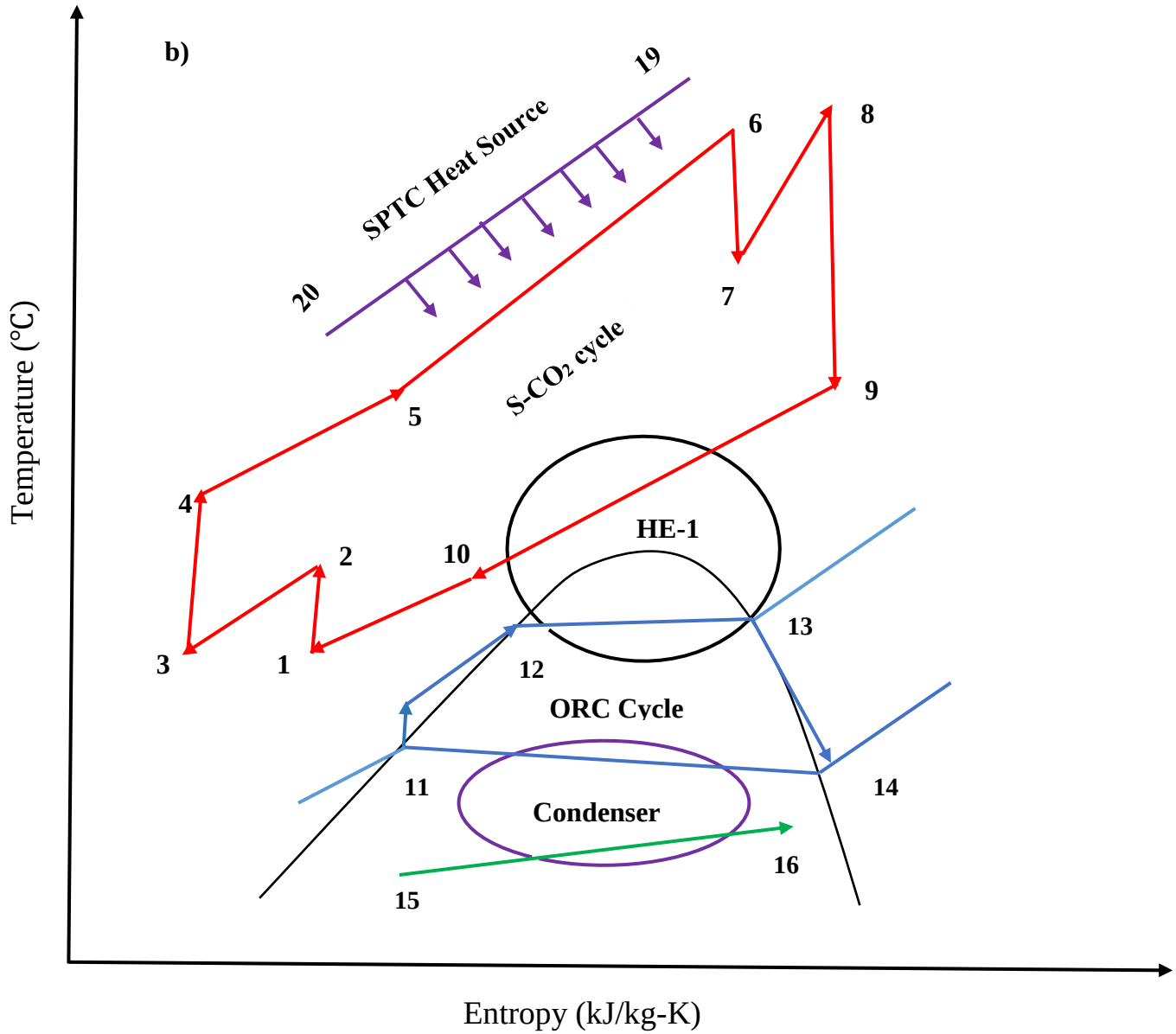

Figure 5.1 a) Schematic diagram of the combined cycle for parabolic Trough solar power plant.

b) Temperature entropy (T-S) diagram of combined cycle (SCO_2-ORC)

5.2.2.1. Energy Balance Equation for S-CO_2 and ORC in the Present Work

The thermal efficiencies of all the proposed cycles are obtained by simulation for different temperatures and pressures based on the First Law and the second law of Thermodynamics. The supercritical CO_2 Brayton cycle is of interest both to the solar energy and nuclear energy communities. One characteristic that is driving interest in the S-CO_2 the cycle is that the working fluid operates at or near its critical point (at 30.98 °C and 7 .38 MPa) where it has an extremely high density. The density of carbon dioxide as the function of temperature for a range of pressures at and above the critical point is shown in Appendix B.2. As can be seen in Appendix B.2, CO_2 density changes quickly near the critical point. High fluid density offers the potential to reduce both compressor power and size; thereby, leading to greater efficiency than an ideal-gas Brayton cycle and greater power density when compared to a superheated Rankine cycle.

Table 5.1 The following design given parameter is made for the thermodynamic analysis of the supercritical carbon dioxide power cycles and ORC [26][47]:

Parameter	**Value**
S-CO_2 Turbine inlet temperature	380°C
S-CO_2 cycle high pressure	25MPa
Isentropic efficiency turbine &Compressor	90% & 89%
Pinch point temperature	5°C
Recuperator effectiveness	95%
Heat exchanger effectiveness	92%
S-CO_2 cycle precompressor (LP) inlet temperature (T1)	32 °C
S-CO_2 cycle pressure precompressor (LP)	10MPa
Pressure ratio	2.5
Isentropic efficiency turbine &pump efficiency in ORC	85% & 90%
regenerator effectiveness	80%
ORC cycle pump inlet pressure(P11)	154.7kPa
ORC Pump inlet temperature (T11)	40

The energy equations are follows

For lower pressure compressor at (state 1)

$$W_{C1} = \dot{m}_{co2}(h_2 - h_1) \tag{5.18}$$

Where W_{c1} is the work done by the compressor (input work), h_1 is the specific enthalpy of inlet fluid to the compressor and h_2 present the enthalpy of the outlet from the compressor.

For S-CO_2 Intercooling at (state 2)

In this cycle, multistage compression with intercooling is employed. Recompression with intercooling is a common addition to gas cycles that decreases compression work. This arrangement also benefits the S-CO_2 cycle by decoupling the main compressor inlet pressure from the low-pressure turbine outlet pressure.

$$\dot{m}_{co2}(h_2 - h_3) = \dot{m}_{water}(h_{18} - h_{17}) \tag{5.19}$$

For High-Pressure compressor at (state3)

$$W_{C2} = \dot{m}_{co2}(h_4 - h_3) \tag{5.20}$$

Where W_{c2} is the work done by the compressor (input work), h_3 is the specific enthalpy of inlet fluid to the compressor and h_4 present the enthalpy of the outlet from the compressor.

Recuperator (state 4)

It makes use of the waste heat from the turbine exhaust to preheat the compressor discharge before it enters the heat-exchanger unit, lowering the requirement on heat-input for the same work and thus improving system efficiency. However, at higher-pressure ratios, the compressor discharge temperature might be higher than the turbine exhaust temperature to make this option ineffective.

$$\dot{m}_{co2}(h_5 - h_4) = \dot{m}_{co2}(h_9 - h_{10}) \tag{5.21}$$

$$\varepsilon_{recuperator} = \frac{T_5 - T_4}{T_9 - T_4} \tag{5.21}$$

For Gas heater Heat exchanger one (state 5)

$$\dot{Q}_{HE1} = \dot{m}_{VP-1}(h_{19} - h_{20}) = \dot{m}_{co2}(h_6 - h_5) \tag{5.22}$$

For high-pressure turbine (state 6)

$$W_{T1} = \dot{m}_{co2}(h_6 - h_7) \tag{5.23}$$

For Gas heater Heat exchanger, two (state 7)

$$\dot{Q}_{HE2} = \dot{m}_{VP-1}(h_{21} - h_{22}) = \dot{m}_{co2}(h_8 - h_7) \tag{5.24}$$

For lower pressure turbine (state 8)

$$W_{T2} = \dot{m}_{co2}(h_8 - h_9) \tag{5.25}$$

For evaporate at (sate 10)

Heat transfer rate in the evaporator, by neglecting any heat loss to the surroundings, can be expressed as [47].

$$\dot{Q}_{eva} = \dot{m}_{orc}(h_{13} - h_{12}) = \dot{m}_{co2}(h_{10} - h_1) \tag{5.26}$$

For pump (state 11)

If the pump is adiabatic, then. $\dot{Q} = 0$ So pump work can be written as [47].

$$W_{Pump} = \dot{m}_{ORC}(h_{12} - h_{11})$$

$$\eta_{Pump} = \frac{w_s}{w_a} = \frac{v_{11}(P_{12} - P_{11})}{h_{12} - T_{11}} \tag{5.27}$$

For ORC turbine at (state 13)

For an adiabatic turbine $\dot{Q} = 0$. So, turbine work [47],

$$W_{ORC} = \dot{m}_{ORC}(h_{13} - h_{14})$$

$$\dot{W}_{ORC} = \dot{m}_{ORC}(h_{13} - h_{14S}).\eta_{turb} \quad (5.28)$$

For ORC condenser (state 14)

Heat transfer rate in the condenser, by neglecting any heat loss to the surroundings, can be expressed as [47].

$$\dot{Q}_{cond} = \dot{m}_{orc}(h_{14} - h_{11}) = \dot{m}_{water}(h_{16} - h_{15}) \quad (5.29)$$

5.2.2.2. Exergy Balance Equation for S-CO_2 and ORC

Exergy balance equations are derived by modifying equation (5.14)

For any particular point, e.g. point i, the specific flow exergy is found by equation (5.6)

$$e_{fi} = (h_i - h_0) - T_0(s_i - s_o) \quad (5.30)$$

Compressor 1:

Exergy balance for lower pressure compressor at (state 1)

$$\dot{W}_{C1} = \dot{m}_{co2}(e_{f2} - e_{f1}) + E_{d,comp} \quad (5.31)$$

$$\dot{E}_{d,comp} = \dot{W}_{C1} - \dot{m}_{co2}(e_{f2} - e_{f1})$$

The second law efficiency[48]

$$\eta_{II} = \frac{\dot{m}_{Co2}(e_{f2} - e_{f1})}{\dot{W}_{C1}} \quad (5.32)$$

Intercooler:

Exergy balance For S-CO_2 Intercooling at (state 2)

$$\dot{m}_{co2}(e_{f2} - e_{f3}) = \dot{m}_{water}(e_{f18} - e_{f17}) + \dot{E}_{d,\text{intercooler}} \quad (5.33)$$

Compressor 2:

Exergy balance for the High-Pressure compressor at (state3) [48].

$$\dot{W}_{C2} = \dot{m}_{co2}(e_{f4} - e_{f3}) + \dot{E}_{d,comp} \quad (5.34)$$

$$\dot{E}_{d,comp} = \dot{W}_{C2} - \dot{m}_{co2}(e_{f4} - e_{f3})$$

The second law efficiency[48],

$$\eta_{II} = \frac{\dot{m}_{Co2}(e_{f4} - e_{f3})}{\dot{W}_{C2}} \quad (5.35)$$

Recuperator:

Exergy balance equation for Recuperator at (state 4)

$$\dot{m}_{co2}(e_{f9} - e_{f10}) = \dot{m}_{Co2}(e_{f5} - e_{f4}) + \dot{E}_{d,reuperator} \quad (5.36)$$

Heat exchanger 1:

Exergy balance for Gas heater Heat exchanger one (state 5)

$$\dot{m}_{VP-1}(e_{f19} - e_{f20}) = \dot{m}_{Co2}(e_{f6} - e_{f5}) + \dot{E}_{d,HE1} \quad (5.37)$$

Turbine-1:

Exergy balance equation for the turbine is obtained from equation 5.5 (state 6)

$$\dot{W}_{T1} = \dot{m}_{co2}(e_{f6} - e_{f7}) - \dot{E}_{d,turbine1}$$

$$\dot{E}_{d,turbine1} = \dot{m}_{co2}(e_{f6} - e_{f7}) - \dot{W}_{T1} \quad (5.38)$$

The second law efficiency[48]

$$\eta_{II} = \frac{W_{T1}}{\dot{m}_{Co2}(e_{f6} - e_{f7})} \quad (5.39)$$

Heat exchanger 2:

Exergy balance for Gas heater Heat exchanger one (state7)

$$\dot{m}_{VP-1}(e_{f21}-e_{f22})=\dot{m}_{Co2}(e_{f8}-e_{f7})+\dot{E}_{d,HE2} \quad (5.40)$$

Turbine-2:

Exergy balance equation for the turbine is obtained from equation 5.5 (state 8)

$$\dot{W}_{T2}=\dot{m}_{co2}(e_{f8}-e_{f9})-\dot{E}_{d,turbine2}$$

$$\dot{E}_{d,turbine2}=\dot{m}_{co2}(e_{f8}-e_{f9})-\dot{W}_{T2} \quad (5.41)$$

The second law efficiency[48]

$$\eta_{II}=\frac{W_{T2}}{\dot{m}_{Co2}(e_{f8}-e_{f9})} \quad (5.42)$$

For evaporate at (sate 10)

Exergy balance equation for evaporator is obtained from equation (5.14)[48],

$$\dot{m}_{Co2}(e_{f10}-e_{f1})=\dot{m}_{ORC}(e_{f13}-e_{f12})+\dot{E}_{d,eva}$$

$$\dot{E}_{d,eva}=\dot{m}_{Co2}(e_{f10}-e_{f1})-\dot{m}_{ORC}(e_{f13}-e_{f12}) \quad (5.43)$$

The second law efficiency[48],

$$\eta_{II}=\frac{\dot{m}_{ORC}(e_{f13}-e_{f12})}{\dot{m}_{Co2}(e_{f10}-e_{f1})} \quad (5.44)$$

For pump (state 11)

Exergy balance equation for the pump is obtained from equation 5.5 [48],

$$\dot{W}_{Pump}=\dot{m}_{ORC}(e_{f12}-e_{f11})+\dot{E}_{d,Pump}$$

$$\dot{E}_{d,Pump}=\dot{m}_{ORC}(e_{f11}-e_{f12})-\dot{W}_{Pump} \quad (5.45)$$

The second law efficiency [48],

$$\eta_{II} = \frac{\dot{m}_{ORC}(e_{f12} - e_{f11})}{\dot{W}_{Pump}} \tag{5.46}$$

For ORC turbine at (state 13)

Exergy balance equation for the turbine is obtained from equation 5.5

$$\dot{W}_{T,ORC} = \dot{m}_{ORC}(e_{f13} - e_{f14}) - \dot{E}_{d,turbine,ORC}$$

$$\dot{E}_{d,turbine,ORC} = \dot{m}_{ORC}(e_{f13} - e_{f14}) - \dot{W}_{T,ORC} \tag{5.47}$$

The second law efficiency [48],

$$\eta_{II} = \frac{W_{T,ORC}}{\dot{m}_{ORC}(e_{f13} - e_{f14})} \tag{5.48}$$

Condenser:

Exergy balance equation for evaporator is obtained from equation (5.14), at (state 14)

$$\dot{m}_{ORC}(e_{f14} - e_{f11}) = \dot{m}_{water}(e_{f16} - e_{f15}) + \dot{E}_{d,condenser}$$

$$\dot{E}_{d,condenser} = \dot{m}_{ORC}(e_{f14} - e_{f11}) + \dot{m}_{water}(e_{f15} - e_{f16}) \tag{5.49}$$

The second law efficiency [48]

$$\eta_{II} = \frac{\dot{m}_{water}(e_{f16} - e_{f15})}{\dot{m}_{ORC}(e_{f14} - e_{f11})} \tag{5.50}$$

Overall System Analysis

The network is done:

$$\dot{W}_{net} = (\dot{W}_{T1} + \dot{W}_{T2} + \dot{W}_{T,ORC}) - (\dot{W}_{C1} + \dot{W}_{C2} + \dot{W}_{Pump}) \tag{5.51}$$

Heat energy in the system

$\dot{Q}_{in-1} = \dot{m}_{co2}(h_6 - h_5)$ And

$$\dot{Q}_{in-2} = \dot{m}_{co2}(h_8 - h_7)$$

$$\dot{Q}_{IN-Total} = \dot{Q}_{in-1} + \dot{Q}_{in-2} \tag{5.52}$$

Thermal Efficiency/1st law Efficiency [48],

$$\eta_I = \frac{\dot{W}_{net}}{\dot{Q}_{IN-Total}} \tag{5.53}$$

Second Law Efficiency[48].

$$\eta_{II,sys} = \frac{\dot{W}_{net}}{\dot{E}_{x-in}} \tag{5.54}$$

Thermal efficiency and second law efficiency are key performance criteria of S-CO_2 and ORC because they quantify how much of the input energy or exergy is being transformed into desired output.

Based on the thermodynamic model developed in this chapter, proper simulation is performed. The simulation results are the primary topics of the next chapter or in chapter 6.

CHAPTER SIX

6. SIMULATION RESULT AND DISCUSSION

6.1 Solar Parabolic Trough Collector (SPTC) Model Result

The performance of the PTCs solar field is evaluated through an energy parametric study. Therefore, first, an energy analysis is developed in which is the reference block diagram Figure 5.1 is utilized to identify the different energy streams flowing into or out of a control volume plotted around the PTCs solar field system. The PTC energy analysis also considers the heat losses and the required power for HTF circulations as well as evaluate the energy efficiency of the PTCs. The EES software and REF PRO software are used to evaluate the state properties and solve the proposed models.

The Therminol VP-1 mass flow rates and other thermal parameters at the various states, as numbered in Figure 5.1 are listed in Table 6.2. Different average monthly hourly solar radiations listed on the Appendix A. For the design purpose and to compare previous literature figure 6.1 Weather conditions of 16th February 2017 average a solar beam radiation of 850 W/m^2 are taken, wind velocity of 2 m/s, and an ambient temperature of 28 °C presented based on using calculated data collected form Ethiopian methodology site. The calculated and analysis of the direct normal irradiance on the earth surface at zero angles of incidence. All the states calculated data are listed here in Table 6.1& Table 6.2 are for the HTF Therminol-PV1. In this case, Total solar radiation, incident on the field of aperture area 7.618 MWth and the solar field produces a total 5.104 MWth directly sent to the power block.

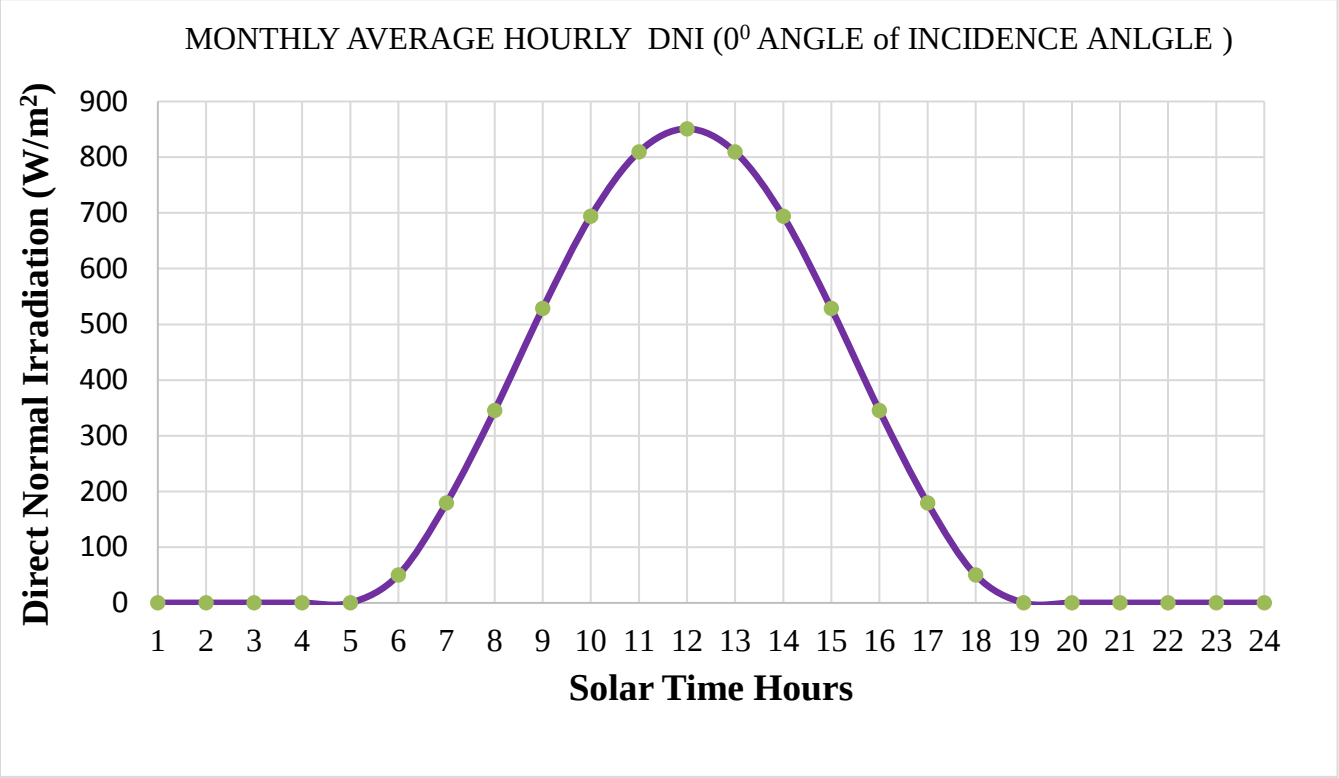

Figure 6.1 DNI on 16th February 2017 calculated result in Adigala.

Table 6.1. The parabolic solar trough different output result base on the Design point parameters In the Adigala site.

Parameter	**Output**	**Unit**
Total aperture area (SCA) in a single loop	2180	m^2
Total reflective aperture area in the field	8,963.	m^2
Solar Filed area	17440	m^2
Total Land Area	24416	m^2
Design Solar Field Inlet Temperature	280	℃
Design Solar Field Outlet Temperature	390.447	℃
Solar Filed Nominal Design Thermal Output	5.1041	MW
Total solar radiation, incident on the field of the aperture area	7.618	MW
Mass flow rate on per loop of the system	8	kg/s

Table 6.2 the thermal parameters at the different states shown in Figure 5.1corresponding to the reference case.

State No	Fluid	P(kPa)	T (^{0}C)	$\dot{m}$ (kg/s)	H (kJ/kg)	S (kJ/kgK)
19	Therminol VP-1	131.1	390	4.222 [1]	1010.88	2.09
20	Therminol VP-1	131.1	280	4.222 [1]	643.16	1.79
21	Therminol VP-1	131.1	280	3.778 [1]	643.16	1.79
22	Therminol VP-1	131.1	390	3.778 [1]	1010.88	2.09
23	Therminol VP-1	131.1	280	8	643.16	1.79
24	Therminol VP-1	131.1	280	8	643.16	1.79
25	Therminol VP-1	131.1	390	32	1010.88	2.09
26	Therminol VP-1	131.1	390	8	1010.88	2.09

6.2 Heat Transfer Fluid (HTF) Temperature and Solar field heat loss result

Validation of the working solar collector has been possible through the comparison of current model results with the theoretical study of Al-Sulaiman [49] as shown in Table 6.3. The variation in heat loss was calculated corresponding to the change in average temperature above the ambient temperature of fluid flowing inside the receiver. The results of the current model show good agreement with the existing of theoretical study.

Figure 6.3 Change in heat losses with an average temperature of the fluid above the ambient of the absorber.

Temperature Difference (^{0}C)	Heat loss (W/m^2) Current model	Heat loss (W/m2) (Al-Sulaiman.et al [48])	Error Estimation (%)
100.6	10.78	10.6	1.69%
149.1	17.24	19.3	-11.9%
196.7	32.15	30.6	4.82
245.8	54.48	45.4	16.66%
290.447	67.69	62.9	7.076

The heat loss of the receiver in meter-by-meter simulation used the vacuum SCHOTT PTR 70 heat loss correlation coefficients result presented by using EES software based on the given input value Table 4.3, Table 4.4, and Table 4.5 respectively.

Figure 6.2 shows the temperature rise of the HTF. The temperature rise is linear with a negligible change in temperature rise per meter of 0.201°C at T_{HTF} =280°C to 0.181°C at T_{HTF} = 390.447°C (0.02 difference). The net gain of energy decreases as the fluid progresses through the loop because heat loss increases as the HTF temperature increases. The heat loss in the loop is shown in fig. 6.3.

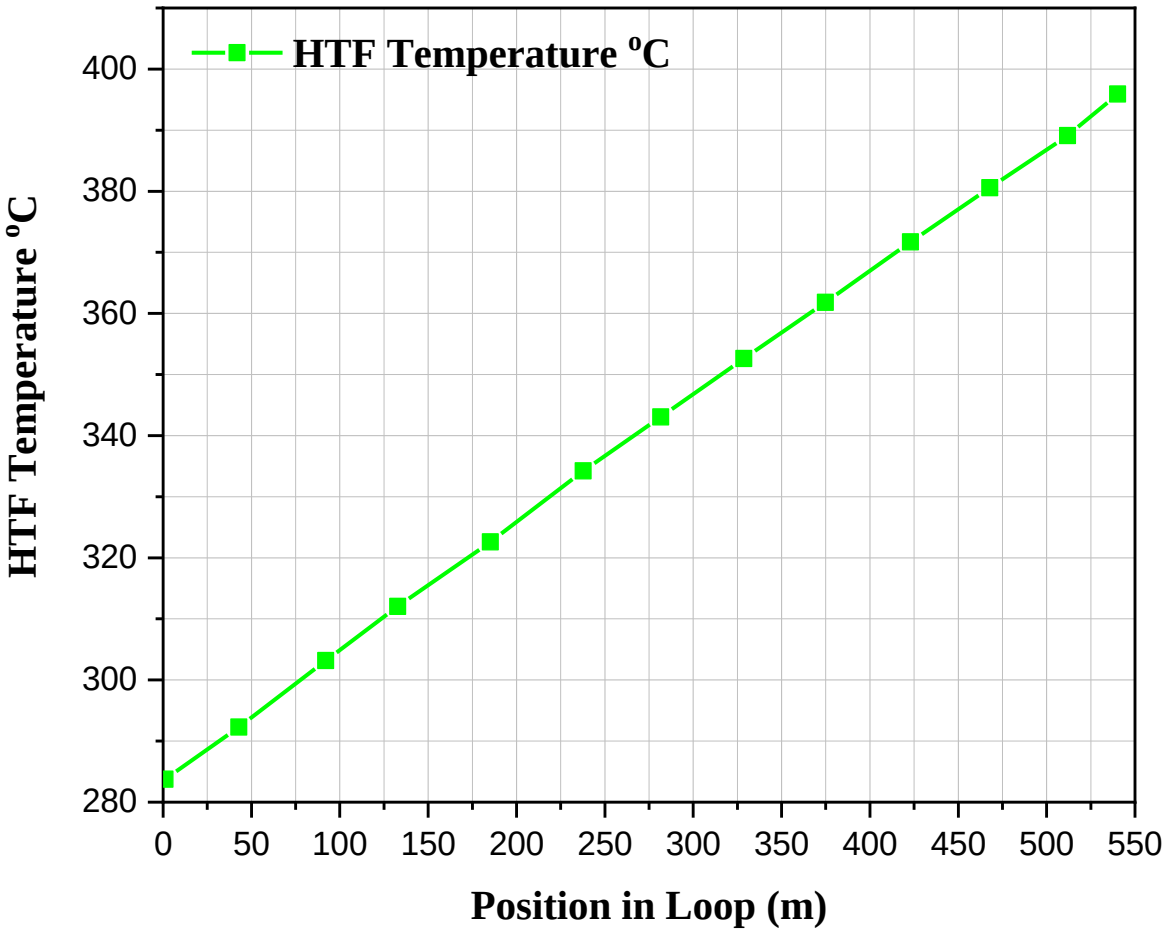

Figure 6.2. HTF temperature increase as it flows through one loop

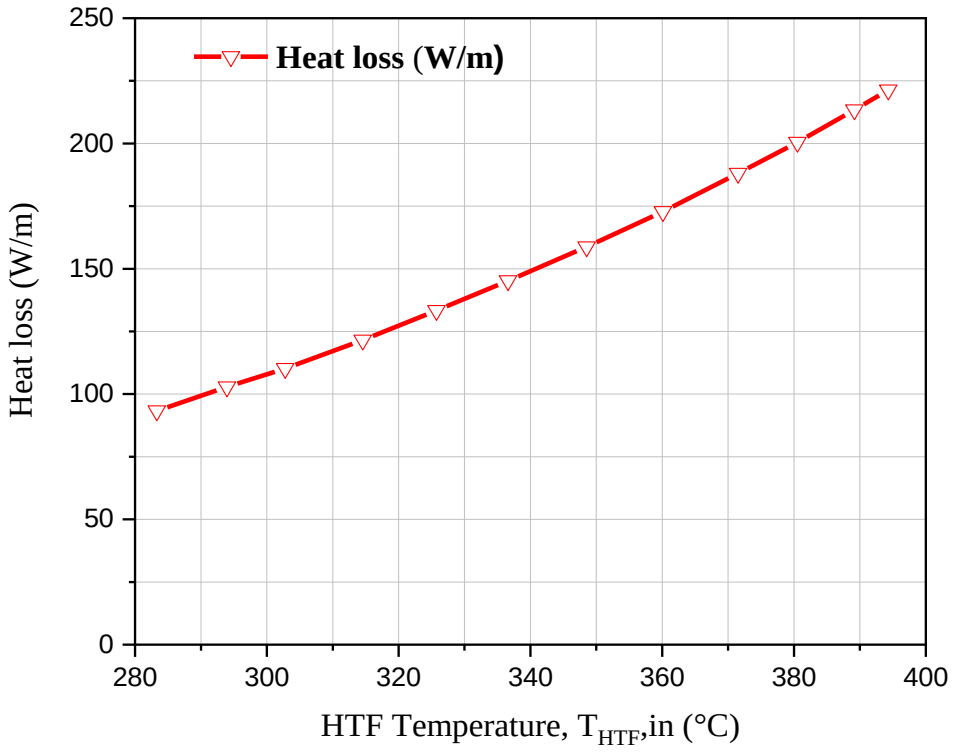

Figure 6.3. Heat loss as a function of HTF temperature

For the purpose of validation of SPTC considered system, numerous researcher [49] are selected from the available literature. The error estimation is recommended between -25% up to 25% [50]. Therefore, based on the simulation results of current study as well as results of the previous research are shown in Table 6.3 and the comparison indicates that the simulation results of the present model properly agree with that of literature work at the same baseline conditions, therefore it can be used to analyse the performance of combined cycle for the next step.

6.3. Results of energetic and exergetic performance analysis of S-CO_2 combined ORC power cycle and its validation.

The basic assumptions and input data for the simulation of the considered system are outlined in Table 5.1. To verify the results of thermodynamic simulations for each of the sub-cycles of the proposed combined cycle the results available in the literature are used. The obtained results in the present work, for S-CO_2 Brayton and ORC systems, are compared with those reported by Yari et al. [51][52]. The comparison is shown in Fig. 6.4 (a) and (b) which indicates a satisfying agreement between them.

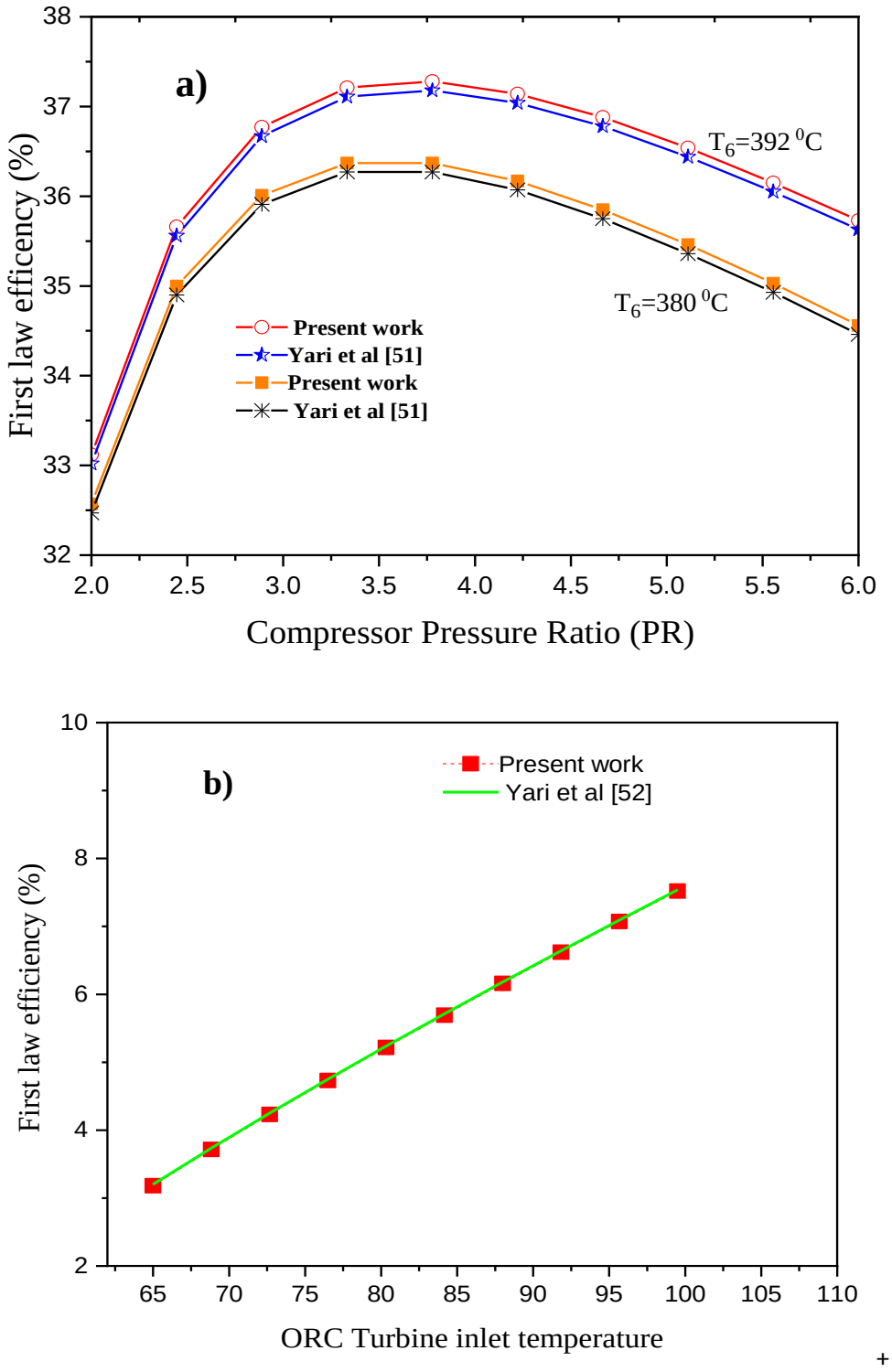

Figure 6.4: **a)** Verification of thermodynamic simulation in the present work with the previously published data on the S-CO_2 Brayton cycle. **(b)** Verification of thermodynamic simulation in the present work with the previously published data on Organic Rankine cycle.

6.3.1. Energy analysis of CPTS and thermodynamic cycle S-CO_2 combined with ORC

A numerical code is established using EES software to perform the calculations required for the thermal and exergy plant analysis in appendix C. The values of the different operating parameters for real working conditions are indicated in Table 6.4&6.5. Based on the design parameter the over-all energy of CPTS and thermodynamic cycle S-CO_2 combined with ORC are evaluated, the results of the analysis for each subsystem, at a typical operating condition, are outlined in Table 6.4. From energy analysis results, as presented in Table 6.4, indicate that the power plant can generate 1048 kW electrical energy from 7618 kW solar irradiance energy or thermal energy in addition to the overall total thermal efficiency of the system is 13.7%. In this case, the solar field produces a total of 5.104MWth out of which about 2.010MWth is sent to the power block while 3.094 MWth is pumped in to the storage tank. Thus, the TES is operating in charging mode as long as the solar field production is higher than that required for the power block to meet the targeted operation capacity of one MWe. In addition to, it can be seen that the thermodynamic S-CO_2 combined with ORC power cycle has relatively high-energy efficiency (52.13%) the analysis was done using EES software (see Appendix C).

Table 6.4 Energy analysis results at a typical operating like T_6 = 380℃; PR =2.5; T_{13} =100℃; DNI =850 W/m^2; condition.

Subsystem	**Energy**			
	Input (kW)	Output (kW)	Loss (kW)	Energy efficiency (%)
Total solar radiation, incident on the field of the aperture area	7618	5104.06	2513.94	67.8
Power cycle	2010	1048	962	52.13
Overall power plant	7618	1048	3475.94	13.7

Table 6.5 Energy and exergy analysis results at a typical with constant T6 =380℃, T13=100℃, PR=2.5, DNI= 850W/m2 operating condition

Parameter	**Energy Output**	**Exergy Output**	**Exergy Destruction**	**Unit**
(LP) Compressor Work	71.6	70.2	1.4	kW
Heat at intercooler	209.7	190.7	19	kW
(HP) Compressor Work	175	173.9	1.1	kW
Heat exchanger HE 1	1.608	1.4152	0.1928	MW
Heat exchanger HE 2	0.4013	0.3838	0.0175	MW
High presser Turbine work	317.4	318.7	1.3	kW
Low pressure Turbine work	831.4	835.8	4.4	kW
Heat evaporator	897.6	817.3	80.3	kW
ORC turbine	160.4	162.9	2.5	kW
ORC pump	14.79	14.66	0.13	kW
ORC condenser	180.6	164.5	16.1	kW
Total Thermal input on the cycle	2.010	1.799	0.211	MW
Network on the combined S-CO2&ORC system	1.048	1.048	0.48164	MW
The thermal efficiency of the combined S-CO_2 & ORC system	52.13	58.25	-	%

The analysis of energy as well as exergy efficiency, rate exergy destruction and overall efficiency power plant model is done using EES software in table 6.4&6.5 and the Reference Fluid Thermodynamic and Transport Properties (REFPROP) software is used to find the properties of S-CO_2 and ORC at different pressures and temperatures. This model is used to determine all the state points, the values of temperature, pressure, mass flow rate, enthalpy and entropy are outlined in Table 6.6, for each state point according to the stream numbers shown in Fig. 5.1.

6.3.2. Exergy distraction of different thermodynamics components.

Abdullah A et .al [1] reported that to produce 1MW electric output the maximum exergy destruction rate within the integrated CSP occurs in the PTCs solar field with about 65% while the remaining 35 % of exergy destruction rate occurs within the power block. For the present studied paper, the results of exergy analysis only on the thermodynamics combined S-CO_2 and ORC show that the highest exergy destruction occurs in the heat exchanger, which is due to the fact that there is a large temperature difference in HE-1 between the inlet of HTF and S-CO_2 with temperature inlet is 390℃ and 169℃ respectively. In addition to heat transfer between the flow pressure losses due to fluid friction and dissipation of energy to the environment, the four phenomena can also occur simultaneously. Second major irreversibility in the ORC evaporator because of phase change of steam. Exergy loss in the S-CO_2 turbine is higher as compare to ORC steam turbine because of very high inlet temperature and law expansion ratio that increases the irreversibility. ORC turbine has a higher expansion ratio but law temperature at the inlet of the turbine that reduces the irreversibility. Now to evaluate the Exergy destruction rates of thermodynamics combined S-CO_2 and ORC power plant with different components, determined for state-of-the-art conditions are presented in Table 6.5 and Figure 6.5. The minimum irreversibility rates are obtained for the ORC pump (0.13 kW), the (HP) Compressor Work (1.1 kW) and the High presser Turbine work (1.3 kW) followed by the evaporator intercooler and condenser. The heat exchangers present an irreversibility rate of about 0.1928 MW.

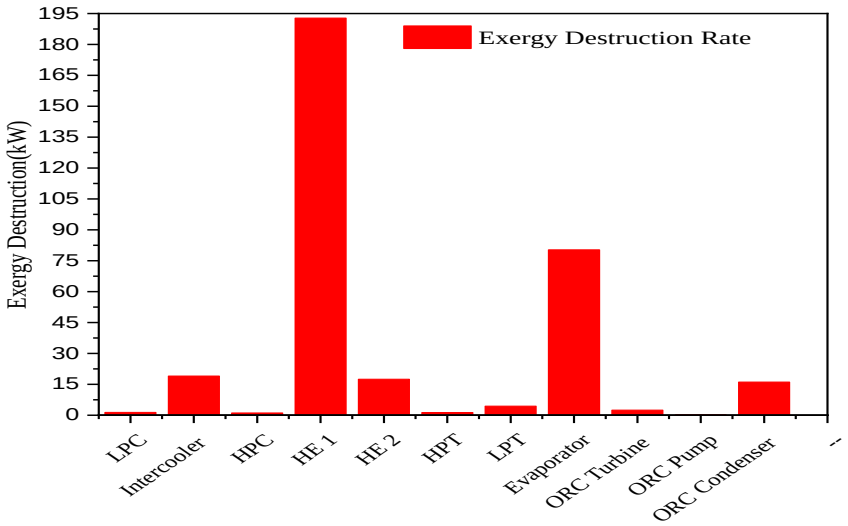

Figure 6.5 Exergy destruction rates of thermal power plant components.

Table 6.6 Calculated thermodynamic properties and mass flow rates for the considered system

State No.	Fluid	P(kPa)	T (^{0}C)	$\dot{m}$ (kg/s)	H (kJ/kg)	S (kJ/kgK)
1	S-CO2	10000	32.000	12	278.36	1.2442
2	S-CO2	14000	38.570	12	284.19	1.2461
3	S-CO2	14000	32.000	12	266.69	1.1893
4	S-CO2	25000	44.180	12	281.33	1.1944
5	S-CO2	25000	169.00	12	535.25	1.8746
6	S-CO2	25000	380.00	12	822.02	2.4082
7	S-CO2	19600	354.70	12	795.62	2.4129
8	S-CO2	19600	382.00	12	829.04	2.4650
9	S-CO2	10000	309.90	12	759.70	2.4782
10	S-CO2	10000	151.00	12	573.20	2.1040
11	R123	154.7	27	30	228.3	1.098
12	R123	786.8	27.29	30	228.8	1.099
13	R123	786.8	100	30	442.5	1.694
14	R123	154.7	57.48	30	420.2	1.711
15	Cooling Water	100	25	130.6	104.8	0.3669
16	Cooling Water	100	35	130.6	146.7	0.5049
17	Cooling Water	100	25	130.6	104.8	0.3669
18	Cooling Water	100	35	130.6	106.8	0.5049
19	Therminol VP-1	131.1	390	4.122	1010.88	2.09
20	Therminol VP-1	131.1	280	4.122	643.16	1.79
21	Therminol VP-1	131.1	280	3.778	643.16	1.79
22	Therminol VP-1	131.1	390	3.778	1010.88	2.09
23	Therminol VP-1	131.1	280	7.9	643.16	1.79
24	Therminol VP-1	131.1	280	7.9	643.16	1.79
25	Therminol VP-1	131.1	390	7.9	1010.88	2.09

6.4. Energy and Exergy efficiency of the combined S-CO_2 and ORC plant with the behavior of internal disturbances.

In this study is directed to inspect the effects on the power plant performance of key operating parameters of both solar and CO_2 power cycle and ORC sub-systems. The effects of important parameters including compressor pressure ratio, gas turbine inlet temperature (T_6), direct normal irradiance (DNI), and the parabolic trough solar field efficiency are examined as result variables. Such a thermodynamic analysis is necessary to design efficient and cost-effective new generations of this type of power plants.

6.4.1 The Effect of Compressor Pressure Ratio in CPTS power plant overall efficiency

One of the most important parameters affecting the system performance in terms of efficiency and output power is the compressor pressure ratio with the constant parameter like the evaporator temperature (T_{13}) and the direct normal irradiance.

Figure 6.6 shows the effects of this parameter on the energy efficiencies as well as the net output power for the overall power plant. In addition, the figure brings out that; there are optimum values for Pressure Ratio at which the efficiencies and the net output power can be maximized. This trend can be explained as follows as Pressure Ratio increases, the generated power by the turbine and the consumed power by the compressors are increased too. However, at lower pressure ratios than the optimum, one the increment of turbine-generated power dominates the increment of compressor power consumed and at higher-pressure ratios, the trend is vice versa. Now from the figure, the maximum values of thermal efficiency and Network output power are 15.81% and 1233.5 kW for the overall power plant at the pressure ratio of 3.714. Therefor as can be seen from the graph by changing the pressure ratio from 2.5 to 3.714 it can be improved the efficiency and Network output 13.7% to 15.81%, and 1048 kW to 1233.5 kW respectively.

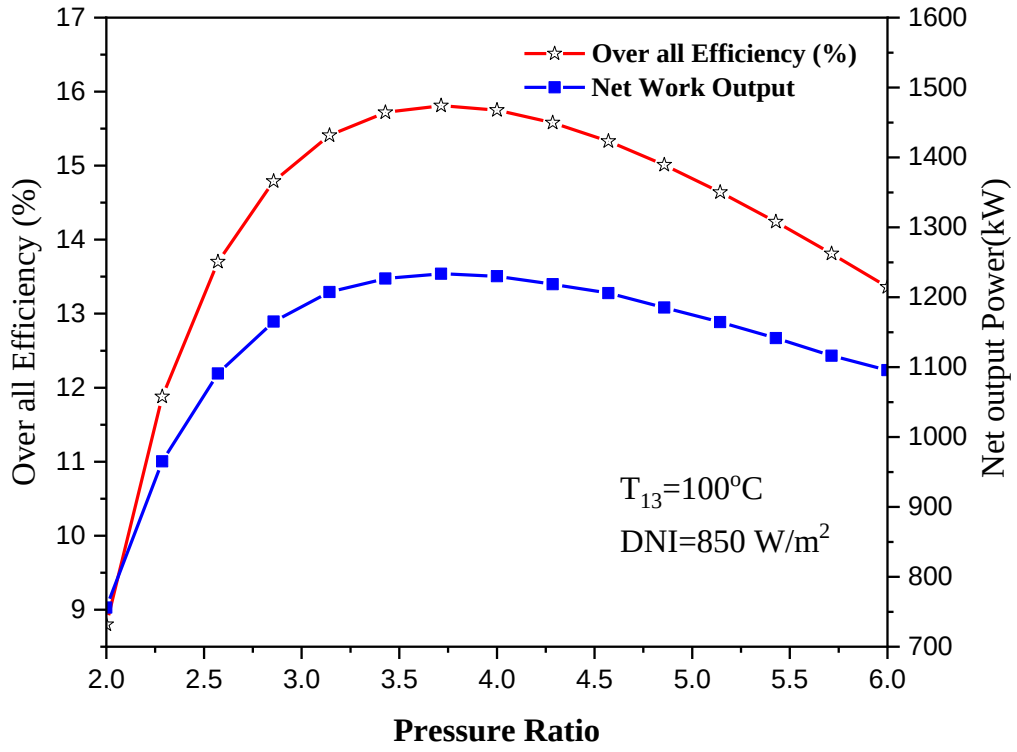

Figure 6.6 the effect of pressure ratio on CPTS power plant overall efficiency

6.4.2 The Effect of Compressor Pressure Ratio on the Power Cycle energy and exergy Efficiency.

The effect of compressor pressure ratio on the energy and exergy efficiency values of the combined S-CO_2 Brayton cycle and ORC power cycle are presented in Fig. 6.7 it is seen from the figure the energy and exergy efficiency increasing rapidly at lowest compressor pressure ratios between 2 up to 4.5 and reaches the peak point. In addition, the highest amount of energy efficiency is obtained for the cycle is 53.76% is at the pressure ratio of 3.8 and the best exergy efficiency is about 60.59% at a pressure ratio of 3.5.

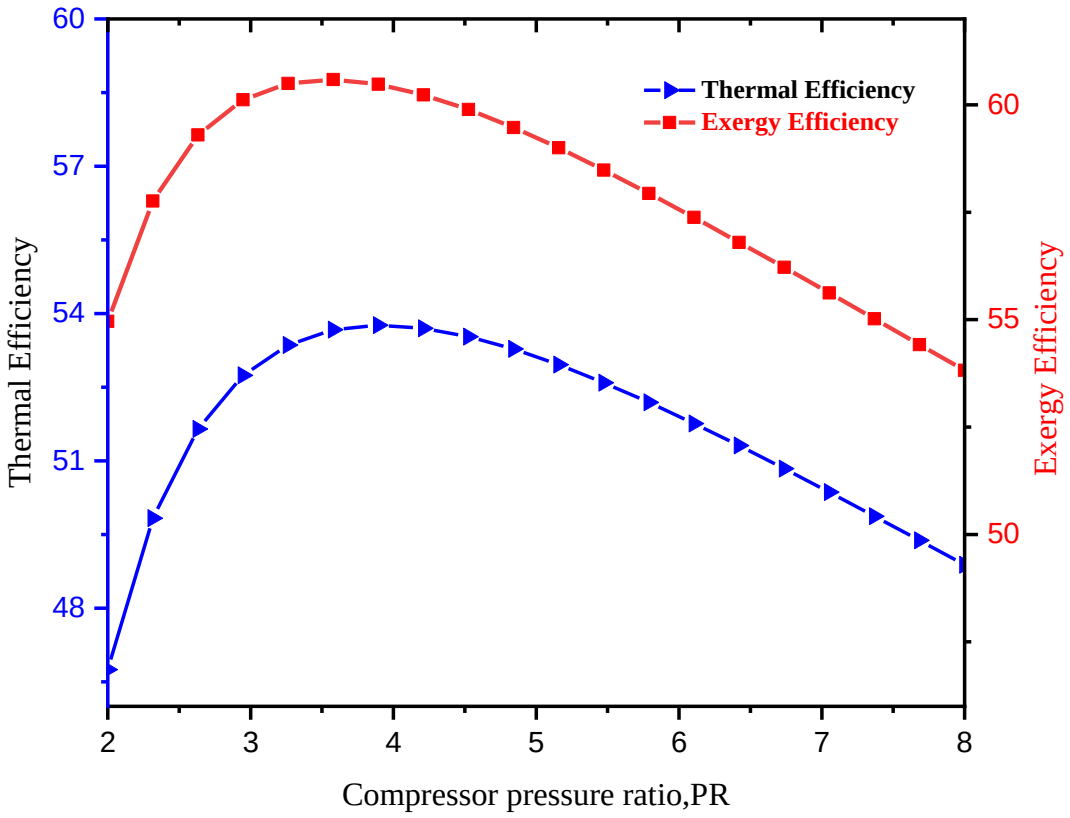

Figure 6.7 The Effect of Compressor Pressure Ratio on the Power Cycle Efficiency.

6.4.3 Comparison of thermal efficiency of stand-alone Brayton cycle and the combined cycle

To disclose the performance improvement of the Supercritical Carbon Dioxide Brayton Cycle with Intercooling, Reheat and Regenerator Brayton cycle by combining the ORCs with it, the thermal efficiency of the stand-alone S-CO_2 Brayton cycle is compared with that of the combined cycle in Fig. 6.8. The figure indicates a significant efficiency improvement of the Brayton cycle when the ORCs are combined within it. As can be seen, the thermal efficiency of the Brayton cycle is increased from around 44.5% to about 53.7% at nearly optimum operating conditions. According to the result by adding an ORC, bottoming cycle can increase the overall cycle efficiency by 9.2 percentage points under the specified conditions.

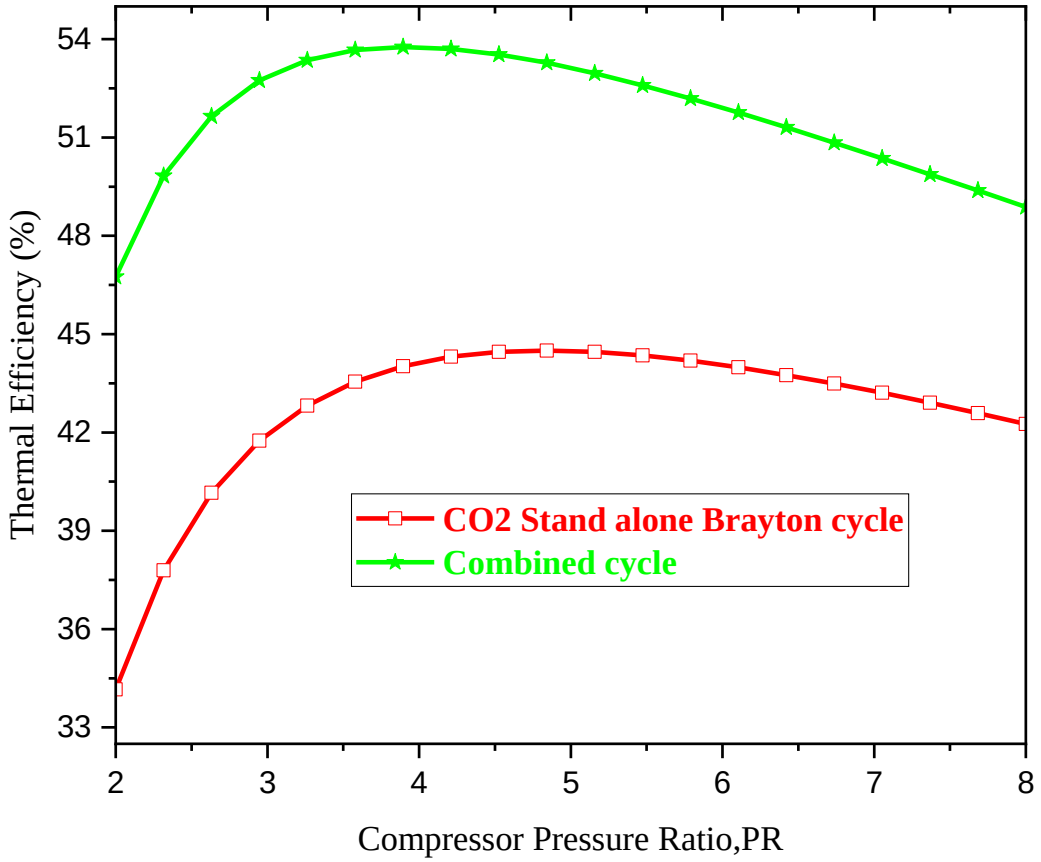

Fig. 6.8 Comparison of thermal efficiency of stand-alone Brayton cycle and the combined cycle

6.4.4 Effect of S-CO_2 inlet temperature on the overall power plant efficiency and Network output power

As shows in figure 6.9, the effect of differences in inlet temperature (T_6) at an S-CO_2 high-pressure turbine on the energy and thermal efficiency performance of the considered S-CO_2-ORC. With an increase in inlet temperature, energy and thermal efficiency of S-CO_2 with ORC also increase, as analyzed under constant baseline conditions such as compression pressure ratio, direct normal irradiance, evaporator temperatures (T_{13}), Mass flow rate S-CO2 = 12 kg / s and P_6 = 25 MPa as shown in Fig. 6.9.indicates that increasing the turbine temperature increases the Network is increased due to the increase of turbine power as its inlet temperature increases, because the enthalpy inflow to the turbine increases correspondingly, that is resulting in an increase in the work output of the turbine. Therefore, inlet temperature from 330 °C to 400 °C results in an increase in thermal efficiency from 9.54% to 14.5% in output power (from 725.3 kW to 1104 kW).

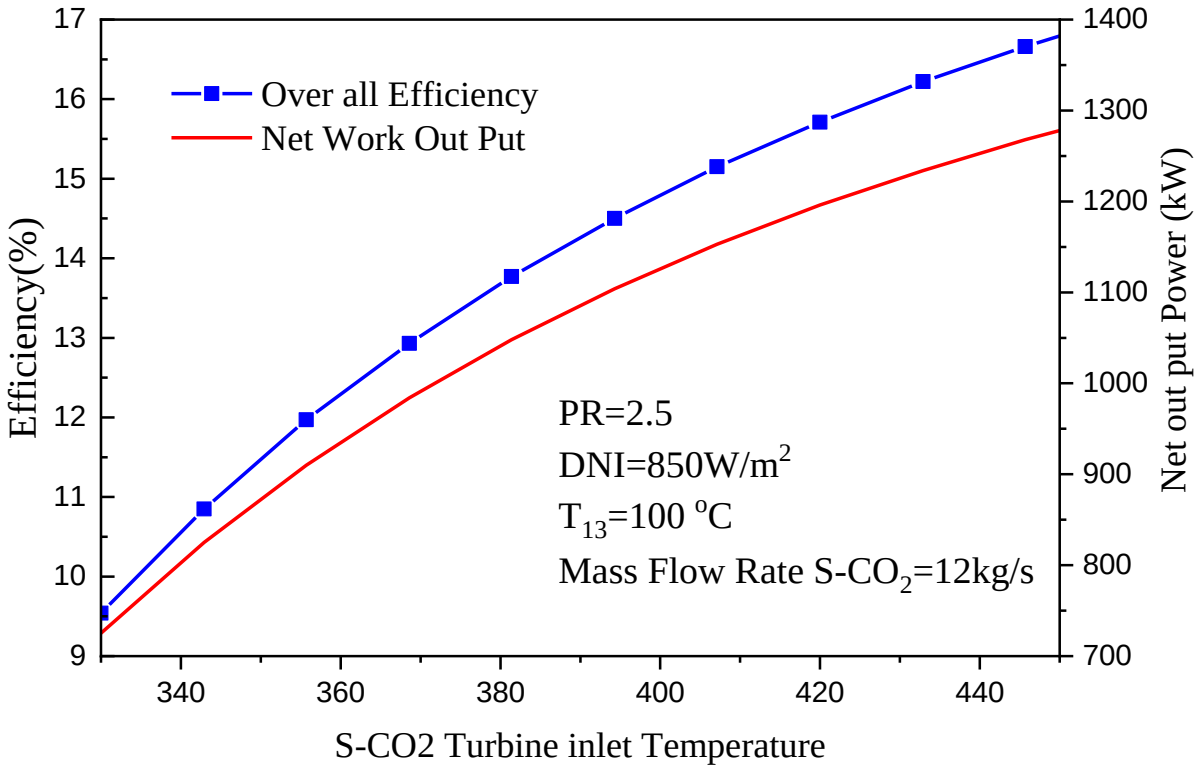

Figure 6.9 Effect of S-CO_2 inlet temperature on the overall power plant efficiency and net output power

6.4.5 The Effect S-CO_2 Brayton Turbine and Compressor Efficiency and ORC Turbine Efficiency on the Power Plant Exergy Efficiency

Improving the turbine and compressor an essential parameter for future technology maximizing energy and exergy efficiency. In an S-CO_2 Brayton cycle, turbine and compressor efficiencies are important factors affecting the Power Plant system performance. The effects of S-CO_2 turbine and compressor efficiencies on the power plant exergy efficiency are revealed in Figure. 6.10a. as can be seen, these parameters are crucial for the system performance. The S-CO_2 turbine efficiency and compressor efficiency does have an essential influence on power plant performance. For instance, for the case of DNI = 900 W/m^2, a reduction in turbine and compressor efficiencies by 8.495% leads to a reduction of the exergy efficiency from 67.58% to 59.085% S-CO_2 combined with ORC power plants.

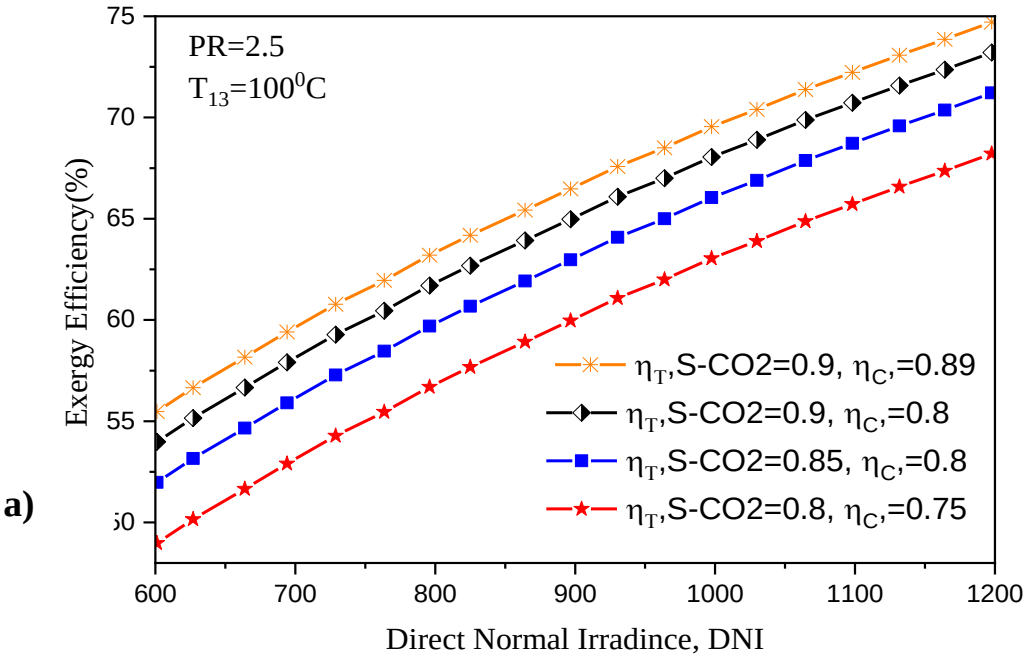

a)

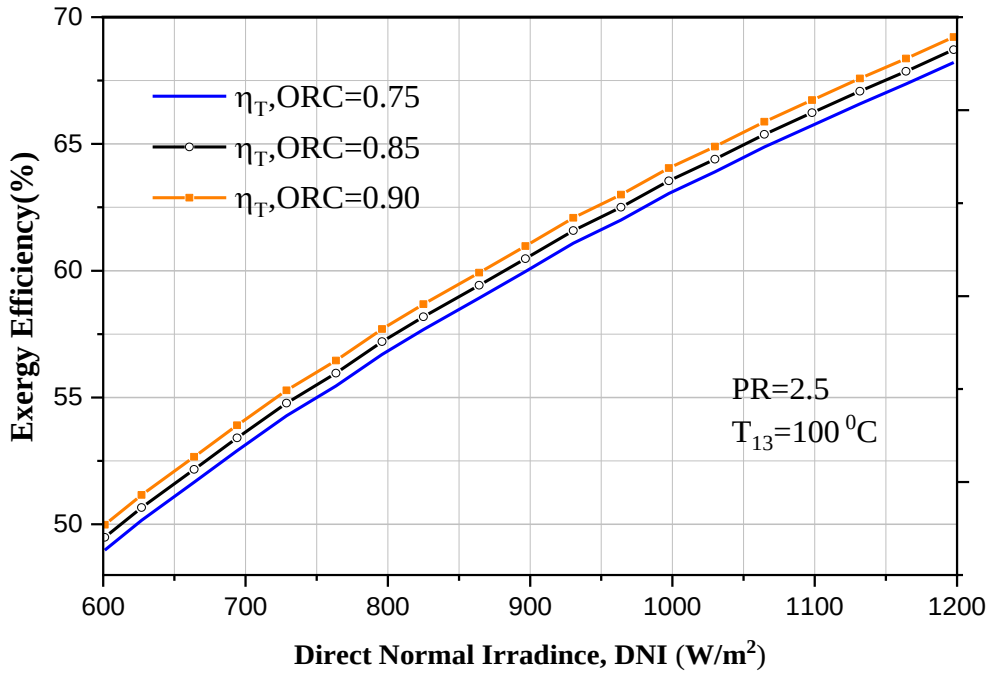

b)

Figure 6.10; a) effect of ORC turbine efficiency on the power cycle **(b)** effect of ORC turbine efficiency on the power cycle

In S-CO_2 Brayton cycle combined with ORC power cycle, the performance of the ORC system is mostly affected by its turbine isentropic efficiency, the effect of which is reported in Figure 6.10b on the power plant exergy efficiency. As the figure indicates the ORC turbine efficiency does not have an essential influence on power plant performance with different isentropic turbine efficiency 0.75, 0.85 and 0.9 then the amount of exergy efficiency are resulted 57.68%, 58.1% and 58.68% respectively. Which is the net output power of the ORC system is lower than that of the Brayton cycle. In addition, since the pump consumed power is very low as compared to the turbine-generated power in all types of Rankine cycles, the variations of the pump isentropic efficiency is not investigated.

6.5. Optimize and simulation of the maximum efficiency and energy power production.

The effects of the critical design and operating parameters on maximum efficiency and energy power production are illustrated. In addition, optimizing of the pressure ratio of the S-CO_2 Brayton cycle combined with the ORC cycle and also the maximum efficiency and power production with a variation of DNI.

6.5.1. Optimization of the Effect of Pressure Ratio on Compressor and Turbine Work

It is important to mention that the range of the pressure ratio considered for the combined cycles during optimization are larger than the stand-alone cycles. The maximum pressure ratio for a recompression and reheating S-CO_2 combined with ORC cycle is configurations is limited to 7 for the partial cooling cycle [9]. Therefore, for the present work to optimize the Effect of Pressure Ratio on Compressor and Turbine Work is there is a variation of Work in, Work out and efficiency with a pressure ratio of the cycle at turbine inlet temperature (T_6 = 380 °C), is shown in figure 6.11. As can be seen in the figure both works experienced a steady rise in value, which is 66.6% and 50.3% for Work in and Work out respectively for pressure ratio range of 2.5 to 3.7. Now the maximum efficiency achieved in the pressure ratio of 3.7. Therefore, in order to minimize the metallurgical effect and to increase the life expectancy of the power plant is the optimum pressure ratio operating condition is between 2.5 up to 3.7 with a better work output (1633kW) and thermal efficiency (53.76%).

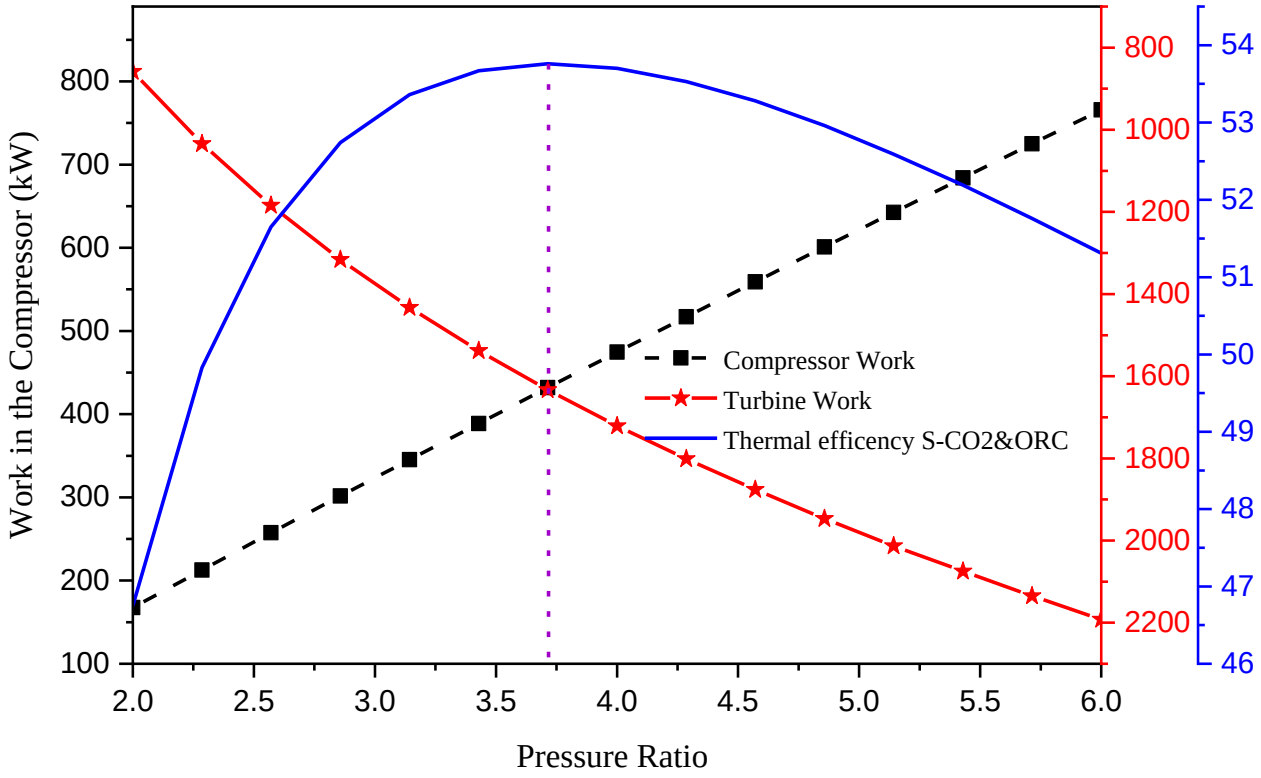

Figure 6.11 Optimization of the Effect of Pressure Ratio on Compressor and Turbine Work

6.5.2 The efficiencies of the overall plant with the variation of DNI.

The effects of the variations in direct normal irradiance on the overall CSP plant's performance are presented in figure 6.12. Where energy efficiencies of the overall plant are assessed under a widespread range of direct normal irradiance intensity. The S-CO_2 closed Brayton cycle Combined with Organic Rankine cycles for Parabolic Trough Solar Power Plant shows better performance at higher solar intensities. The energy efficiency varies from 11.49% at 500 W/m^2 to 14.45% at 1200 W/m^2 with an increase of 2.96% over the entire range. Therefore, the direct normal radiance one of the parameter it affects overall efficiencies range in the CSP plant.

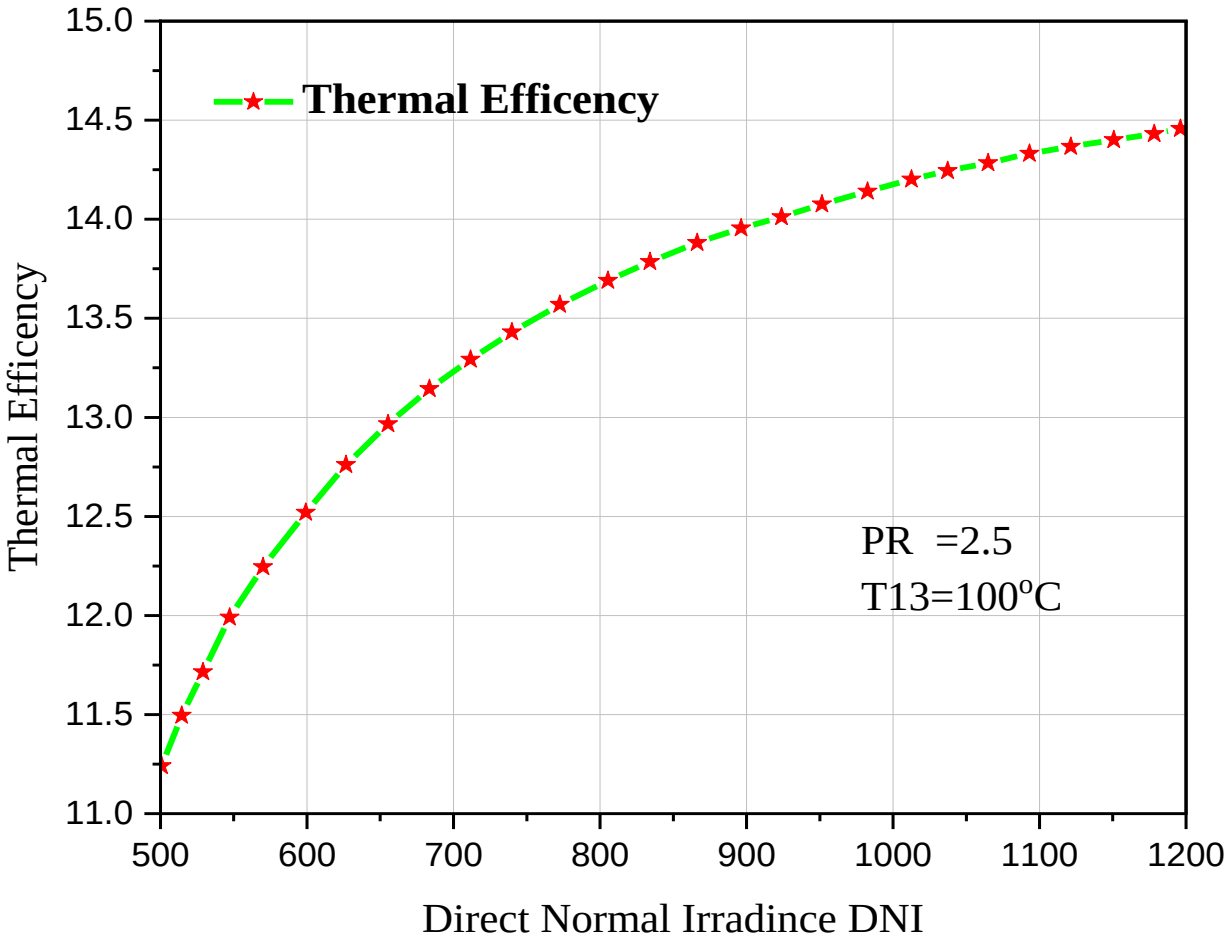

Figure 6.12. The effect of the change in DNI on the overall system energy efficiency

6.5.3 Monthly Average Hourly Energy output and overall efficiency on the selected site

The change in monthly average hourly energy output and efficiency during a day are presented in Fig.6-13. For the summer months, which include June, July and August, is observed that the lost energy output and efficiency this is because of the decreasing of direct normal irradiance and sunshine hours availability**.**

On the other hand, the maximum energy output and efficiency occurred on hours for the winter, spring and autumn seasons, which are February, January, may, October and November. It is notable to mention that the energy and overall efficiency have a direct relation with the rate of radiation which received by the solar field which is just affected by DNI and sunshine hours. Therefore, from the result the maximum and minimum monthly average hourly energy output are obtained on December (10053.408kWh) and August (6552 kWh) respectively, on the other hand,

the maximum and minimum overall efficiency of the power plant is May (14.201%) and August (12.246%).

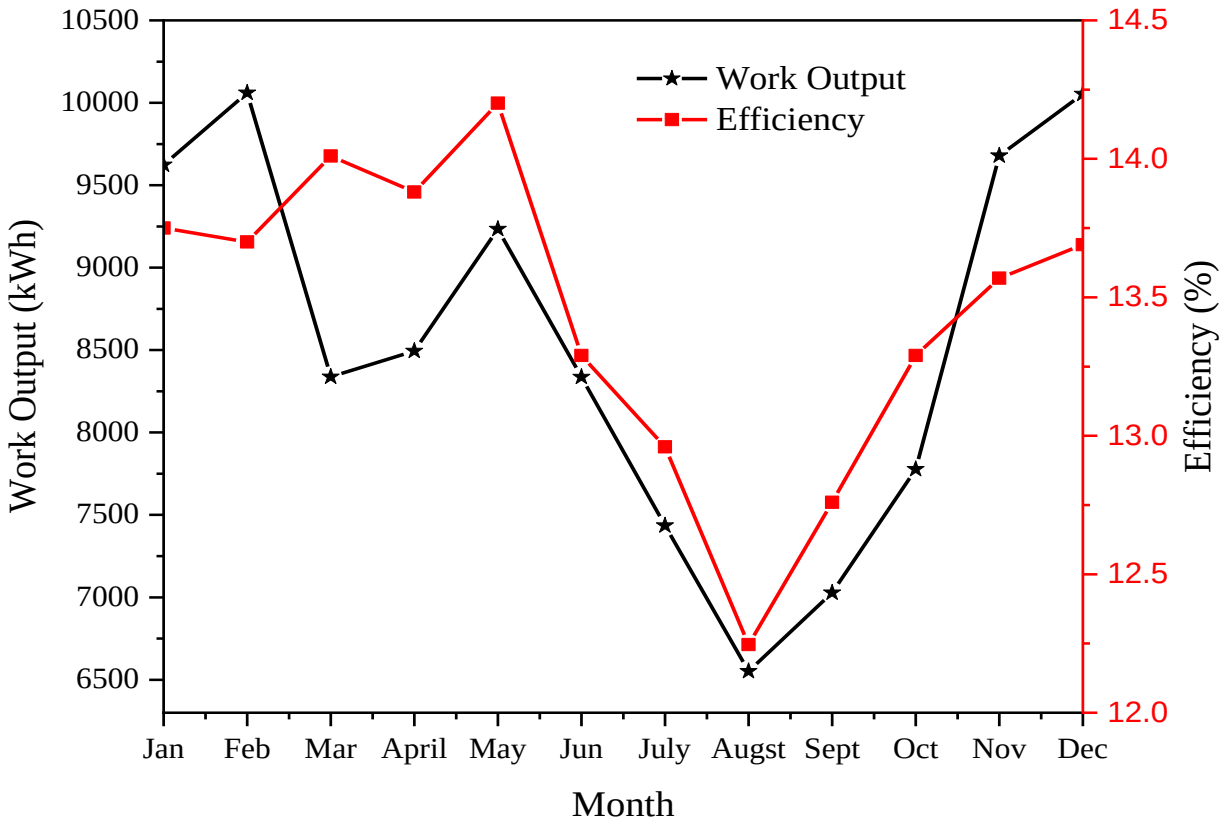

Figure 6.13 monthly average hourly energy output and efficiency

6.5.4 Performance comparison of present work with previously proposed power cycles

To evaluate the performance of the present work is compared with other researchers in previous works, for the same solar subsystem conditions. The results of such a comparison are presented in Table 6.7 reveals the superiority of the power cycle proposed in the present paper over the previously proposed systems. For instance, for a given conditions of the solar subsystem, the overall thermal efficiency of the power cycle proposed in this work is 13.7% in addition Exergy on the power cycle Efficiency (58.9%) and thermal on the power cycle Efficiency (52.13%), while the Parabolic trough solar power plant using carbon dioxide power cycle, at the same solar field conditions have the cycle efficiencies of 12%, 38.51% and 33% respectively. A higher efficiency of the power cycle results in a higher efficiency of the overall power plant as Table 6.7 indicates. In addition, as compared with Energy and exergy analyses of a parabolic trough solar power plant

using carbon dioxide power cycle, the power cycle proposed in the present work performs better than the previous work CO_2-based Brayton cycles.

Table 6.7 Performance comparison of the present work with previously proposed power cycles

Research Title	DNI(W/m^2)	Exergy on the power cycle Efficiency (%)	Thermal Efficiency cycle (%)	Overall Thermal Efficiency cycle (%)
Parabolic trough collectors driven combined supercritical CO2 and organic Rankine cycle[26]	950	78.07	43.49	12.87
Combined Cycle in the Present work	950	82	54	14.1
Parabolic trough solar power plant using carbon dioxide power cycle[1]	850	38.51	33	12
Combined Cycle in the Present work	850	58.25	52.13	13.7

CHAPTER SEVEN

CONCLUSION AND RECOMMENDATION

7.1 CONCLUSION

In this study, the ability to utilize parabolic solar trough power plant by using S-CO_2 closed Bryton power cycle combined with ORC in producing energy in low-grade heat sources and recovering waste heat has been investigated. The present work power plant model is one MW CSP system was developed in Adigala, Somalia, Ethiopia.

The integrated CSP is thermodynamic models are developed to analyze the proposed system performance based on energy and exergy perspectives. In addition to, the thermal efficiencies of the solar field PTCs and S-CO_2 closed Bryton cycle combined with ORC power cycle as well as the overall combined system are evaluated. Moreover, the exergy efficiencies S-CO_2 closed Bryton cycle combined with ORC power cycle are also evaluated. The factor affected of the CSP design parameters and operating conditions on the performance of the CSP system are investigated. Such parameters are the Direct Normal Irradiance, Pressure ratio, Gas turbine inlet temperature, Turbine Efficiency, Compressor Efficiency, on the Power Plant are evaluated. In addition, the operating conditions, such as solar radiation intensity, PTCs solar field inlet temperature, and average ambient temperature, are also studied. The energy losses and the effect of the internal and external disturbance on the overall CSP energy efficiencies and exergy destructions on the power cycle and exergy efficiencies are investigated.

The present work results show that the energy efficiency of the PTC solar field is 67.8%. While the solar field input and output temperatures at 280°C, and 390°C, respectively. The proposed Parabolic Trough Solar Power Plant system analyses on the specific location of in Adigala, Somalia, Ethiopia and the total CSP plant targeted capacity is 1 MW electric output. The total collector area needed is found to be 8,963 m^2 based on SM of two. In the power cycle, maximum exergy destruction rate occurs in the heat exchanger one next to in the ORC evaporator is with about 192.8 kW and 80.3 kW respectively. The S-CO_2 closed Brayton cycle combined with the ORC power cycle achieved an energy efficiency of about 52.13 %. Thus, the overall combined CSP efficiency reached 13.7% at the pressure ratio of 2.5 and 850 W/m^2 solar radiation. Therefore the present work proposed cycle is better efficiency (13.7%) than Parabolic trough solar power

plant using carbon dioxide power cycle (12.0%) [1]. In case of higher solar radiation 950 W/m^2, the present work power plant is better efficiency (14.1%) while Parabolic trough collectors driven combined supercritical CO2 and organic Rankine cycle (12.87%) [26].

7.2 RECOMMENDATION

This present study forms a foundation and should be considered as a starting point for further studies. It is a basic development for a very promising technology which is the parabolic trough collector system. In the future with required developments and research, these systems can be more commercially viable. Suggestions to improve on this present modeling and simulation work are as follows:

- The current model does not include storage. Storage can be implemented to improve the availability of this system and shift electricity production closer to peak electricity demand.
- In future, if the detail parabolic solar trough exergy analyses are done it will give a better quality of the overall power plant.
- It would be interesting if a CSP power plant was modeled and analyses under the transient condition to get the relevant output of the overall power plant.
- It is interesting if experimental work is done to validate and improve the applicability of results obtained on during the investigations.
- Parabolic trough plants are capital-intensive projects and cost reduction should be investigated and improved.

APPENDIX A

A1. Adigala Calculated Data Sheet

a) Monthly Averages of Daily Mean Global and diffuse Radiation on the Horizontal Surface for Adigala,

n	Θ(rad)	Month	δ	tanδ	φ	tanφ	ωs=Acos(-tanφtanδ)	ωs (rad)	Ns	Isc	H (x10e+6)	a	b	H(bar) (x10e+6)	Hd bar (x10e+6)	Globale Radiation	Diffuse Dadiation
17	5.18	Jan	-20.94	-0.383	10.44	0.18	86.00	1.50	11.47	1367	37.58	0.3788	0.3711	25.36	7.14	1004.46	148.30
47	5.70	Feb	-13.01	-0.231			87.61	1.53	11.68		37.60	0.3866	0.3544	25.49	6.68	985.93	135.49
75	6.18	Mar	-2.49	-0.043			89.59	1.56	11.94		37.61	0.3315	0.4728	24.05	9.64	968.08	217.78
105	6.69	Apr	9.34	0.1644			91.78	1.60	12.24		37.61	0.3323	0.4711	24.08	9.60	968.87	216.79
135	7.21	May	18.74	0.3391			93.63	1.63	12.48		37.58	0.3410	0.4523	24.39	9.19	977.53	205.26
162	7.67	Jun	23.07	0.4257			94.54	1.65	12.61		37.56	0.3312	0.4734	24.01	9.64	866.86	317.74
198	8.29	Jul	21.23	0.3882			94.15	1.64	12.55		37.56	0.3141	0.5102	23.25	10.34	845.79	337.16
228	8.81	Aug	13.54	0.2407			92.59	1.62	12.34		37.59	0.3200	0.4976	23.54	10.12	853.96	331.12
258	9.33	Sep	2.33	0.0406			90.47	1.58	12.06		37.61	0.3139	0.5106	23.27	10.36	946.37	237.74
288	9.84	Oct	-9.49	-0.167			88.28	1.54	11.77		37.61	0.3310	0.4738	24.03	9.66	967.51	218.32
318	10.36	Nov	-18.84	-0.341			86.44	1.51	11.53		37.59	0.3824	0.3633	25.42	6.93	1006.25	142.40
344	10.81	Dec	-23.03	-0.425			85.56	1.49	11.41		37.57	0.3929	0.3408	25.54	6.28	1009.43	124.51

b) Monthly Average Daily Sunshine Duration in Adigala

Month	Jan	Feb	March	Apr	May	Jun	July	Aug	Sept	Octob	Nov	Dec
Sunshine hours	9.15	9.6	7.78	8	8.5	8.2	7.5	7	7.2	7.7	9.325	9.6

c) Monthly Ambient Temperature Pattern in Adigala, from 2012 to 2017 Years

Month	Jan	Feb	Mar	Apr	May	Jun	Jul	Aug	Sep	Oct	Nov	Dec
Tmax	23.6	28.8	30.2	28.8	29.8	35.4	39.6	41.2	39.3	39.2	33	25.1
Tmin	13.4	17.9	17.6	18.1	19.4	22.5	25.1	26.4	21	19.2	13.8	12.7
Tava	18.5	23.35	23.9	23.45	24.6	28.95	32.35	33.8	30.15	29.2	25.45	18.9

A.2 Monthly Average Hourly Beam Radiation on a Horizontal Surface

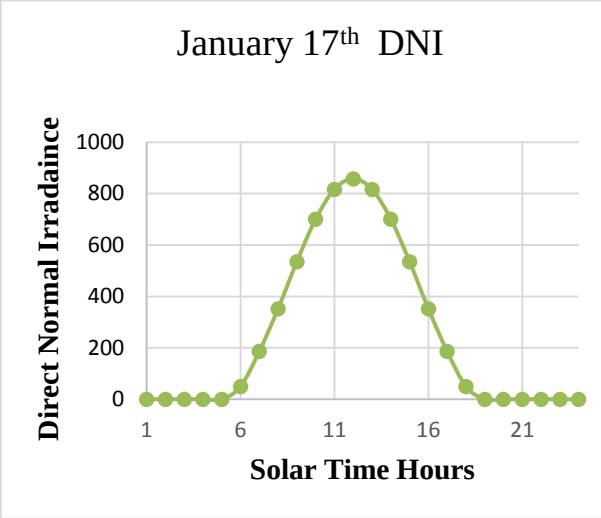

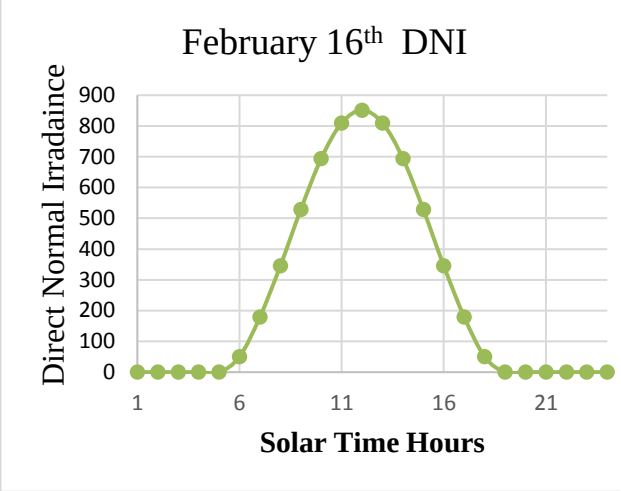

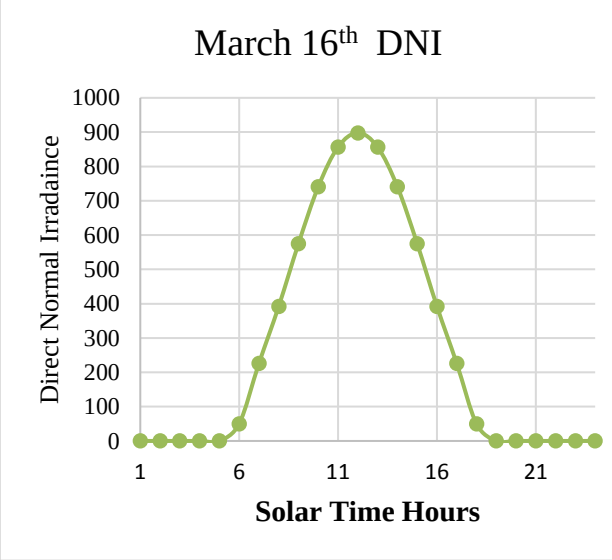

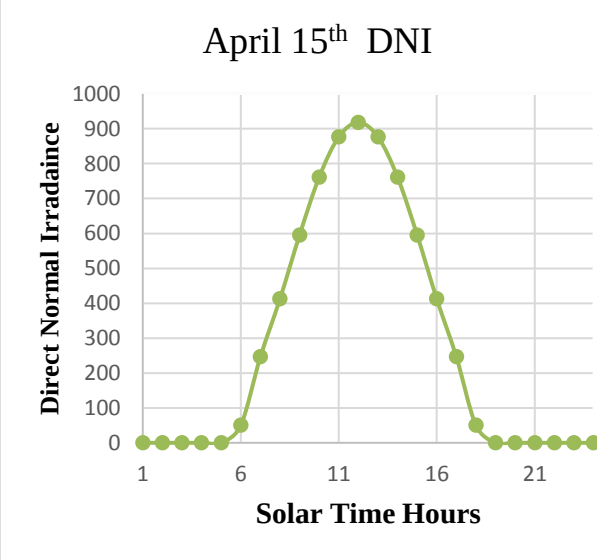

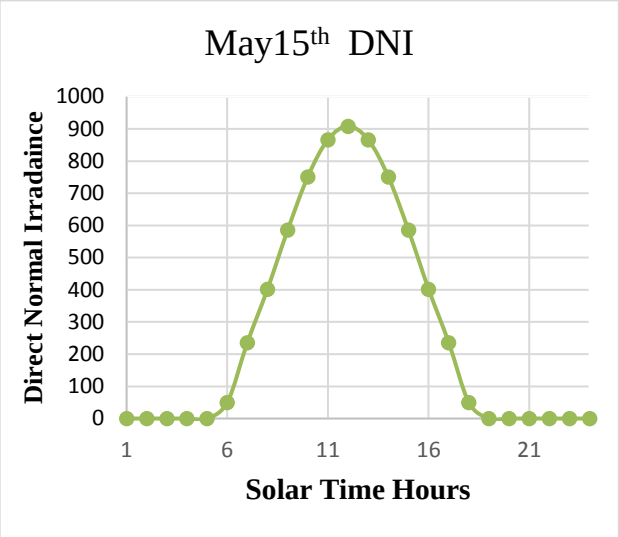
May15th DNI
Direct Normal Irradaince
1000
900
800
700
600
500
400
300
200
100
0
1
6
11
16
21
Solar Time Hours

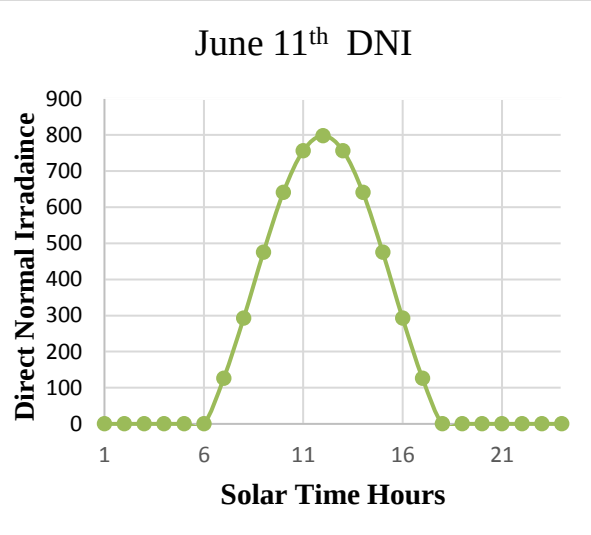
June 11th DNI
Direct Normal Irradaince
900
800
700
600
500
400
300
200
100
0
1
6
11
16
21
Solar Time Hours

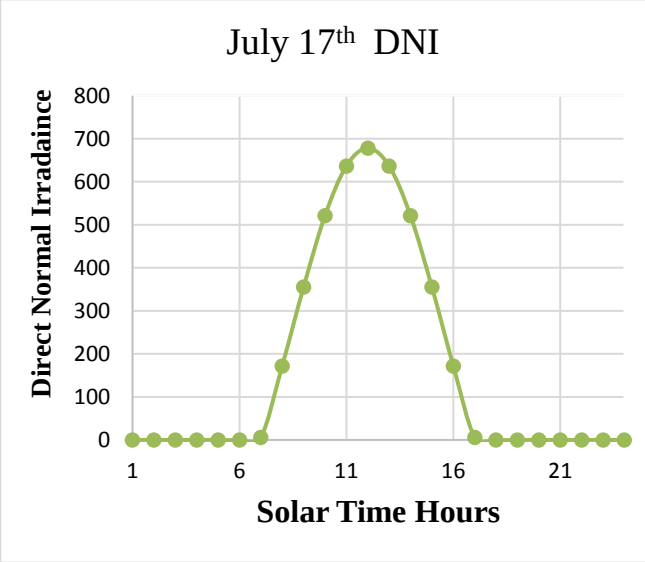
July 17th DNI
Direct Normal Irradaince
800
700
600
500
400
300
200
100
0
1
6
11
16
21
Solar Time Hours

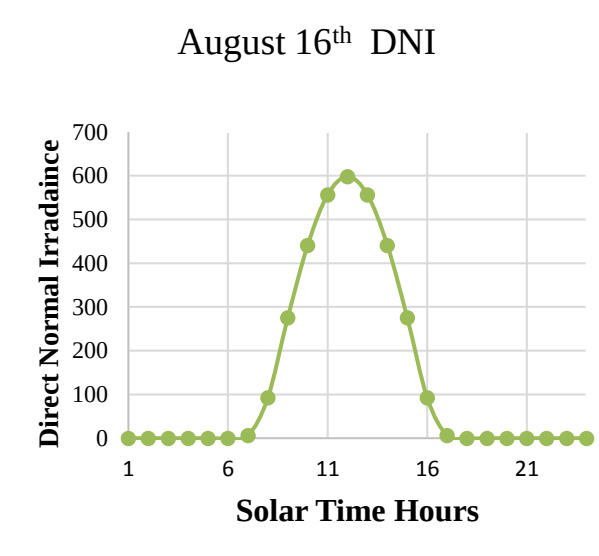
August 16th DNI
Direct Normal Irradaince
700
600
500
400
300
200
100
0
1
6
11
16
21
Solar Time Hours

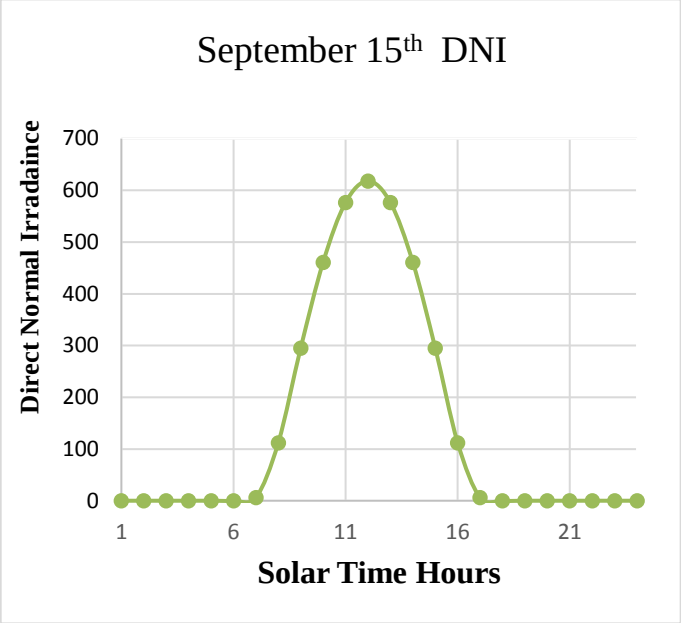
September 15th DNI
Direct Normal Irradiance
700
600
500
400
300
200
100
0
1
6
11
16
21
Solar Time Hours

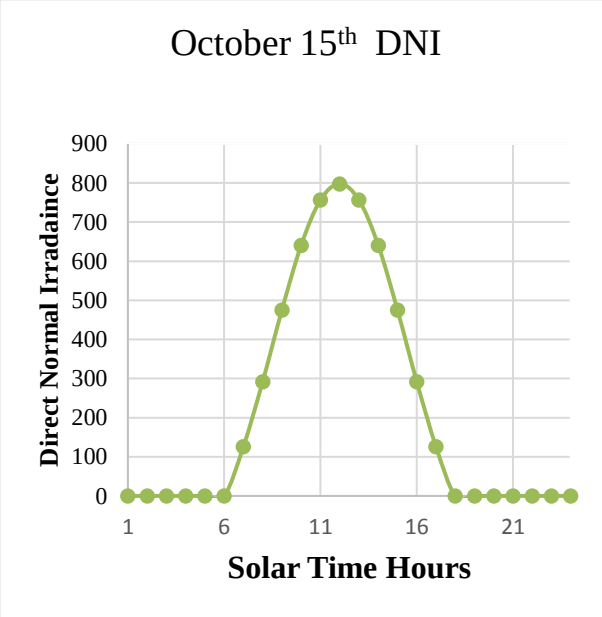
October 15th DNI
Direct Normal Irradiance
900
800
700
600
500
400
300
200
100
0
1
6
11
16
21
Solar Time Hours

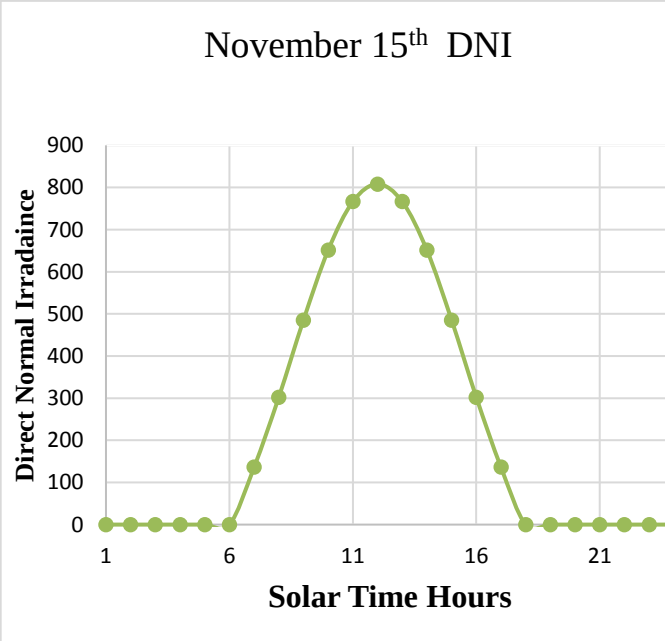
November 15th DNI
Direct Normal Irradiance
900
800
700
600
500
400
300
200
100
0
1
6
11
16
21
Solar Time Hours

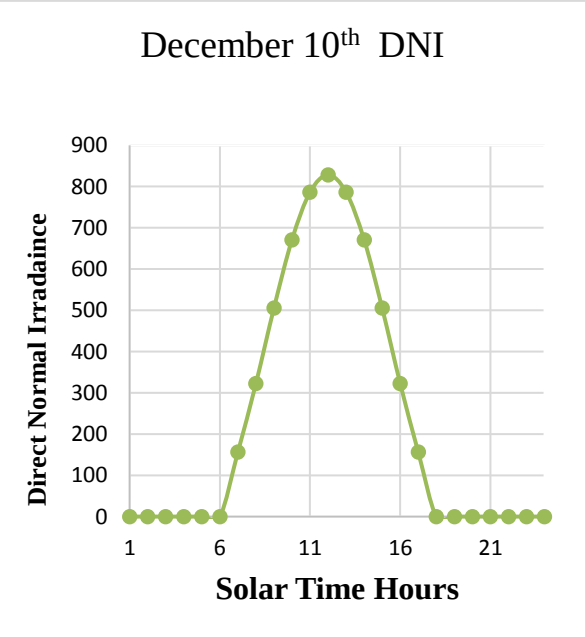
December 10th DNI
Direct Normal Irradiance
900
800
700
600
500
400
300
200
100
0
1
6
11
16
21
Solar Time Hours

APPENDIX B

FLUID PROPERTIES

B.1 VP-1 Properties

The VP-1 thermal oil properties are described Equation B.1 to Equation B.4 and represented in Figure B.1 to Figure B.4 [53].

Heat Capacity [kJ=kg · K]:

$Cp = 1.498+0.002414(T) + 5.9591\ e^{-6}\ (T)^2 - 2.9879e{-}8(T)3 + 4.4172e{-}11(T)^4$…..….……B.1

Density [kg=m3]:

$\rho = 1098.5 - 0.9729(T)$ ……...…..……..B.2

Enthalpy [kJ=kg]:

$h = -18.175 + 1.4968(T) + 0.0014(T)^2$ ……..……B.3

Viscosity [mPa s]:

$\mu = 179{:}43(T) - 1{:}167$……...B.4

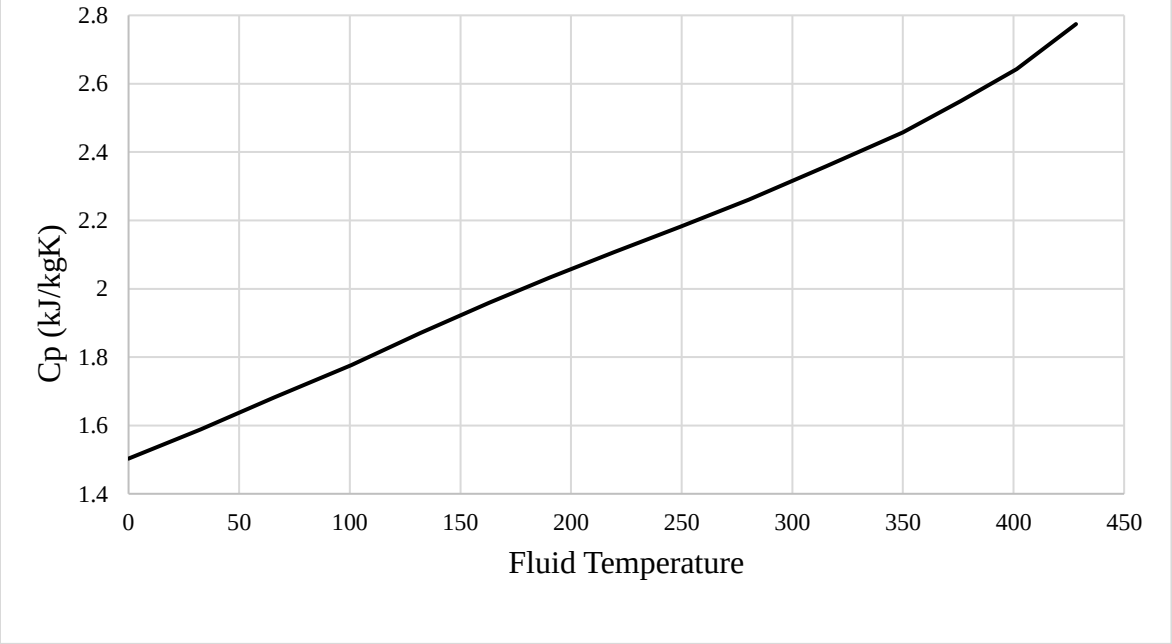

Figure B.1: Heat Capacity

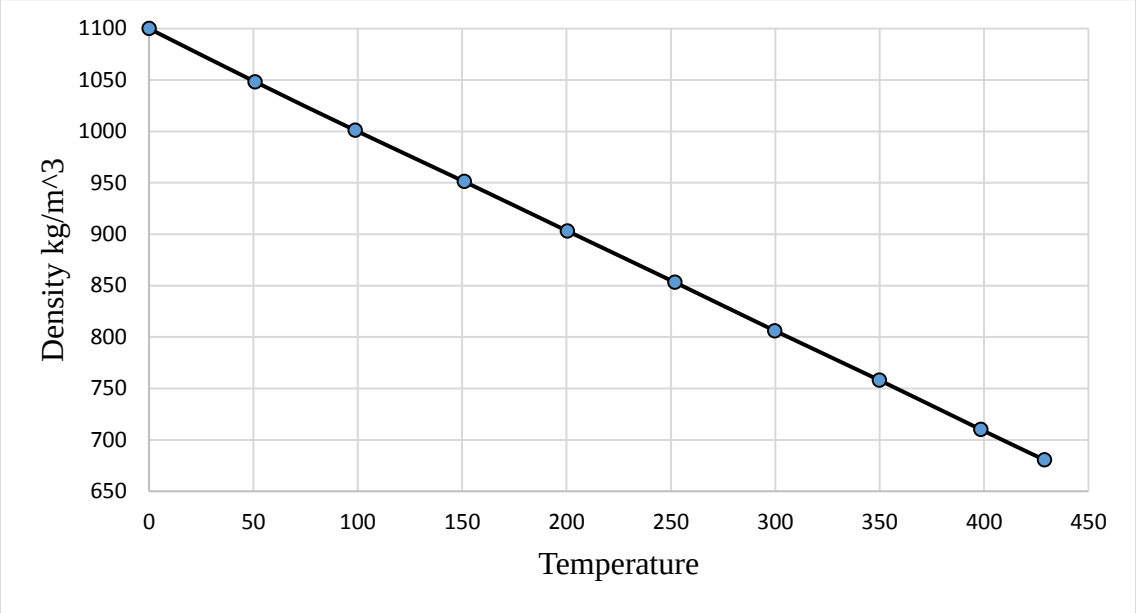

Figure B.2: Density

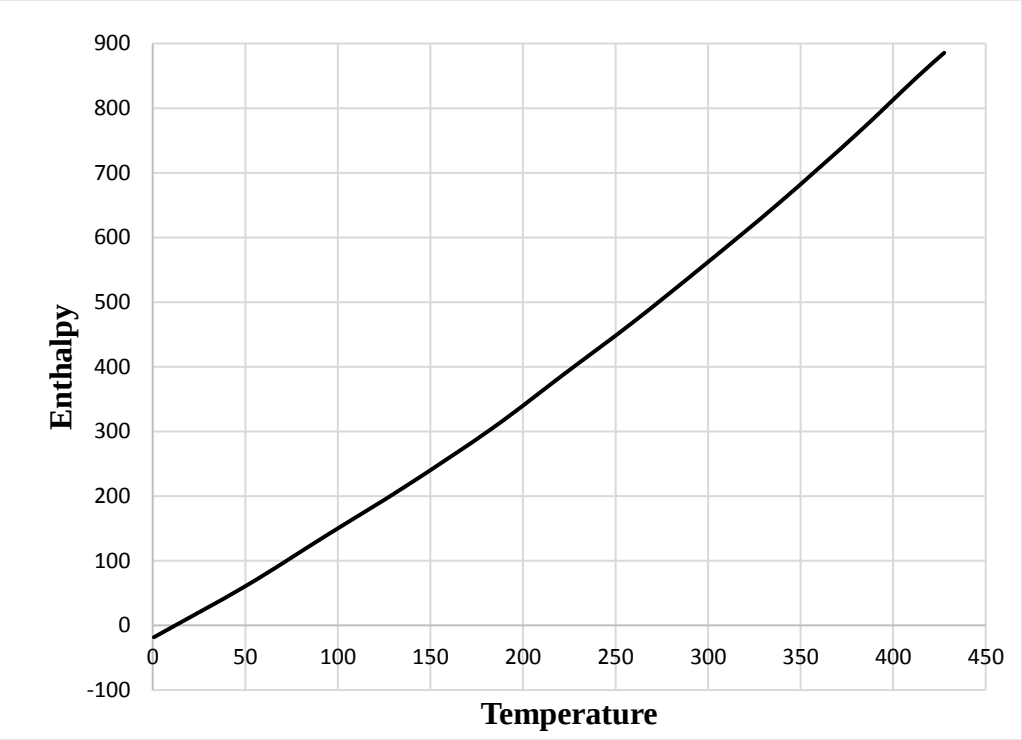

Figure B.3: Enthalpy

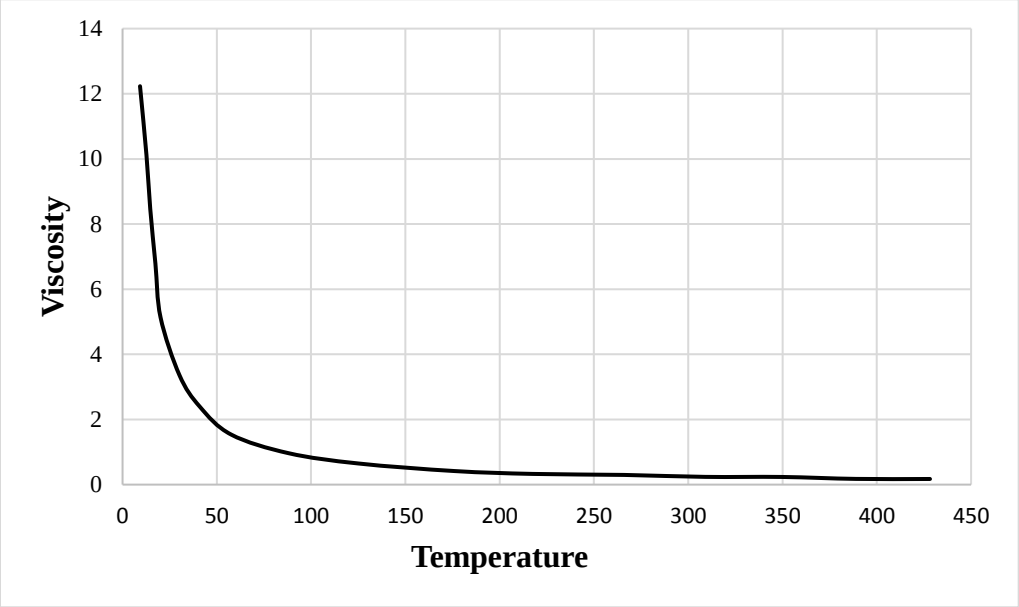

Figure B.4: Viscosity

B.2 S- CO2 Properties

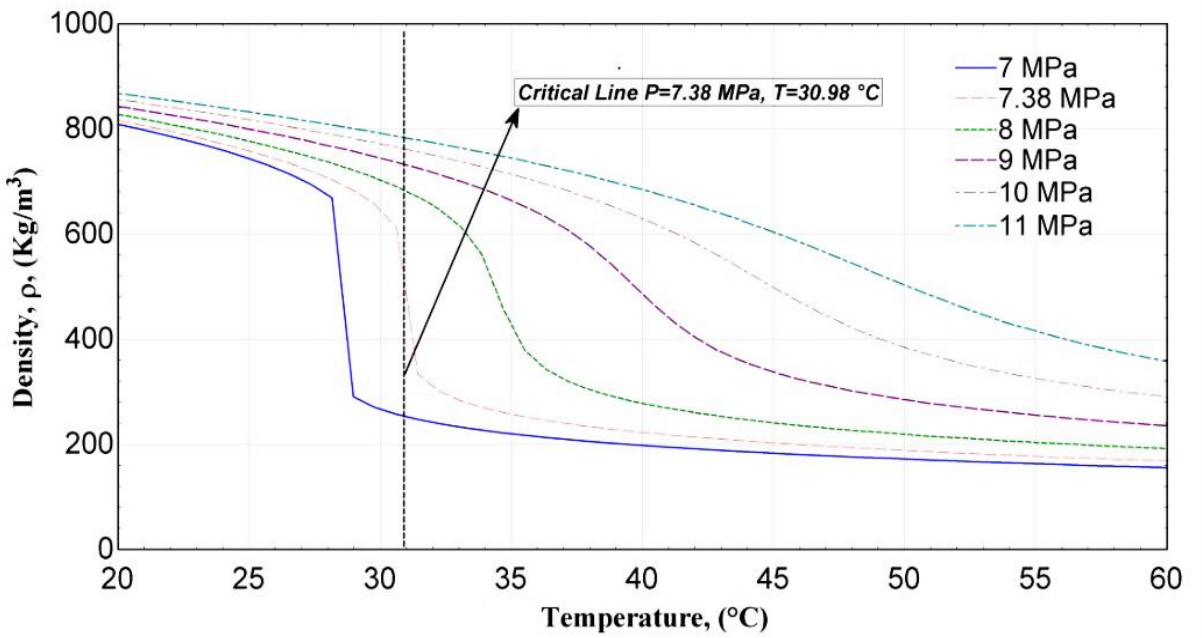

Figure B.2 CO_2 Density near Critical Point using REFPRO software

B.3 ORC R123 of Property

Table B.3 Properties of the ORC123 fluids used in this study

Working Fluid	T_{cr} (℃)	P_{cr}(MPa)	T_{tmax}(℃)
R-123	183.68	3.66	166.05

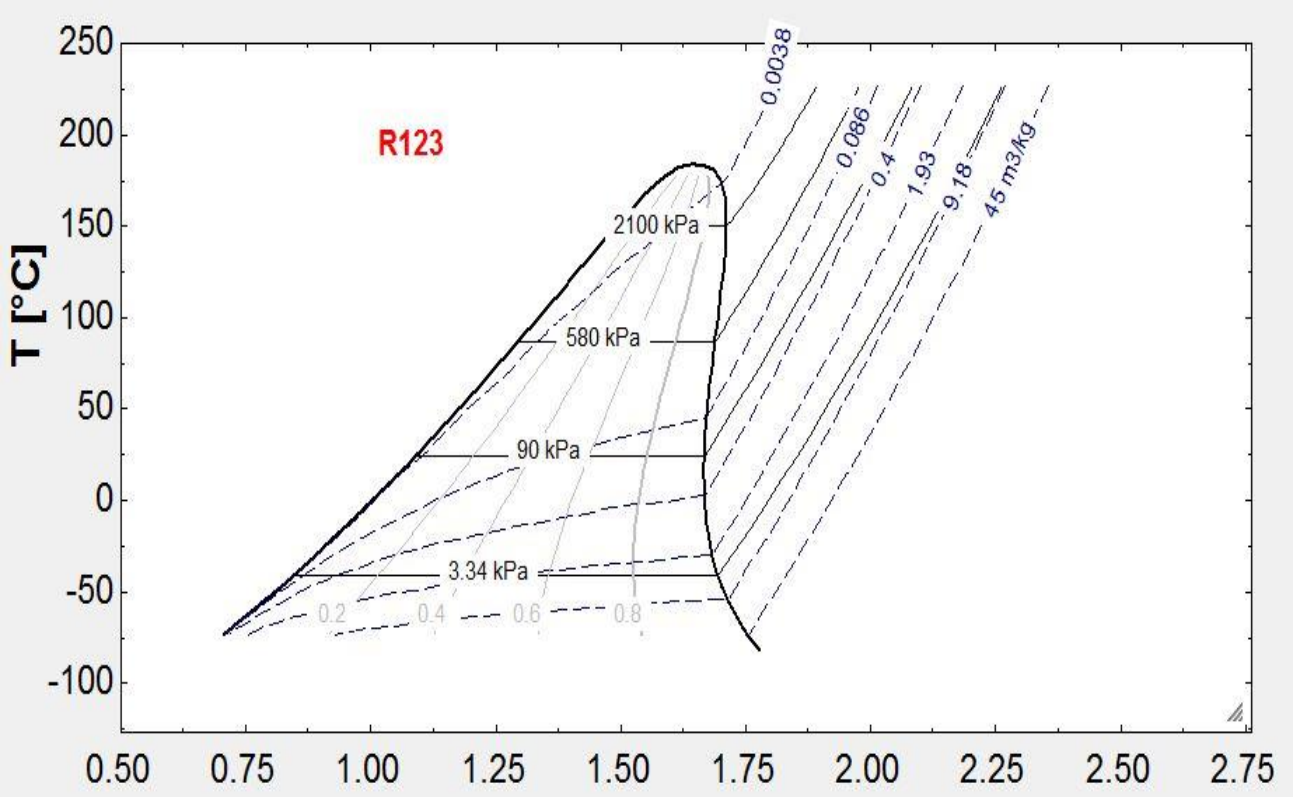

Figure B.3. Temperature vs Entropy of R-123 Organic Rankine fluid

APPENDIX C

The EES Code for parabolic solar trough Super Critical Carbon Dioxide Brayton Cycle combined ORC

C1. One-Dimensional Energy Balance Model Parabolic Solar Trough

"YOHANNES ALEMU PARABOLIC SOLAR TROUGH CODE AND SUPER CRITICAL CARBON DIOXIDE BRAYTON CYCLE COMBINED ORC "

"EES code of PTSC"

"Instruction:- Before go into ran the command code it needs to generate the lookup table for the property of Therminol VP1 heat transfer working fluid and Adin to the EES "

"Thermal model of parabolic trough solar collector PTSC"

"Preliminary Sizing"

"Input variables"

I_b =850 " the direct normal radiation W/m2 "

SM=2 "The solar multiplier"

eff_th_nom=0.35 " the nominal cycle efficiency"

eff_th_SF=0.75 "The nominal solar field efficiency"

Wpb_nom=1 "gross electrical power out put of both plants"

Q_SF=(Wpb_nom*SM)/eff_th_nom "solar field thermal output at design"

Qpb_nom=Q_SF/SM " thermal power required by the power block at the nominal "

Qin_nom=Q_SF/eff_th_SF "total incident thermal energy"

A_eff=(Qin_nom/I_b)*1000000 "the effective aperture area "

Function fq_12conv(T_1in, T_2, v_1in)

$COMMON D_2, v_1in, p_1in, T_o

{If(Fluid$='Therminol VP1') Then

If(T_1ave<12) or (400<T_1ave) Then CALL WARNING('The result may not be accurate, since water fluid properties are out of recommended temperature range: 12 C <T_1ave<400 C. See procedure pq_12conv. T_1ave=xxxA1',T_1ave)

EndIf}

"thermophysical properties for HTF"

```
RHO_1in:=Density(Therminol VP1,P=P_1in,T=T_1in) "[kg/m^3]"
MU_1 := viscosity(Therminol VP1,P=P_1in,T=T_1in) "[N-s/m^2]"
k_1 := conductivity(Therminol VP1, T=T_1in, P=P_1in) "[W/m-k]"
Cp_1in := CP(Therminol VP1, T=T_1in, P=P_1in) "[kJ/kg-k]"
Re_D2:=(RHO_1in*D_2*v_1in)/Mu_1
pr_1:=(Cp_1in*1000*Mu_1)/k_1
If(Re_D2<=2300) Then
Nu#_D2:=4.36
Else
Nu#_D2:=0.023*Re_D2^0.8*pr_1^0.4
EndIf
h_1:=Nu#_D2*k_1/D_2
fq_12conv:=h_1*D_2*PI*(T_2-T_1in)  "[w/m]"
END
FUNCTION fA_cs(D_2)
fA_cs := PI * (D_2 ^2 )/ 4 "[m^2]"
END
"pHCEdimensions"
PROCEDURE pHCEdimensions(CollectorType$: D_2, D_3, D_4, D_5,  L_aperture,
A_aperture)
$COMMON CollectorType$, A_aperture
if(CollectorType$='LS_3') Then
D_2:=0.066    "meter, inner diameter of the absorber"
D_3:=0.070     "meter, outer diameter of the absorber"
D_4:=0.114     "meter, inner diameter of the glass envelope"
D_5:=0.125     "meter, outer diameter of the glass envelope"
w:=5.76          "The parabolic reflector aperture m^2"
L_HCE := 4.1       "[m]"
```

```
L_aperture := 100 "[m]"

A_aperture := (w-D_5)*L_aperture "545" "[m^2]"

Number_HCE := 134

EndIf

END

"FUNCTION fq_34rad : Radiation heat transfer rate between the absorber surface and glazing

inner surface"

FUNCTION fq_34rad(T_3, T_4)

$COMMON D_3, D_4, L_aperture, T_o, sigma, EPSILON_3, EPSILON_4

fq_34rad := PI * D_3 * sigma * ((T_3 + T_o)^4 - (T_4 + T_o)^4) / (1 / EPSILON_3+ (D_3
/D_4) * ( 1 / EPSILON_4 - 1)) "[W/m]"

END

"Convective heat transfer rate from the glazing to the atmosphere"

FUNCTION fq_56conv(T_5, T_6)

$Common D_5, L_aperture, P_6, v_6, T_o

" Thermophysical Properties for air "

MU_6 := VISCOSITY(Air,T=T_6 ) "[N-s/m^2]"

k_6 := CONDUCTIVITY(Air,T=T_6) "[W/m-K]"

Rho_6 := DENSITY(Air,T=T_6, P=P_6) "[kg/m^3]"

Re_D5 := v_6 * D_5 * Rho_6 / MU_6

If(Re_D5<=1000) Then

Nu#_6 :=0.4+0.54*Re_D5^0.52

Else{EndIf

If (Re_D5 >1000) and (Re_D5<=5000) Then}

Nu#_6 :=0.3+0.54*Re_D5^0.6

EndIf

h_6 := Nu#_6 * k_6 / D_5 "[W/m^2-K]"

fq_56conv := h_6 * PI * D_5 * (T_5 - T_6) "[W/m]"
```

```
End

"FUNCTION fq_57rad : Radiation heat transfer rate between the glazing outer surface and the sky"

"FUNCTION fq_57rad(T_5, T_7)"

FUNCTION fq_57rad(T_5, T_7)

$COMMON EPSILON_4, D_5, L_aperture, sigma, T_o

fq_57rad := EPSILON_4 * PI * D_5 * sigma * ((T_5 + T_o)^4 - (T_7 + T_o)^4) "[W/m]"

END

"FUNCTION fk_23: Absorber conductance"

Function fq_23cond(T_3, T_2, k_23, D_3, D_2)

fq_23cond = 2 * PI * k_23* (T_3 - T_2) / (LN(D_3 / D_2) )"[W/m]"

End

Function fq_45cond(T_4, T_5)

$COMMON K_45, D_4, D_5

fq_45cond = 2 * PI * K_45 * (T_4 - T_5) /( LN(D_5 / D_4)) "[W/m]"

End

"FUNCTION fk_23(T_2, T_3)"

FUNCTION fk_23(T_2, T_3)

$COMMON AbsorberMaterial$, T_o T_23 := T_o+(T_2 + T_3)/2   [k]

If (AbsorberMaterial$ = '304L')

fk_23 := 0.013 * T_23 + 15.2   "[W/m-K]"

EndIf

If (AbsorberMaterial$ = '321H') Then

fk_23 := 0.0153 * T_23 + 14.775   "[W/m-K]"

EndIf

END

{FUNCTION fETA_Col(q_12conv, q_i)

fETA_Col := q_12conv/q_i
```

```
END}

"PROCEDURE pSelectiveCoatingProperties(T_3: EPSILON_3)"

PROCEDURE pSelectiveCoatingProperties(SelectiveCoating$,T_3:
EPSILON_3,TAU_envelope , Alpha_abs)

$COMMON SelectiveCoating$, T_o

" Do-Loop to calculate emissivity for all the HCE increments, and to return optical properties for
chosen selective coating type "

If (SelectiveCoating$ = 'Luz cerment') Then

TAU_envelope := 0.935

Alpha_abs := 0.92

EPSILON_3 := 0.08

Endif

END

"OpticalEfficiency of collector"

PROCEDURE pOpticalEfficiency(CollectorType$:OptEff_env,OptEff_abs)

$COMMON Reflectivity, TAU_envelope

If(CollectorType$='LS_3') Then

shadowing:=0.974

TrackingError:=0.994

GeomEffect:=0.92

rho_mirror_clean:=0.937

Dirt_mirror:=Reflectivity/rho_mirror_clean

Dirt_HCE:=(1+Dirt_mirror)/2

Error:=0.96          "miscellaneous factor"

EndIf

If(Dirt_mirror>1) Then

Dirt_mirror:=1

Dirt_HCE:=1

EndIf
```

```
OptEff_env:=shadowing*TrackingError*GeomEffect*rho_mirror_clean*Dirt_mirror*Dirt_HCE
*Error

OptEff_abs:=OptEff_env*TAU_envelope

END

"Heat loss"

FUNCTION fHeatLoss( q_56conv, q_57rad)

fHeatLoss := q_56conv + q_57rad "[W/m]"

END

FUNCTION fq_5SolAbs(q_i)

$COMMON Alpha_env, OptEff_env

fq_5SolAbs := q_i * OptEff_env * Alpha_env "[W/m]"

End

PROCEDURE Pq_56conv(q_45cond, q_5SolAbs, q_57rad: q_56conv)

q_56conv := q_45cond+ q_5SolAbs - q_57rad "[W/m]"

END

CALL pHCEdimensions(CollectorType$: D_2, D_3, D_4, D_5,  L_aperture, A_aperture)

{CALL Pq_45cond(q_34rad: q_45cond)}

CALL pSelectiveCoatingProperties(SelectiveCoating$ ,T_3: EPSILON_3, TAU_envelope ,
Alpha_abs)

CALL pOpticalEfficiency(CollectorType$:OptEff_env,OptEff_abs)

CALL Pq_56conv(q_45cond, q_5SolAbs, q_57rad: q_56conv)

q_12conv=fq_12conv(T_1in, T_2, v_1in)

q_34rad = fq_34rad(T_3, T_4)

 A_cs = fA_cs(D_2)

q_45cond = fq_45cond(T_4, T_5)

q_56conv = fq_56conv(T_5, T_6)

q_57rad = fq_57rad(T_5, T_7)

q_23cond = fq_23cond(T_3, T_2, k_23, D_3, D_2)

 k_23 =  fk_23(T_2, T_3)
```

```
{ETA_Col = fETA_Col(q_12conv, q_i)}

HeatLoss = fHeatLoss( q_56conv, q_57rad)

q_5SolAbs = fq_5SolAbs(q_i) "[W/m]"

"Energy Balance"

q_12conv = q_23cond

q_3SolAbs = q_23cond + q_34rad

q_34rad = q_45cond

q_i = I_b * A_aperture / L_aperture "[W/m]"

q_3SolAbs = q_i * OptEff_abs * Alpha_abs "[W/m]"

DELTAL = L_aperture/imax "[m]"

imax= 545

T_1in=280

p_1in=4000

I_b = 850 "beam radiation"

m_dot =8  "mass flow rate "

alpha_env=0.02   "[absorbtivity of glass]"

Reflectivity=0.94  "0.93 for Luz_3"

CollectorType$='LS_3'

AbsorberMaterial$ = '304L'

SelectiveCoating$ = 'Luz cerment'

"v_1in = v_1volm / (A_cs) "[m/s]""

T_o=273.15

T_6 = 28.2;  T_7 = T_6  - 8

EPSILON_4 = 0.86

sigma=5.67E-8     "[w/m^2-k^4]"

P_6 = 76.757 [kPa]

v_6 = 0.8 [m/s]

k_45=1.04          "[thermal condactivity of glass W/m_k]"
```

```
m_dot = v_1in * RHO_1in * A_cs "[kg/s]"

RHO_1in = Density(Therminol VP1, T=T_1in, P=P_1in) "[kg/m^3]"

"Duplicate i = 1, (imax-1)"

T_1in[1] = T_1in   "[k]"

v_1in[1] = v_1in     "[m/s]"

Duplicate i = 1, (imax-1)

T_1in[i+1] = T_1out[i] "[C]"

v_1in[i+1] = v_1out[i] "[m/s]"

RHO_1in[i+1] = RHO_1out[i]

End

Duplicate i = 1,imax

L[i]=i*DELTAL

v_1ave[i] = (v_1in[i] + v_1out[i])/2 "[m/s]"

pr_1[i] =(Cp_1in[i]*1000*Mu_1[i])/k_1[i]

MU_1[i] = viscosity(Therminol VP1,P=P_1in,T=T_1in[i]) "[N-s/m^2]"

k_1[i] = conductivity(Therminol VP1, T=T_1in[i], P=P_1in) "[W/m-k]"

v_1out[i] = m_dot / (RHO_1out[i] * A_cs) "[m/s]"

" Outlet HTF temperature for each increment "

m_dot *Cp_1in[i]*1000*(T_1out[i] - T_1in[i]) = (q_5SolAbs + q_3SolAbs - HeatLoss[i] )*
DELTAL

Cp_1in[i] = Cp(Therminol VP1,T=T_1in[i], P=P_1in)

RHO_1out[i] = Density(Therminol VP1, T=T_1out[i], P=P_1in) "[kg/m^3]"

HeatLoss[i] = fHeatLoss( q_56conv[i], q_57rad[i]) "[W/m]"

q_12conv[i] = fq_12conv(T_1in[i], T_2[i], v_1in[i])

q_34rad[i] = fq_34rad(T_3[i], T_4[i])

q_45cond[i] = fq_45cond(T_4[i], T_5[i])

q_56conv[i] = fq_56conv(T_5[i], T_6)

q_57rad[i] = fq_57rad(T_5[i], T_7)
```

```
q_23cond[i] = fq_23cond(T_3[i], T_2[i], k_23[i], D_3, D_2)
 k_23[i] =  fk_23(T_2[i], T_3[i])
q_12conv[i] = q_23cond[i]
q_3SolAbs = q_23cond[i] + q_34rad[i]
q_34rad[i] = q_45cond[i]
CALL Pq_56conv(q_45cond[i], q_5SolAbs, q_57rad[i]: q_56conv[i])
{ETA_Col[i] = fETA_Col(q_12conv[i], q_i)}
End
EffectOptEff = (OptEff_abs * Alpha_abs + OptEff_env * Alpha_env)
q_heat_gain = SUM((q_12conv[i] /1000 ), i=1,imax)
q_HeatLoss_ApertureLength = SUM((HeatLoss[j] /1000), j=1, imax)

"=================================================================="
```

C2. " On the other hand, we can calculate without using function and look up table by taking the average constant parameters based on National Renewable Energy Laboratory Technical Report NREL/TP-550-45633 May 2009 it includes experimental work and mathematical modeling are using "

" constant input parameters of the receiver"

D[2]=0.066; "meter, inner diameter of the absorber"

D[3]=0.07; "meter, outer diameter of the absorber"

D[4]=0.114; "meter, inner diameter of the glass envelope"

D[5]=0.125; "meter, outer diameter of the glass envelope"

L=1; " meter, length of the collecto"

In=0.48; "intercept factor"

E_glass=0.89 "emissivety of glass "

TRS_glass =0.96; "the glass envelope of transmittance"

ABS_abs =0.96; "absorbance of the absorber"

ABS_glass =0.02; "Absorptance of the glass envelope"

eff_opt=0.75 "the optical efficiency at normal incidence "

Ap=5.75 "The parabolic reflector aperture m^2"

SM=2 "The solar multiplier"

eff_th_nom=0.35 " the nominal cycle efficiency"

eff_th_SF=0.75 "The nominal solar field efficiency"

Wpb_nom=1 "gross electrical power out put of both plants"

"Input variables"

Ib=950 " the direct normal radiation W/m2 "

IAD=0 "the incidence angle, degrees"

IAM =1 "the incidence angle modifier"

U[5]=5; "m/s, wind speed"

Ta=25; "C ambient temperature"

Tgout=40[C]; "C outer glass temperature"

Tsky=(Ta-8); "C sky temperature"

"Tin=280 in let temperature of the fluid "

m_dot=8[kg/s] "massflow rate "

"Preliminary Sizing"

"Q_SFQ_SF=(Wpb_nom*SM)/eff_th_nom

Qpb_nom=Q_SF/SM

Qin_nom=Q_SF/eff_th_SF

A_eff=(Qin_nom/Ib)*1000000"

"Thermal Model"

"HCE heat loss model and sensitivity study"

Q_solabs=Ib*cos(IAD)*Ap*eff_opt*IAM "The concentrated solar radiation absorbed by the absorber tube W/m"

Q_solabs&glass=(Ib*cos(IAD)*Ap*IAM*ABS_glass*eff_opt)/(TRS_glass*ABS_abs) "the absorption of a small amount of insolation by the glass envelope" "HCE heat loss model and sensitivity study"

"T[inabs]=The inner absorber surface temperatures "

"T[outabs]= The outer absorber surface temperatures "

"T[ingl]=The inner glass surface temperatures, °C."

"The heat transferred from the glass envelope to the environment through radiation and convection "

q_56conv=Pi*D[5]*h_56*(Tgout-Ta) "Heat Transfer from the Glass to the ambient"

h_56=4.9+4.9*U[5]-0.18*U[5]^2 "convective heat transfer coefficient "

sigma=5.67E-08 " the Stefan-Boltzmann constant "

q_56rad =sigma*E_glass*Pi*D[5]*((Tgout+273)^4-(Tsky+273)^4) "Radiation heat transfer from outer glass to sky"

q_loss=q_56conv+q_56rad

x=ln(D[5]/D[4])

q_45cond=(2*Pi*K_glass*(Tingl-Tgout))/x "Heat Transfer from the glass to the Glass Envelope by conduction"

K_glass=1.1

q_45cond+Q_solabs&glass=q_loss

"The heat transferred across the evacuated annulus from the outer absorber surface to the inner glass surface through radiation "

E_abs=0.093 "emissivety of absoreber"

E_ratio=(1/E_abs+((1-E_glass)/E_glass)*(D[3]/D[4])) "emissivity ratio"

q_34rad=sigma*Pi*D[3]*((Toutabs+273)^4-(Tingl+273)^4)/E_ratio "Heat Transfer from the Absorber to the Glass Envelope by radiation"

q_34rad=q_45cond

"The heat transferred through the absorber from the outer absorber surface to the inner absorber surface by conduction (W/m). "

q_23cond=(2*Pi*k[23]*(Toutabs-Tinabs))/ln(D[3]/D[2]) "Conduction Heat Transfer through the Absorber Wall"

T[23]=300

k[23]=(0.0153*T[23])+14.775

"The heat transferred to the HTF from the inner absorber surface through convection (W/m). "

q_12conv=h_1*D[2]*Pi*(Tinabs-Tin) "Convection Heat Transfer between the HTF and the Absorber"

h_1=522+478*m_dot

Tin=280[C] " (Therminol VP1, 6.6 cm inner diameter absorber, average HTF temperature of 340°C) "

Q_solabs=q_23cond+q_34rad

Tout=Tin+(q_12conv/(m_dot*cp))*150 "the HTF temperature leaving the 1 meter section "

Cp=1494+2.76*Tin

"{eff=q_12conv/Qin_nom}"

"=="

EPSILON= mass_flow_rate_Co2*cp (T[6]-T[5])/ m_dot*cp (T[19]-T[5])

C3. Super Critical Carbon Dioxide Brayton Cycle combined ORC

"Instruction:- after ran the EES program you should have to change the enthalpy and entropy of S-CO_2 based on the given temperature and pressure by using REFFPRO software "

"Thermodynamics Power plant Input variables"

"The unit of the temperature and pressure are ℃ and kPa respectively"

T[1]=32

T[6]=380

P[1]=10000

P[2]=14000

P[7]=19600

eta_Pump=0.9

P[13]=786.8

T[11]=27

P[11]=154.7

eta_precompressor=0.89

eta_recompressor=0.89

eta_HPturbine=0.90

eta_LPturbine=0.90

eta_turbineORC1 =0.85

Recuperator=0.8

P_ratio=2.5

EPSILON=0.8

mass_flow_rate_Co2=12

mass_flow_rate_ORC=30

Qin_nom= 7618 [kW]

"=="

"ENVIROMENTAL CONDITION"

T[0]=28 "reference temperature in adigala "

```
P[0]=101.2 "reference pressure in adigala  "
H[0]=Enthalpy(CarbonDioxide,T=T[0],P=P[0])  "reference enthalpy in adigala  "
S[0]=Entropy(CarbonDioxide,T=T[0],P=P[0])    "reference entropy  in adigala "
"state 1" "Inlet to Precompressor"
h[1]=ENTHALPY(CarbonDioxide,T=T[1],P=P[1])
s[1]=ENTROPY(CarbonDioxide,T=T[1],P=P[1])
E[1]=(h[1]-H[0])-T[0]*(s[1]-S[0])
"state 2" "Inlet to Intercooler"
s_s[2]=s[1]
T_s[2]=TEMPERATURE(CarbonDioxide,s=s_s[2],P=P[2])
h_s[2]=ENTHALPY(CarbonDioxide,T=T_s[2],P=P[2])
eta_precompressor=(h_s[2]-h[1])/(h[2]-h[1])
T[2]=temperature(CarbonDioxide,h=h[2],P=P[2])
s[2]=entropy(CarbonDioxide,T=T[2],P=P[2])
E[2]=(h[2]-H[0])-T[0]*(s[2]-S[0])
"state 3" "Inlet to Recompressor"
P[3]=P[2]
T[3]=T[1]
h[3]=ENTHALPY(CarbonDioxide,T=T[3],P=P[3])
s[3]=ENTROPY(CarbonDioxide,T=T[3],P=P[3])
E[3]=(h[3]-H[0])-T[0]*(s[3]-S[0])
"state 4" "Inlet to Regenerator"
s_s[4]=s[3]
P_ratio=P[4]/P[1]
T_s[4]=TEMPERATURE(CarbonDioxide,s=s_s[4],P=P[4])
h_s[4]=ENTHALPY(CarbonDioxide,T=T_s[4],P=P[4])
eta_recompressor=(h_s[4]-h[3])/(h[4]-h[3])
T[4]=TEMPERATURE(CarbonDioxide,h=h[4],P=P[4])
```

s[4]=ENTROPY(CarbonDioxide,T=T[4],P=P[4])

E[4]=(h[4]-H[0])-T[0]*(s[4]-S[0])

"state 5" "Inlet to Combustor"

P[5]=P[4]

EPSILON= (h[5]-h[4])/(h[9]-h[4])

h[5]=ENTHALPY(CarbonDioxide,T=T[5],P=P[5])

s[5]=ENTROPY(CarbonDioxide,T=T[5],P=P[5])

E[5]=(h[5]-H[0])-T[0]*(s[5]-S[0])

"State 6" "Inlet to High Pressure Turbine"

P[6]=P[4]

s[6]=ENTROPY(CarbonDioxide,T=T[6],P=P[6])

h[6]=ENTHALPY(CarbonDioxide,T=T[6],P=P[6])

E[6]=(h[6]-H[0])-T[0]*(s[6]-S[0])

"State 7" "Inlet to Reheater"

s_s[7]=s[6]

T_s[7]=TEMPERATURE(CarbonDioxide,s=s_s[7],P=P[7])

h_s[7]=ENTHALPY(CarbonDioxide,T=T_s[7],P=P[7])

eta_HPturbine=(h[7]-h[6])/(h_s[7]-h[6])

T[7]=TEMPERATURE(CarbonDioxide,h=h[7],P=P[7])

s[7]=ENTROPY(CarbonDioxide,T=T[7],P=P[7])

E[7]=(h[7]-H[0])-T[0]*(s[7]-S[0])

"State 8" "Inlet to Low Pressure Turbine "

T[8]=T[6]

P[8]=P[7]

s[8]=ENTROPY(CarbonDioxide,T=T[8],P=P[8])

h[8]=ENTHALPY(CarbonDioxide,T=T[8],P=P[7])

E[8]=(h[8]-H[0])-T[0]*(s[8]-S[0])

"State 9" "Outlet of Low Pressure Turbine"

```
s_s[9]=s[8]
P_ratio=P[6]/P[9]
T_s[9]=TEMPERATURE(CarbonDioxide,s=s_s[9],P=P[9])
h_s[9]=ENTHALPY(CarbonDioxide,T=T_s[9],P=P[9])
eta_LPturbine=(h[9]-h[8])/(h_s[9]-h[8])
T[9]=TEMPERATURE(CarbonDioxide,h=h[9],P=P[9])
s[9]=ENTROPY(CarbonDioxide,T=T[9],P=P[9])
E[9]=(h[9]-H[0])-T[0]*(s[9]-S[0])
"state 10" "Regenerator Outlet"
P[10]=P[1]
h[4]+h[9]=h[5]+h[10]
T[10]=Temperature(CarbonDioxide,h=h[10],P=P[10])
s[10]=Entropy(CarbonDioxide,T=T[10],P=P[10])
E[10]=(h[10]-H[0])-T[0]*(s[10]-S[0])
"========================================================="
"ORC CYCLE "
H[15]=Enthalpy(R123,T=T[0],P=P[0]) " reference point of the local site "
S[15]=Entropy(R123,T=T[0],P=P[0]) " reference point of the local site "
"state11"  " inlet to the pump ORC 1"
H[11]=Enthalpy(R123,P=P[11],T=T[11])
S[11]=Entropy(R123,P=P[11],T=T[11])
V=Volume(R123,T=T[11],P=P[11])
E[11]=(H[11]-H[15])-T[0]*(S[11]-S[0])
"State 12 inlet to the evaporator "
P[12]=P[13]
WPs1=V*(P[13]-P[11])
H_s[12]=H[11]+V*(P[13]-P[11])
eta_Pump=(H_s[12]-H[11])/(H[12]-H[11])
```

```
S[11]=S_s[12]
S[12]=Entropy(R123,P=P[12],H=H[12])
T[12]=Temperature(R123,P=P[12],H=H[12])
E[12]=(H[12]-H[15])-T[0]*(S[12]-S[0])
"State 13 inlet to the turbine"
EPSILON=(h[13]-h[12])/(h[10]-h[12])
H[13]=Enthalpy(R123,T=T[13],P=P[13])
S[13]=Entropy(R123,T=T[13],P=P[13])
E[13]=(H[13]-H[15])-T[0]*(S[13]-S[0])
"State 14 inlet to the turbine"
P[11]=P[14]
S[13]=S_s[14]
H_s[14]=Enthalpy(R123,S=S_s[14],P=P[14])
eta_turbineORC1=(H[13]-H[14])/(H[13]-H_s[14])
T[14]=Temperature(R123,P=P[14],H=H[14])
S[14]=Entropy(R123,H=H[14],P=P[14])
E[14]=(H[14]-H[15])-T[0]*(S[14]-S[0])
"=========================================================="
"Energy Balance Equations"
w_out_HPturbine_co2=abs(h[7]-h[6])*12
w_out_LPturbine_co2 =abs(h[9]-h[8])*12
w_out_co2=w_out_HPturbine_co2+w_out_LPturbine_co2
w_in_precompressor_co2=abs(h[2]-h[1])*12
w_in_recompressor_co2=abs(h[4]-h[3])*12
w_in_co2=w_in_precompressor_co2+w_in_recompressor_co2
w_net_co2=w_out_co2-w_in_co2
q_in_combustor_co2=abs(h[6]-h[5])*12
q_in_reheater_co2=abs(h[8]-h[7])*12
```

```
q_in_co2=q_in_combustor_co2+q_in_reheater_co2
q_out_intercooler_co2=abs(h[2]-h[3])*12
q_out_reg_co2=abs(h[7]-h[6])*12
q_out_precooler_co2=abs(h[10]-h[1])*12
q_out_co2=q_out_intercooler_co2+q_out_reg_co2+q_out_precooler_co2
w_out_ORC_turbine=(h[13]-h[14])*30
w_in_ORC_pump=(h[12]-h[11])*30
w_net_ORC= w_out_ORC_turbine
W_NET_TOTALE= w_net_co2 + w_net_ORC
"=================================================="
"Exergy Balance Equations"
w_out_HPturbine_EX=abs(E[7]-E[6])*12
w_out_LPturbine_EX=abs(E[9]-E[8])*12
w_out_EX=w_out_HPturbine_EX+w_out_LPturbine_EX
w_in_precompressor_EX=abs(h[2]-h[1])*12
w_in_recompressor_EX=abs(E[4]-E[3])*12
w_in_EX=w_in_precompressor_EX+w_in_recompressor_EX
w_net_EX=w_out_EX-w_in_EX
q_in_combustor_EX=abs(E[6]-E[5])*12
q_in_reheater_EX=abs(E[8]-E[7])*12
q_in_EX=q_in_combustor_EX+q_in_reheater_EX
q_out_intercooler_EX=abs(E[2]-E[3])*12
q_out_reg_EX=abs(E[7]-E[6])*12
q_out_precooler_EX=abs(E[10]-E[1])*12
q_out_EX=q_out_intercooler_EX+q_out_reg_EX+q_out_precooler_EX
w_out_ORC_turbine_EX=(E[13]-E[14])*30
w_in_ORC_pump_EX=(E[12]-E[11])*30
w_net_ORC_EX= w_out_ORC_turbine_EX - w_in_ORC_pump_EX
```

"Thermal Efficiency"

Eta_th=W_NET_TOTALE/q_in_co2

Eta_th_CO2=w_net_co2/q_in_co2

"EXERGY Efficiency"

Eta_ex=W_NET_TOTALE/q_in_EX

"over all thermal efficiency"

over_all_eff =W_NET_TOTALE/ Qin_nom

REFERENCE

[1] A. A. Alzahrani and I. Dincer, "Energy and exergy analyses of a parabolic trough solar power plant using carbon dioxide power cycle," *Energy Convers. Manag.*, vol. 158, no. September 2017, pp. 476–488, 2018.

[2] M. Mesfin, "Modeling , Simulation and Performance Evaluation of Parabolic Trough Solar Collector Power Generation System," no. September, 2009.

[3] *Solar Energy Engineering - Processes and Systems 2009*. 2009.

[4] A. Baghernejad and M. Yaghoubi, "Energy , exergy and second law performance of parabolic Trough collector integration into combined cycle system (ISCCS)," pp. 1–6, 2009.

[5] E. N. E. P. (2ND DRAFT), "Table of Contents," *Ethiop. Natl. ENERGY POLICY (2ND Draft.*, 2013.

[6] S. T. Teferie and A. Assefa, "Addis Ababa Institute of Technology School of Graduate Studies Energy Center Simulation of Parabolic Trough Concentrating Solar Power Generation System Addis Ababa Institute of Technology School of Graduate Studies Energy center," no. April, 2014.

[7] R. Dang and S. K. Mangal, "Energy & Exergy Analysis of Thermal Power Plant at Design and Off Design Load," vol. 3, no. 5, pp. 29–36, 2016.

[8] C. Xu, Z. Wang, X. Li, and F. Sun, "Energy and exergy analysis of solar power tower plants," *Appl. Therm. Eng.*, vol. 31, no. 17–18, pp. 3904–3913, 2011.

[9] S. M. Besarati, "Analysis of Advanced Supercritical Carbon Dioxide Power Cycles for Concentrated Solar Power Applications," 2014.

[10] F. A. Al-sulaiman, "Exergy analysis of parabolic trough solar collectors integrated with combined steam and organic Rankine cycles," *ENERGY Convers. Manag.*, vol. 77, pp. 441–449, 2014.

[11] W. Vogel and H. Kalb, *The Potential of Solar Thermal Power Plants for the Energy Supply : Capacity Factor , Availability of Solar Energy , and Land Availability*. 2010.

[12] S. Thermal and P. Systems, *10 10.1*. 2014.

[13] S. Kuravi, J. Trahan, D. Y. Goswami, M. M. Rahman, and E. K. Stefanakos, "Thermal energy storage technologies and systems for concentrating solar power plants," *Prog. Energy Combust. Sci.*, vol. 39, no. 4, pp. 285–319, 2013.

[14] G. Cinti, A. Baldinelli, A. Di, and U. Desideri, "Integration of Solid Oxide Electrolyzer and Fischer-Tropsch : A sustainable pathway for synthetic fuel," *Appl. Energy*, vol. 162, pp. 308–320, 2016.

[15] S. Hou, Y. Wu, Y. Zhou, and L. Yu, "Performance analysis of the combined supercritical CO 2 recompression and regenerative cycle used in waste heat recovery of marine gas turbine," *Energy Convers. Manag.*, vol. 151, no. August, pp. 73–85, 2017.

[16] R. Chacartegui, J. M. M. De Escalona, D. Sánchez, B. Monje, and T. Sánchez, "Alternative cycles based on carbon dioxide for central receiver solar power plants," *Appl. Therm. Eng.*, vol. 31, no. 5, pp. 872–879, 2011.

[17] M. K. Gupta and S. C. Kaushik, "Exergy analysis and investigation for various feed water heaters of direct steam generation solar – thermal power plant," *Renew. Energy*, vol. 35, no. 6, pp. 1228–1235, 2010.

[18] E. Bellos, C. Tzivanidis, and K. A. Antonopoulos, "A detailed working fluid investigation for solar parabolic trough collectors," *Appl. Therm. Eng.*, 2016.

[19] V. V. Wadekar, "Ionic liquids as heat transfer fluids – An assessment using industrial exchanger geometries," *Appl. Therm. Eng.*, vol. 111, pp. 1581–1587, 2017.

[20] E. Bellos, C. Tzivanidis, and D. Tsimpoukis, "Thermal , hydraulic and exergetic evaluation of a parabolic trough collector operating with thermal oil and molten salt based nano fl uids," *Energy Convers. Manag.*, vol. 156, no. July 2017, pp. 388–402, 2018.

[21] P. D. Myers and D. Y. Goswami, "Thermal energy storage using chloride salts and their eutectics," *Appl. Therm. Eng.*, vol. 109, no. July, pp. 889–900, 2016.

[22] G. Srilakshmi, V. Venkatesh, N. C. Thirumalai, and N. S. Suresh, "Challenges and opportunities for Solar Tower technology in India," *Renew. Sustain. Energy Rev.*, vol. 45,

pp. 698–709, 2015.

[23] C. Zhou, “Hybridisation of solar and geothermal energy in both subcritical and supercritical Organic Rankine Cycles,” *ENERGY Convers. Manag.*, vol. 81, pp. 72–82, 2014.

[24] Y. Ahn *et al.*, “ScienceDirect REVIEW OF SUPERCRITICAL CO 2 POWER CYCLE TECHNOLOGY,” *Nucl. Eng. Technol.*, no. August, pp. 1–15, 2015.

[25] J. D. Osorio, R. Hovsapian, and J. C. Ordonez, “Dynamic analysis of concentrated solar supercritical CO2-based power generation closed-loop cycle,” *Appl. Therm. Eng.*, vol. 93, pp. 920–934, 2016.

[26] H. Singh and R. S. Mishra, “Performance analysis of solar parabolic trough collectors driven combined supercritical CO2and organic Rankine cycle,” *Eng. Sci. Technol. an Int. J.*, 2018.

[27] A. A. Alzaharani, I. Dincer, and G. F. Naterer, “Performance evaluation of a geothermal based integrated system for power , hydrogen and heat generation,” *Int. J. Hydrogen Energy*, vol. 38, no. 34, pp. 14505–14511, 2013.

[28] A. A. Alzahrani and I. Dincer, “ScienceDirect Design and analysis of a solar tower based integrated system using high temperature electrolyzer for hydrogen production,” *Int. J. Hydrogen Energy*, no. 2016, pp. 1–15, 2015.

[29] X. Li, H. Huang, and W. Zhao, “A supercritical or transcritical Rankine cycle with ejector using low-grade heat,” *Energy Convers. Manag.*, vol. 78, pp. 551–558, 2014.

[30] C. Sarmiento, J. M. Cardemil, A. J. Díaz, and R. Barraza, “Parametrized analysis of a Carbon Dioxide transcritical Rankine cycle driven by solar energy,” *Appl. Therm. Eng.*, 2018.

[31] H. Li, W. He, G. Feng, and Y. Qin, “Design of New Type Waste Gas/Wastewater Dual - Source Heat Pump Energy Cascade Recovery System in Campus Bath,” *Procedia Eng.*, vol. 205, pp. 3328–3333, 2017.

[32] J. Andreasen, W. Liu, H. Spliethoff, F. Haglind, and J. Abildskov, “Working fl uid

selection for organic Rankine cycles e Impact of uncertainty of fl uid properties," vol. 109, 2016.

[33] H. Singh and R. S. Mishra, "Engineering Science and Technology , an International Journal Performance analysis of solar parabolic trough collectors driven combined supercritical CO 2 and organic Rankine cycle," *Eng. Sci. Technol. an Int. J.*, 2018.

[34] J. A. D. Deceased and W. A. Beckman, *of Thermal Processes Solar Engineering*. .

[35] R. Foster, A. Cota, and F. Group, "SOLAR and the Environment," *Sol. Energy*, 2010.

[36] N. S. meteorology and S. E. – Location, "NASA Surface meteorology and Solar Energy – Location."

[37] L. Magistrale, "Evaluation of ORC processes and their implementation in solar thermal DSG plants," 2013.

[38] P. Garg, K. Srinivasan, P. Dutta, and P. Kumar, "Comparison of CO 2 and steam in transcritical Rankine cycles for concentrated solar power," *Energy Procedia*, vol. 49, pp. 1138–1146, 2014.

[39] F. Burkholder and C. F. Kutscher, "Heat loss testing of Schott's 2008 PTR70 parabolic trough receiver," *NREL Tech. Rep.*, no. May, p. 58, 2009.

[40] Y. Messele, "Addis Ababa Institute of Technology Department of Mechanical Engineering Thermal Analysis , Design and Experimental Investigation of Parabolic Trough Solar Collector," no. February, 2012.

[41] M. Günther, M. Joemann, and S. Csambor, "Advanced CSP Teaching Materials Chapter 5 Parabolic Trough Technology Authors," *2011*, pp. 1–43, 2011.

[42] P. Gilman and A. Dobos, "System Advisor Model , General Description System Advisor Model , General Description," no. February, 2012.

[43] E. N. M. Agency, "Agency, Ethiopian National Meteorology."

[44] M. Abdulazeez and A. Alfellag, "Modeling and Experimental Investigation of Parabolic Trough Solar Collector," 2014.

[45] B. and B. Moran, Shapiro, "NFundamentals of Engineering Thermodynamics, 8th Editiono Title."

[46] M. MJ, "Availability analysis: a guide to efficient energy use. 1982."

[47] W. S. R.V. Padilla, Y.C.S. Too, R. Benito, "Exergetic analysis of supercritical CO2 Brayton cycles integrated with solar central receivers, Appl. Energy 148 (2015) 348–365."

[48] M. Engineering, "ENERGY AND EXERGY ANALYSIS OF WASTE HEAT RECOVERY SYSTEMS USING ORGANIC RANKINE CYCLE Department of Mechanical Engineering ," 2016.

[49] "F.A. Al-Sulaiman, Exergy analysis of parabolic trough solar collectors integrated with combined steam and organic Rankine cycles, Energy Convers. Manage. 77 (2014) 441–449."

[50] "V.E. Dudley, G.J. Koib, A.R. Mahoney, T.R. Mancini, C.W. Matthews, M. Sloan, D. Keamey, SEGS LS-2 solar collector test results. Report of Sandia National Laboratories. SANDIA94-1884, 1994."

[51] M. Yari, A. S. Mehr, V. Zare, S. M. S. Mahmoudi, and M. A. Rosen, "Exergoeconomic comparison of TLC (trilateral Rankine cycle), ORC (organic Rankine cycle) and Kalina cycle using a low grade heat source," *Energy*, vol. 83, pp. 712–722, 2015.

[52] S. Moghanlou, "Thermodynamic Study of the Supercritical, Transcritical Carbon Dioxide Power Cycles for Utilization of Low Grade Heat Sources Application," *East. Mediterr. Univ.*, no. February, 2014.

[53] R. C. Barnes, "Reece Christian Barnes," no. December, 2017.